Politecnico di Torino

Politecnico di Torino

Corso di Laurea Magistrale In Ingegneria Dell'Autoveicolo
Tesi di Laurea Magistrale
Anno Accademico 2023/2024
Sessione di Laurea 03/2025

Development and assessment of a GT-SUITE model of an SI engine running with methanol, ethanol and syngas fuels

Relatori:
Prof. Ing. Stefano D'ambrosio
Prof. Ing. Roberto Finesso
Ing. Omar Marello
Ing. Alessandro Mancarella

Candidato:
Simone Perrini

INDEX

LIST OF FIGURES

LIST OF TABLES

INTRODUCTION

The internal combustion engine (ICE) has long been a cornerstone of the transportation industry, playing a pivotal role in both passenger and freight transport. Its widespread adoption can be attributed to several key advantages: simplicity, compactness, and cost-effectiveness compared to other propulsion systems. Additionally, the ICE boasts a favourable power-to-weight ratio, largely due to the high energy density of liquid fuels such as gasoline and diesel.

However, the internal combustion engine does not come without drawbacks: it suffers from relatively low efficiency and relies heavily on fossil fuels, which are non-renewable resources. This dependence on fossil fuels has significant environmental implications, including the emission of carbon dioxide (CO2), a greenhouse gas that contributes to global warming, and other pollutants resulting from incomplete combustion processes. These pollutants pose serious risks to both the environment and human health.

In contrast, electric motors offer several advantages over internal combustion engines, including higher efficiency, lower emissions, and reduced reliance on fossil fuels. Electric vehicles (EVs) produce zero tailpipe emissions, making them a cleaner alternative to traditional ICE-powered vehicles. However, the transition to electric propulsion is not without challenges: issues such as energy storage, charging infrastructure, and the environmental impact of battery production and disposal must be addressed.

In recent years, increasingly stringent emissions regulations have been implemented worldwide to mitigate the environmental impact of transportation. These regulations aim to reduce greenhouse gas and other pollutants emissions, driving the automotive industry to explore and adopt cleaner technologies. While the electrification of the powertrain is seen as a long-term solution, the internal combustion engine will continue to play a crucial role in the near future. As a result, ongoing research and development efforts are focused on improving the efficiency and reducing the emissions of ICEs through advanced technologies such as after-treatment systems, exhaust gas recirculation (EGR), and variable valve timing.

However, the transition to Fully Electric Vehicles (FEVs) presents numerous challenges that must be addressed to achieve global scale deployment. One of the primary obstacles is the need for a robust and widespread charging infrastructure: currently, the lack of sufficient charging stations poses a significant barrier to the adoption of electric vehicles, particularly in regions with less developed infrastructure.

Another critical issue is the capacity of the electrical grid: as the number of electric vehicles increases, so does the demand for electricity; this surge in demand can strain existing power grids, leading to potential overloads and reliability concerns. Ensuring that the grid can handle this increased load requires substantial investment in grid modernization and expansion.

The production and disposal of batteries also present environmental and logistical challenges. The extraction of raw materials for batteries, such as lithium, cobalt, and nickel, has significant environmental impacts. Additionally, the recycling and disposal of used batteries pose further environmental concerns. Developing

sustainable and efficient methods for battery production and recycling is crucial for the long-term viability of electric vehicles.

Furthermore, the cost of electric vehicles remains a significant barrier to widespread adoption. Although prices have been decreasing, electric vehicles are still generally more expensive than their internal combustion engine counterparts. This cost disparity can deter potential buyers, particularly in developing countries where affordability is a key consideration.

Lastly, the transition to electric vehicles requires a shift in consumer behaviour and acceptance. Many consumers are still hesitant to adopt electric vehicles due to concerns about range, charging times, and the availability of charging infrastructure. Overcoming these perceptions and building consumer confidence in electric vehicles is essential for their widespread adoption.

In conclusion, while the electrification of the automotive industry offers significant environmental benefits, several challenges must be addressed to achieve global scale deployment of Fully Electric Vehicles. These include developing a comprehensive charging infrastructure, ensuring grid capacity, addressing environmental impacts of battery production and disposal, reducing costs, and shifting consumer behaviour. Addressing these challenges will require coordinated efforts from governments, industry stakeholders, and consumers alike.

To develop these concepts quickly, research has turned to the use of predictive combustion models through numerical simulations. Predictive combustion models allow for more reliable evaluations of phenomena such as EGR and injection timing compared to non-predictive models. Although 3-D CFD (Computational Fluid Dynamics) simulation tools accurately reproduce the combustion process in engines, they have high simulation times. Therefore, today, zero/one-dimensional (0-D/1-D) tools are mostly considered, as they have acceptable simulation times and provide accurate results for automotive applications.

In addition to this, my project for the company Holdim Group, specifically with Ecomotive Solutions, concerns the creation of a mono-dimensional predictive model of a real engine, which originally was a CI engine but has been converted to SI. The goal is to validate this model, so that it can be used by the company in order to experimentally test the real engine, without direct bench testing and so at zero cost, and assess whether this engine can run on less polluting fuels; tests with methanol and ethanol have, indeed, already been performed.

1. FEATURES OF A SPARK IGNITION ENGINE

1.1 Flame Propagation

Spark Ignition (SI) engines are a fundamental type of internal combustion engine (ICE), widely exploited in various applications and particularly in the automotive industry. These engines operate on the principle of igniting an air-fuel mixture using a spark plug, which initiates the combustion process. The development and refinement of SI engines have played a crucial role in the evolution of modern transportation, providing a reliable and efficient mean of conversion of chemical energy into mechanical work.

As SI engines run with low reactivity fuels, this implies that, when the fuel is mixed with the air, due to a compact molecular structure of the fuel, the oxidation reactions are very slow and so there is no risk of spontaneous combustion process. Indeed, as already stated, the combustion process is started at a proper time by an external device, the spark plug, which provides an electrical voltage between two electrodes that produce an electrical arc, bringing the initial kernel at temperatures above 3000 K, so to achieve a temperature level that is high enough to break the molecular bonds of the hydrocarbons and to trigger the combustion process. Even though the energy imparted to the mixture by the electrical discharge is minimal (typically around 10 mJ) compared to the total energy released during the entire combustion process (approximately $1\,kJ$ in an automotive engine), it remains crucial to initiate the exothermic chemical reactions that are necessary to sustain a propagating flame.

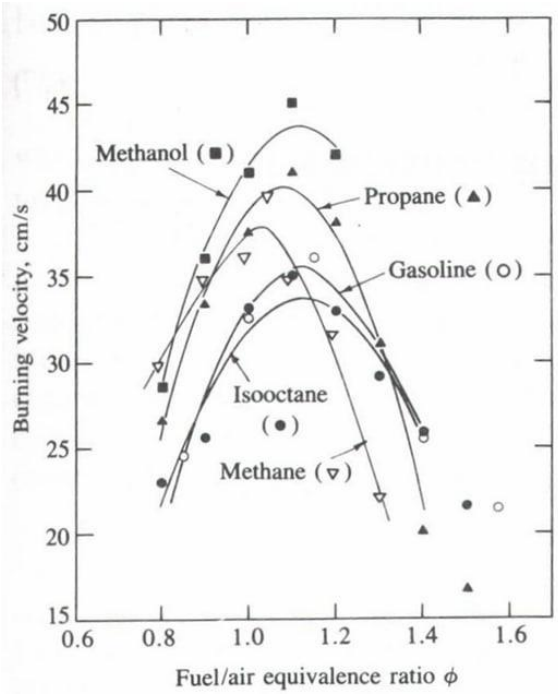

Figure 1 - Burning velocity in function of the air-fuel ratio [8]

Once the initial kernel is ignited, a flame front begins to spread radially outward: this occurs due to the intense heat transfer from the hot, burned gases to the surrounding layer of fresh, unburned mixture. Layer by layer,

the flame front progresses, with a thickness (especially in SI engines) being on the order of magnitude of $0.1\ mm$. The flame front is the surface or thin layer that separates the fresh, unburned mixture from the burned gases. Exothermic chemical reactions occur within the flame front, while heat transfer takes place through it.

However, the flame propagation cannot occur within the short time interval available in internal combustion engines (ICEs) under laminar conditions, even when using near-stoichiometric mixtures to maximize flame speeds, as the burning velocity values would be approximately two orders of magnitude lower than required.

As stated, if the flame front was to propagate with a laminar flame speed, extremely sensitive to the mixture composition, the combustion process would not progress with the required speed. However, temperature and pressure, such as those reached inside the ICE, are able to significantly increase the flame propagation speed. In fact, the high values of temperature and pressure affect the density of the charge, and, by turn, the heat transfer between the burned gasses and the fresh mixture is affected, as well as the temperature gradient between the fresh mixture and the burned gasses. On the other hand, it is necessary to consider that the increment of the pressure negatively affects the increment of the flame speed, since the layer that receives the heat from the burned gasses is much more dense, and, subsequently, it requires a higher amount of energy to be enhanced to a temperature at which the chemical reactions can proceed. However, the extremely positive effect of the high value of the temperature completely counteracts the negative effect of the pressure, with an overall increment of the flame speed. In addition to this, the negative effect of the composition of the mixture inside the cylinder has to be taken into account: in fact, in the ICE, not only the fresh mixture and the fuel are present, but also some dilutants that are burned gasses of the previous cycle; the amount of these gasses can obviously change depending on the operating conditions of the engine. The effect is that the chemical reactions are slowed down, since there are some inert gasses in the mixture which make the collisions between the molecules ineffective, and so the laminar flame speed further decreases. Typically, the amount of unburned gasses residual of the previous cycle is quite limited when the engine is operating at full load, due to the fact that, in this condition, the fresh mixture fills in all the engine displacement, and so the amount of inert gasses is the one contained inside the clearance volume at the end of the exhaust stroke. Instead, at part load, the amount of residuals is indicatively the same, since is the one contained in the clearance volume, but the amount of fresh mixture is reduced, and the consequence is that the concentration of the burned gasses significantly increases. So, at part load, a slower combustion process is expected, due to the presence of a more diluted and, as a result, less reactive mixture. Likely, the flame front becomes stretched and wrinkled due to the turbulent motion of the charge, particularly because of the presence of large vortices: this significantly increases its surface area and, consequently, the heat exchange between the burned gases and the fresh mixture. Smaller vortices, or eddies, increase the thickness of the flame front, creating a complex geometry similar to fractals.

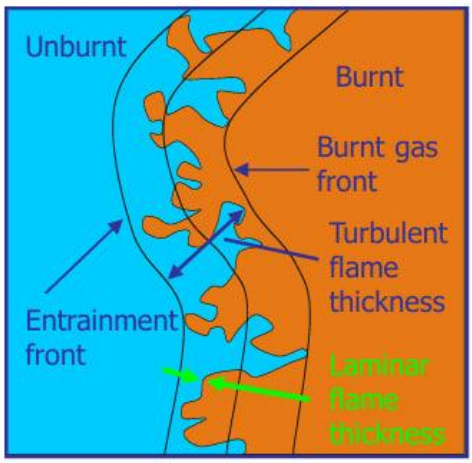

Figure 2 - Flame Front

As a result, turbulence corrugates the flame front, increasing the heat exchange area and thus the flame propagation speed. Since turbulence intensity rises with engine revolution speed, and the flame front speed is proportional to turbulence intensity, the flame front speed increases with the engine speed, thereby compensating for the reduced available time for combustion.

According to Damkohler, the increase of the flame speed under turbulent conditions compared with laminar flame speed can be attributed to the increase in the flame front surface. Moreover, the increase of the flame front surface is proportional to the turbulence intensity, which, by turn, is proportional to the mean piston speed. So, at the end, all these effects lead to a correct flame propagation speed and so to a desired combustion process. Besides to this, two important features of the SI engine, which are strictly related to the mixture compositions, have to be accounted for: firstly, the air and the fuel have to be properly mixed in order to ensure an homogenous and stoichiometric mixture; secondly, the load regulation process has to ensure a stoichiometric mixture as well. In fact, since the flame speed has to be sufficiently high to guarantee a correct combustion process and the peak of the flame speed is reached at a stoichiometric condition of the mixture, in order to reduce the load, and so the power provided by the engine, it is necessary to both reduce the fuel injected and the amount of intake air into the cylinder. This arises the need of a device, the throttle valve, that can be seen as a restriction, as it reduces the pressure of the intake air and, as a consequence, the density of the air, in order to guarantee that the ratio of air and fuel is always equal to the stoichiometric value, which changes depending on the fuel itself [8].

1.2 Main Phases

The combustion in a spark ignition engine can be divided into three phases: the development phase, which is assumed to occur when 5% or 10% of the mixture has been burned; the rapid burning phase, in which, typically, 95% or 90% of the charge is burned; the termination phase, in which the last 5% or 10% of the charge is burned.

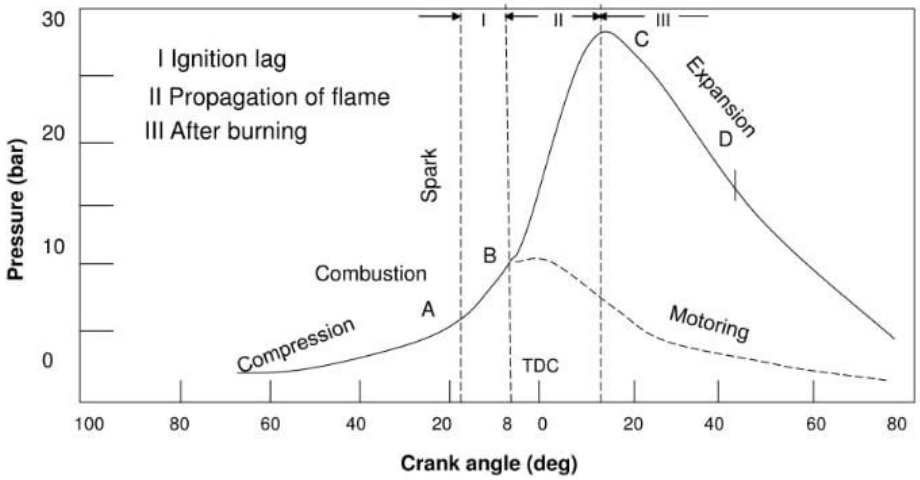

Figure 3 - Trend of Cylinder Pressure as a Function of Crank Angle

During the first phase, the amount of energy that is released due to the ignition of the first kernel, which grows until the flame front is developed, is locally high in terms $of\ J/mm^3$; however, on average, the thermodynamic conditions inside the combustion chamber are not impacted in a significant way. Indeed, an increment in terms of pressure is produced, but it is typically too small to be even perceived. The second phase is characterised by the flame front propagation through the combustion chamber and until the walls are reached, with a speed that is proportional to the turbulence intensity. As stated above, the second phase has a conventional end when the flame front reaches the region of the end gasses, which is far from the spark, and this typically is at $90 \div 95$ % of the mass fraction burned. An optimal engine calibration should release spark in a way that 50% of the mass fraction burned occurs between 8 °CA and 10 °CA after the top dead centre: this corresponds to the peak of the combustion efficiency, because, if the spark was to occur too late, and so the centre of gravity of the combustion (which is the crank angle when 50% of the mass fraction is burned) is higher than 10°CA, the combustion would mainly develop during the expansion stroke, so the chemical energy of the mixture would be converted and released into heat and then into mechanical work with too much delay. This would not allow to exploit all the expansion stroke of the piston. On the other hand, if the spark occurs too early to try to have a centre of gravity of the combustion process close to the TDC, and so also to obtain a combustion process as similar as possible to an ideal thermodynamic process and to be able to exploit all the energy coming from the combustion, then it may happen that the combustion starts to develop significantly during the last portion of the compression stroke and, as a consequence, the compression work increases. This is the reason why the spark timing that ensures an optimal combustion process and the centre of gravity at $8 \div 10$ ° CA after the top

dead centre is called the “Maximum Brake Torque” timing (MBT). In the third phase, the flame front has reached the walls and the last portion of the charge completes its oxidation process.

In addition to this, by acting on the spark timing, the engine control unit is capable of producing an immediate change of torque, that can be very useful in various possible situations in which the engine control unit has to react extremely quickly to sudden torque requests and a reaction of the ECU through a throttle cannot be fast enough. A possible example of this situation is when the engine is in idle conditions and, suddenly, the air conditioning system turns on; so, in this new condition, if the spark timing is not properly tuned, the new torque requested to the engine due to an increase of the load could slow the revolution speed of the engine down to the worst condition, which is when the engine stops. So, a possible solution to this problem, without any action on the throttle valve since the driver is not properly able to understand this situation, is to use a by-pass circuit, which can be opened by the electronic control unit, by-passing the throttle valve: an additional fresh mixture is provided to the engine in order to burn more fuel and to produce an higher torque. However, this kind of action is not the most proper one, since it involves the fluid dynamic field and so a transient phase during which the pressure in the intake manifold progressively rises due to the opening of the by-pass circuit, until the torque delivered by the engine is high enough to balance the new requested torque. On the contrary, if the ECU acts on the spark timing, an immediate response can be obtained by the engine. Of course, to make this possible, it is necessary to have a spark timing during the idle condition that allows a certain *torque back-up*. This has an impact not only on the drivability of the vehicle, but also on the capability of the engine control unit to provide a smooth response to the driver and to avoid any possible torque fluctuation that can be perceived by the driver. Besides this, the combustion efficiency becomes lower, and this also implies that the engine always operates at a lower efficiency. So, at idle, more fuel than necessary is lost in order to have this torque back-up.

Moreover, the three phases of the combustion have a different sensitivity to the engine operating conditions. Indeed, for what concerns the sensitivity to the engine speed, only the second phase scales with the engine speed, becoming faster as the engine speed increases. This is due to the fact that the flame propagation speed scales with the engine speed thanks to the turbulent flame front propagation, which, as explained before, is proportional to the mean piston speed and so to the engine speed. On the contrary, the other two phases solely depend upon the chemical reactions, and so they are not influenced by the turbulence. This means that their duration, in terms of crank angle, increases when the engine speed increases, while the duration of the rapid burning phase remains almost constant. So, all in all, the total duration of the combustion process can be increased by increasing the engine speed. As a consequence, the spark advance should be increased by increasing the engine speed as well. For what concerns the engine load, also in this situation the spark advance has to be shifted: in fact, if, for instance, the engine load decreases (so going from an open throttle condition to a partial load), the spark advance should be increased in order to compensate the slower propagation, as, by reducing the opening of the valve, the intake air reduces but the residuals increase, and this slows down the flame propagation speed and so the reactivity of the fuel.

Moreover, it must be considered that the flame propagation speed is further increased by the expansion of the burned gases, which pushes the fresh mixture towards the periphery of the combustion chamber. Therefore, the observed velocity of the flame front is equal to the sum of the burning velocity and the transport velocity, which plays a fundamental role. Due to the expansion of the burned gases, which typically have a density about four times lower than the fresh mixture, the relationship between the burned mass fraction and the burned volume fraction is highly nonlinear: when 50% of the mass has been burned, about 80% of the chamber volume has been involved in the combustion process, and the remaining 50% of unburned mixture has been compressed into 20% of the chamber volume.

1.3 Features About The Flame Propagation

As much as the turbulence is important when it comes to governing the flame propagation phenomena, it is also equally important to describe the main design options of the intake valves that can be chosen to promote high turbulence levels inside the combustion chamber. In fact, when the combustion process occurs in spark-ignition engines, the charge is typically in a turbulent state due to the large-scale gas motions generated during the intake stroke, which are influenced by the shape of the intake ports (such as tumble and swirl motions), or during the compression stroke, due to the shape of the piston and the cylinder head (such as squish motions). Due to the gas viscosity, these structured, large-scale motions continuously break down into smaller eddies, thereby transferring the kinetic energy of the flow to progressively smaller scales. These organized charge motions are mainly of three types: *tumble motion, swirl motion and squish motion [9].*

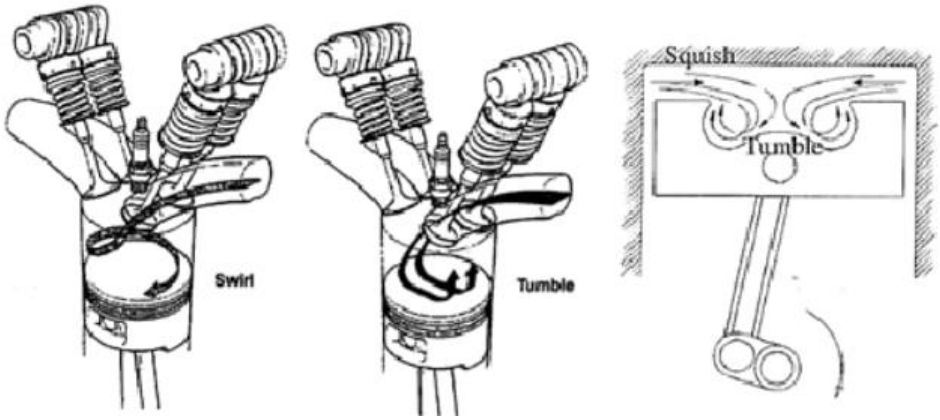

Figure 4 - Organised Charge Motions [9]

1.3.1 Tumble Motion

The tumble motion is characterized by a microscopic vortex that spins around an axis that is perpendicular to the cylinder axis, and it is typically obtained in a four valves SI engine. The tumble motion is generated during the intake stroke through an appropriate design of the intake ports, because, indicatively in the middle of the

intake stroke, the maximum flow velocity is reached. As stated, it must be oriented towards the region beneath the exhaust valves, thereby compelling the flow to tumble during the intake. Subsequently, during the compression stroke, the vortex tends to "spin up", meaning it increases its rotational speed to maintain its angular momentum, as the piston motion forces the vortex to decrease its radius.

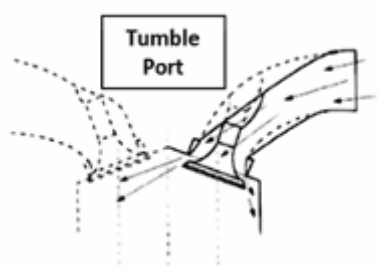

Figure 5 - Tumble Port [9]

As can be seen by these figures, the success in obtaining this organised structure of the flow is dependent upon the design of the intake port: in the case in which a direct port is used, the flow, during the intake stroke, is directed along a direction that is quite close to the cylinder axis; what can happen is that part of the flow enters into the cylinder on one side of the valve, while the other part of the charge enters on the other side. The result of this is a quite chaotic motion of the flow into the cylinder, instead of having an organised structure. An opposite solution would be to use a *high tumble* port, which is designed in a particular way: instead of having a bend and directing the flow in a direction close to the cylinder axis, the flow is directed in an almost tangential way under the cylinder head. Thus, most of the flow is directed in a way so that it enters in the cylinder remaining close to the cylinder head, passing below the exhaust valve. Then, it is forced to rotate by the cylinder wall. On the contrary, the other side of the valve contain is almost unused, as only a small quantity of flow goes into the cylinder from that side, and this is due to the fact that the design of the port is made in order to direct most of the flow on the other portion of the valve contain. As a result, an organised structure is obtained inside the cylinder, and this has an intensity that, from an angular moment point of view, is maximum in the middle of the intake stroke when the velocity of the flow entering into the cylinder is at its maximum level. The angular momentum of the flow structure tends to peak again during the compression stroke: this is due to the so called spinning up phenomenon, because the piston compresses the charge and, by doing it, it forces it to rotate on a progressively smaller rotational radius; so, the vortex tries to keep its momentum and the only way to do it is by increasing the rotational speed. This is beneficial since we are able in this way to increase the rotational speed during the compression itself. This phenomenon increases the velocity gradient, which increases the viscous strain inside the flow and which, in turn, tends to break down the structure into smaller eddies. This is what is necessary so to have smaller eddies near the TDC close to the end of the compression stroke when a high turbulence is fundamental to have a fast combustion process. For what concerns the swirl motion, the previous phenomenon cannot be expected to occur from it, since this organised gas motion rotates around the cylinder axis. This is the reason why the swirl tends to persist as a kind of rigid body motion and it can be useful to obtain mixture mixing, while tumble tends to be destroyed into eddies and

for this reason it is much more efficient when it comes to enhancing the flame propagation speed. Therefore, it is our first choice in the design of a port for an SI engine.

A drawback of an high tumble port is the occurrence of higher flow losses from a port of this type, as it forces all the flow to enter only from one side of the valve, by paying a penalty in terms of flow coefficient. This is the reason why there is a trade-off between achieving a suitable permeability of the port, that is a high enough flow coefficient from one side of the valve, and having a strong enough tumble motion.

1.3.2 Swirl Motion

The swirl motion is a microscopic vortex of the intake charge, which spins around an axis that is either coincident or parallel with respect to the cylinder axis. It is typically obtained by means of a proper design of the intake port, in particular resorting to an helix port shape or through a different orientation between the two intake ports in a four valves cylinder head. It is more universally adopted in compression ignition engines (CI) to promote the air and fuel mixing at the end of the compression stroke, since it quite often tends to maintain its structure during the entire intake and the following compression stroke by not being dissipated into smaller structures when the fuel is injected. Design solutions to achieve a target swirl level are: *Shrouded Valve, Directed Port* and *Helical Port.*

The shrouded valve type is the most intuitive one, but it is not actually feasible for a real engine, because it produces significant stresses on the valves, it limits the cross section at the valve opening and, as a result, it reduces the intake flow. However, it is sometimes used in laboratory engines, which are just motored (that is without the combustion) in order to develop methodologies to characterise the turbulence intensity and the flow motion.

The direct port is a more practical solution, since it is characterised by a port which is blanching directly into the cylinder head and it is typically directing the flow in a way such that the flow can be deflected by the cylinder wall and it can contribute to establish this organised motion rotating around the cylinder axis. In addition, directed ports generally struggle to generate significant swirl levels at low valve lifts due to the low velocity of the flow, which fails to produce a non-uniform distribution of the intake flow at the valve curtain. At higher lifts, they are more effective in generating swirl; however, their design typically results in low flow coefficients, as only a portion of the available valve curtain area is exploited. An enhancement of swirl levels at low valve lifts can be achieved through the use of helical ports. In addition to this, CI engines, typically with four valves per cylinder, are characterised by two different intake ports: a direct port and an helical port. The former one is intended to supply most of the flow and to produce a swirling effect at high flow, because it directs the flow along the cylinder wall; however, it cannot be sufficiently effective when the engine is operated at low speed, since at this condition the flow entering the cylinder is more moderated and as a consequence the swirl motion is moderate as well. If, in addition to this condition, the engine is at part load, so low flow

entering into the cylinder, only a direct port turns out to be even more inefficient. This is why for this condition it is more effective to use an helical port, because, even if the flow entering into this second port is limited, the shape of the port will enhance significant swirl effect. A drawback of this layout is to find a trade-off between two complementary conditions, full load and low load, in order to produce an appropriate level of swirl for both the conditions. In fact, an insufficient mixing must be avoided at low load and low speed as well as an over-mixing at high load and high speed due to a too high swirl level, which could lead to fuel jets overlapping one another. Basically, what might happen is that one jet is diverted by the swirl motion, reaching the region in which the neighbour jet has already been burned and has already consumed oxygen, and, as a result of this, soot is produced due to a worse air utilisation. A possible solution to this problem is to use a geometry in the intake that is variable, and in particular characterised by a small flap valve, which controls one of the two ports in order to force the flow to enter into one of the ports according to the load. Obviously, this solution comes with drawbacks as well, especially in terms of fluid dynamic losses of the intake phase, but this is not typically a major issue, since, at part load, the CI engine (differently from SI engine, which always works with a stoichiometric homogenous mixture) can work with an excess of air and so greater losses can be accepted as there is no constrain from the point of view of the volumetric efficiency.

The helical port is a port in which the structure of the flow is forced to rotate around the valve axis, and so it enters into the cylinder with this rotating motion.

1.3.3 Squish Motion

The squish motion is obtained with a proper design of the combustion chamber: in particular, the design of the piston head and of the cylinder head is such that a toroidal vortex can be obtained. This toroidal vortex basically is a fluid ring that covers the entire periphery of the cylinder; so, when the piston is approaching the top dead centre, especially if it has a particular shape such as a bowl shape, it can squish part of the mixture from the periphery of the cylinder to the centre of the chamber. This happens thanks to the presence of a pressure gradient in the cylinder, because of the different local compression ratio due to the particular shapes of both piston and cylinder head. Indeed, these shapes are such that, at the periphery of the cylinder, the gap between them reduces through the increase of the local pressure of the charge at the end of the compression stroke; vice versa, at the centre of the cylinder, the gap between the piston and the cylinder head increases, by reducing the local pressure of the charge. This way, a part of the mixture can be squished from the periphery to the centre of the chamber and a toroidal vortex is obtained all around the cylinder. This motion can be adopted both for SI and CI engines, but with different purposes: in a CI engine, it enhances the mixing between air and fuel and it promotes an efficient air utilisation, so to guarantee that all the air inside the combustion chamber is used for the fuel oxidation; in a SI engine, it creates intense turbulence motion.

1.4 Combustion Duration And Spark Advance

Spark advance, also known as ignition timing, refers to the timing of the spark plug firing in relation to the position of the piston within the cylinder. In a spark-ignition engine, the spark plug ignites the air-fuel mixture, initiating the combustion process: the timing of this ignition is critical when it comes to optimizing the performance of the engine, its efficiency and its emissions. The term "spark advance" specifically denotes the angle, measured in degrees of crankshaft rotation, before the piston reaches top dead centre (TDC) on the compression stroke at which the spark plug fires. Advancing the spark means that the ignition occurs earlier in the compression stroke, while retarding the spark means that the ignition occurs later. The optimal spark advance varies depending on several factors, including engine speed, load, air-fuel mixture, and combustion chamber design. A proper spark advance ensures that the peak pressure from combustion occurs at the most advantageous point in the piston's power stroke, typically just after the TDC. This maximizes the engine's efficiency and power output, while contemporarily minimizing fuel consumption and harmful emissions. Advanced ignition timing allows for a more complete combustion of the air-fuel mixture, which can improve the engine performance and fuel economy. However, excessive spark advance can lead to the knocking or pinging phenomenon, which is a condition in which the air-fuel mixture detonates prematurely, causing potentially damaging pressure spikes within the cylinder. Conversely, retarded ignition timing can result in an incomplete combustion, a reduced power output and increased emissions. Modern engines often employ electronic control units (ECUs) to dynamically adjust spark advance based on real-time operating conditions: this adaptive control helps to maintain an optimal engine performance across a wide range of driving scenarios.

As previously mentioned, the perfect timing for the ignition is the one that corresponds to the “Maximum Brake Torque”. However, there are cases in which it has to be calibrated differently, for instance when the catalyst needs to be warmed up: during the initial phase of the engine operation, particularly after a cold start, the TWC is not immediately effective due to its low temperature. By advancing the spark timing, the combustion process generates additional heat, which is transferred to the exhaust gases, and this increased heat accelerates the warming of the TWC, allowing it to reach its light-off temperature more rapidly. This new strategy is called the " *catalyst light-off mode*", which is an operating condition in spark-ignition engines where the spark advance is strategically adjusted to expedite the attainment of the light-off temperature of the three-way catalytic converter (TWC). It is, in fact, essential to achieve the light-off temperature quickly in order to minimize the emission of pollutants such as hydrocarbons (HC), carbon monoxide (CO), and nitrogen oxides (NOx) during the warm-up period. The catalyst light-off mode, therefore, plays a crucial role in enhancing the overall efficiency of the emission control system and ensuring compliance with stringent environmental regulations.

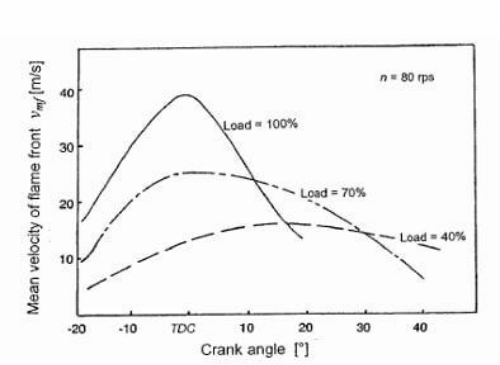

Figure 6 - Flame Front Speed As Function Of The Load

For what concerns the combustion duration, this parameter is influenced by a variety of factors, such as engine load, the composition of the air-fuel mixture, the residuals. For what concerns the engine load, if the load decreases, the flame speed decreases as well, due to an increase of the residuals which leads to a less reactive mixture, and the heat exchange decreases as well, due to a less dense charge. As a result, the combustion duration increases and so also the spark timing has to be increased when the engine load decreases.

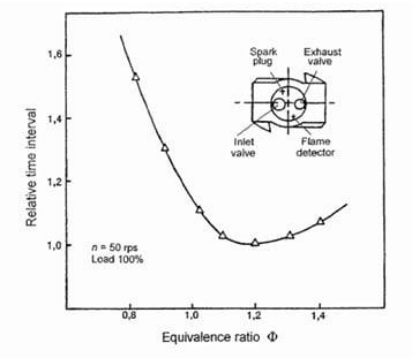

Figure 7- Combustion Duration As Function Of the Equivalence Ratio

As concerns the sensitivity of the combustion duration to the air-fuel ratio, as can be appreciated in the *figure 7* , the combustion duration shows a clear trend which indicatively recalls the one of the flame speed: where the flame speed is at its maximum value, the combustion duration is at its minimum value. This condition is obtained for a slightly rich mixture, at $\lambda = 0.9$, where λ is the ratio between the air-fuel ratio of the mixture and the relative air-fuel stoichiometric ratio. In addition to this, corresponding to this air-fuel ratio, the maximum temperature in the combustion chamber is achieved: this is due to the fact that, at high temperature, even if the hydrocarbons of the fuel are completely burned at stoichiometric condition, the formed carbon monoxides are not fully oxidated. In fact, some of the carbon dioxide molecules dissociate back into carbon monoxide molecules when the temperature is higher than 1850 °C. The dissociation prevents from releasing all of the energy that could potentially be obtained from the burning fuel, as this is an endo-thermic reaction. Instead, if the fuel is burned with a slightly rich mixture, so with a lack of oxygen, the carbon monoxide molecules are still formed, but only a certain amount of them finds the oxygen and then oxidises to form carbon dioxide molecules. In this condition, the environment inside the combustion chamber is such that the concentration of CO molecules is sufficiently high to slow down the dissociation reactions that tend to produce

more CO. Indeed, CO molecules are reactants for the oxidation reactions to form CO_2 molecules, but they are a product of the dissociation reactions. So, with a rich mixture, the dissociation reactions are inhibited due to an higher concentration of CO molecules rather than CO_2 molecules: as a result, with a slightly rich mixture there is a less negative effect of the dissociation, leading to higher temperatures in the combustion chamber.

1.5 Cycle to Cycle Variability

An important measure of the cycle variability is the coefficient of variation in indicated mean effective pressure (IMEP), which is derived from the pressure data. This coefficient is defined as the standard deviation of the IMEP divided by the mean IMEP, and it is typically expressed as a percentage. It has been observed that vehicle driveability issues generally arise when this value exceeds approximately 10 percent. Furthermore, experimental measurements clearly demonstrate that there is a significant variation in the in-cylinder pressure from cycle to cycle, even under fully stabilized engine operating conditions (i.e., constant speed, load, thermal conditions, etc.): this variability can be attributed to fluctuations occurring in the combustion process, which may be due to variations in gas motion at the time of spark ignition, to variations in the mixture composition, particularly in the vicinity of the spark plug, and to the amount of air, fuel, and residuals trapped per cycle. Moreover, the cycle-to-cycle variation must typically be limited to a coefficient of variation in indicated mean effective pressure ($COVimep$) of 3-4%, to avoid fluctuations in the delivered power that can be perceived by the driver. Furthermore, high cycle-to-cycle variation values may cause faster-than-average burning cycles, which result in knocking, and slower-than-average burning cycles to partially misfire, leading to an unacceptable increase in hydrocarbon (HC) emissions. Lean burn or highly diluted mixtures are likely to result in high cycle-to-cycle variation.

1.5 Abnormal Combustion

In a spark-ignition (S.I.) engine, the combustion process may deviate from the normal pattern previously described due to the occurrence of abnormal combustion phenomena. The most significant ones out of all of these phenomena are:

- **Preignition**: anomalous ignition of the mixture occurring before the spark, typically due to surface ignition over a hot spot. This may lead to immediate engine failure if the maximum peak pressure limit is exceeded ($Ppeak > 200\ bar$).
- **Misfire**: failure to ignite the mixture, due to a defective ignition system or mixture characteristics that are unsuitable for ignition (e.g., excessively high residual concentrations). This leads to a dramatic increase in hydrocarbon (HC) emissions and potential permanent damage to the three-way catalyst.

- **Knock**: autoignition of the end gas before it is reached by the flame front, resulting in an abrupt heat release. This produces a sudden increase of the in-cylinder pressure, generating pressure oscillations inside the combustion chamber and causing the engine structure to vibrate and produce a typical metallic noise. Knock may lead to engine damages due to high-temperature fatigue stresses, or it may result in a preignition due to an increased heat exchange with the combustion chamber walls.

1.5.1 Preignition

This is a very damaging event, since the engine cannot be controlled anymore. It is an anomalous ignition of the mixture occurring before the spark, typically due to surface ignition over a hot spot, and it can lead to an immediate engine failure if the maximum peak pressure limit is exceeded ($Ppeak > 200\ bar$). The further advancement of the combustion process caused by preignition increases the heat rejection from the gases towards the combustion chamber walls, due to the higher pressure and temperature peaks reached during combustion. This, in turn, causes a further increase in the walls temperature, which subsequently leads to a further advance in preignition in the following cycle, until the failure of the component is reached. Preignition may be triggered by repeated and prolonged knock, as pressure oscillations caused by knock disturb the thermal boundary layer close to the walls, enhancing the heat exchange and thereby increasing the likelihood of surface hot spot ignition. When this occurs, the preignition is often referred to as *"Megaknock"*. In gasoline direct injection engines, the "megaknock" can often be triggered by the ignition of lubricant oil diluted by the injected gasoline. Zaccardi, together with other researchers at the Institut Français du Pétrole (IFP), was able to identify the location of the preignition in a highly boosted engine with optical accessibility in a quite repeatable manner: the locations close to the spark plug and the exhaust valves suggested that, for the tested engine, the most likely sources of preignition could be surface ignition due to hot spots. Other researchers, working on a highly boosted Volkswagen (VW) engine modified to be optically accessible, excluded the possibility that hot spots could be responsible for preignition. Their findings, instead, indicated that the locations of preignition were randomly distributed within the combustion chamber and that the occurrence of preignition decreased with increasing coolant temperature. So, according to these researchers, the reason at the base of the preignition is not due to the hot spots, like the previous analysis, but it is related to the lubricant oil particles. In fact, the mechanism they proposed for pre-ignition is based on the hypothesis that the fuel spray wetting the cylinder liner leads to increased dilution of the oil film, therefore impairing the lubricant oil properties such as viscosity and surface tension. Consequently, there is a higher probability of releasing droplets that could potentially promote pre-ignition, since, unfortunately, what gives good lubricant properties to the oil is the presence of some additives, which can act as catalysts and promote the combustion reactions.

This hypothesis also explains the increased occurrence of pre-ignition at lower engine temperatures, as lower oil temperatures result in a higher fraction of non-evaporated fuel, leading to a greater degree of oil dilution and, consequently, a higher pre-ignition rate.

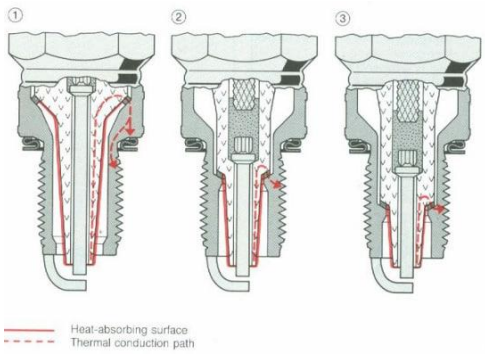

Figure 8 - The Different Spark Plug Types

The most common cause of abnormal preignition is related to the spark plug, and so an incorrect choice of the spark plug may cause misfire or preignition event. As explained in the previous section, a difference of voltage between two electrodes, that are the central and the lateral electrodes, of the spark plug triggers the combustion process. Between these two electrodes there is an isolating material, typically made of ceramic material, which is facing the combustion chamber; indeed, both the electrodes and this isolating material characterise the part of the spark plug that is screwed in a proper seat inside the cylinder head. So, it can occur that, after the combustion, the burned gasses leave some soot particulate, that can create a kind of unburned product layer on the surface of the ceramic material. Unfortunately, this soot layer is primarily made of carbon, which is a perfect material from an electrical point of view to conduct electricity: what may happen is that this layer of carbon creates a kind of short circuit, creating a connection between the two electrodes, and when a voltage differential is applied to trigger the combustion, instead of creating an arc, the current flows through this created carbon path, which does not start the oxidation process. The only way to overcome this problem is to reach, inside of the combustion chamber, a temperature that is sufficiently high to burn the soot that is present along the isolating material. However, the temperature of the part of the spark plug depends both on the geometrical features of the spark plug itself and on the temperature of the combustion process of the previous cycle and so, obviously, on the engine operating conditions. All in all, the choice of the spark plug is dependent upon the characteristics of the engine: a cold spark plug can be used for a high specific power engine, while a hot spark plug for a low specific power engine. In fact, in the first case, the risk of a too high temperature arises, and this can lead to hot spot for the preignition with an hot spark plug, which is a plug characterised by a long *"nose"*, that is the portion of the spark plug screwed inside the combustion chamber. On the other hand, in the second case, a cold spark plug, characterised by a short *"nose"*, leads to a too low temperature, which can be high enough to burn the soot deposit on the isolating material, and as a result it leads to misfire.

1.5.2 Knock

Before delving into the phenomenon of knock, it is essential to focus on the underlying reasons for its occurrence. Knock, also known as detonation, is a critical issue in spark-ignition (S.I.) engines that can significantly impact the engine performance, efficiency and longevity. Understanding the fundamental causes of knock is paramount to develop effective strategies in order to mitigate its effects and enhance the overall operation of internal combustion engines. This introduction aims at providing a comprehensive overview of the factors contributing to knock, setting the stage for a detailed examination of its mechanisms and potential solutions.

The combustion of a generic hydrocarbon, even when in a gaseous phase and fully and homogeneously mixed with air, progresses through a multi-step process known as chain reactions. In this process, intermediate reaction products, such as radicals, play a fundamental role. Before the air-fuel mixture can ignite, chain branching reactions must occur, producing high concentrations of radicals; only when a certain threshold level of radical concentrations has been reached, after a specific time delay, commonly referred to as induction time or ignition delay, the combustion process can commence with a significant release of thermal energy. If, ideally, it was possible to bring the mixture to the desired temperature and pressure (the ones of an ICE), then, initially, nothing would appear, but after a certain time there would be a linear increment of temperature. In ICE, this ignition delay has an order of magnitude of milli seconds, and this is due to the time needed for the intermediate reactions to take place and to reach the concentration of the intermediate reaction. So, during the initial part of the reactions, the formation of the intermediate reactions does not lead to any results in term of energy derogation (so no increment of temperature or pressure) and these reactions are called pre-reactions. Since typical induction times (τ) for practical air-fuel mixtures in internal combustion engines (ICEs) are on the order of milliseconds, measuring τ requires that the mixtures are subjected to high pressures and high temperatures representative of typical ICE conditions in extremely short timescales ($<< \tau$). This task is typically accomplished using Rapid Compression Machines (RCMs), which are single-stroke devices capable of compressing uniform and homogeneous mixtures of fuels and oxidants to engine-like conditions. The compression duration is very brief (it must be $<< \tau$) and, in contrast to engine design, the piston is stopped at the end of the compression to create a constant volume environment inside the chamber. However, in an internal combustion engine (ICE), the mixture is gradually compressed by the piston during the compression stroke. Unlike the Rapid Compression Machine (RCM), the mixture in an ICE remains only for a certain time Δt_i at a pressure P_i and a temperature T_i, at which the mixture would undergo autoignition after an ignition delay τ_i. According to the hypothesis first formulated by Livengood and Wu, the time Δt_i spent by the mixture under thermodynamic conditions corresponding to an ignition delay τ_i consumes a fraction of the intermediate reactions that must be completed before autoignition occurs, equal to $\Delta t_i / \tau_i$. This implies that the autoignition occurs in a mixture exposed to variable thermodynamic conditions only when the intermediate reactions have been completed, that is when the cumulative fraction of the intermediate reactions reaches a critical threshold.

For what concerns the knock phenomenon, it is the autoignition of the end gas, occurring before it is reached by the flame front, resulting in an abrupt heat release. This produces a sudden increase of the in-cylinder pressure, generating pressure oscillations within the combustion chamber. These oscillations cause the engine structure to vibrate, producing a characteristic metallic noise, commonly referred to as "knock". So, this phenomenon happens if the end gasses of the mixture are exposed to thermodynamic conditions for a time that is long enough to consume the intermediate reactions that lead to an autoignition, according to the hypothesis of Livengood and Wu. Due to the cyclic variability, fast-burning cycles are more likely to experience knock, as they reach higher temperatures and pressures in the end gas. The occurrence of abnormal combustion can be mitigated through the control of the spark advance [6].

1.6 Emissions of a Spark Ignition Engine

The emissions produced by spark-ignition (S.I.) engines represent a significant challenge for the automotive industry, as they substantially contribute to air pollution and global warming. This section aims to provide a comprehensive overview of the mechanisms and factors influencing the formation of emissions in S.I. engines. Various types of emissions, including hydrocarbons (HC), carbon monoxide (CO), and nitrogen oxides (NO_x), will be examined, along with the technologies and strategies employed to reduce these emissions. Understanding the complex interplay between engine parameters and emission characteristics is crucial to develop effective solutions to minimize the environmental impact of S.I. engines and support the transition towards sustainable mobility [4][5][6][10].

1.6.1 CO Emission

Carbon monoxide is the last step before the final oxidation into CO_2. However, the oxidation reaction of carbon monoxide (CO) to carbon dioxide (CO_2) is relatively slow compared to the preceding reaction steps. Consequently, in rich mixtures, all the fuel may initiate the oxidation process and reach the intermediate oxidation level of CO, but only a portion of the CO that is formed achieves a complete oxidation to CO_2 (approximately 3% by volume is expected at $\lambda = 0.9$).

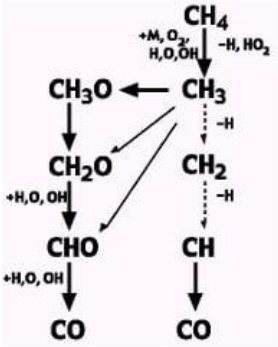

Figure 9 - Oxidation Reactions

The oxidation of CO to CO_2, provided that a sufficient amount of oxygen is available, occurs according to the following reaction:

$$CO + OH = CO_2 + H$$

There could be a formation of CO molecules in significant concentration even with a stoichiometric reaction, since the reversal reaction should be taken into account. At the high temperatures reached during the combustion process (T ≈ 2800 K), reaction rates are sufficiently high to achieve chemical equilibrium. Therefore, even if an adequate amount of oxygen is present to fully oxidize carbon monoxide (CO) to carbon dioxide (CO_2), significant CO concentrations are still expected due to the reverse reaction that leads to the dissociation of CO_2 into CO and hydroxyl radicals (OH). Subsequently, the sudden temperature decrease that occurs during expansion "freezes" the chemical reactions, preventing further oxidation of CO to CO_2. As a result, the CO concentrations found in the exhaust gasses are significantly higher than those predicted on the basis of the chemical equilibrium at exhaust temperatures.

1.6.2 NOx Emission

Nitric oxide (NO) forms throughout the high-temperature burned gas behind the flame front due to oxidation reactions of nitrogen that occur at high temperatures (above 1850 K), without reaching chemical equilibrium. The higher the burned gas temperature, the higher the NO formation rate. Subsequently, during the expansion stroke, as the burned gases cool down, chemical reactions involving NO formation and destruction freeze, leaving NO concentrations to be significantly higher than those corresponding to chemical equilibrium at exhaust conditions. In spark-ignition engines, the majority of NOx emissions consist of NO (approximately 98-99%), while the share of NO_2 is relatively small (about 1-2%). So, this implies that the NO formation is very sensitive to the temperature. The reverse reactions can occur as well, but these mainly happen during the expansion stroke, so, since the variation of the temperature is too fast, the equilibrium level of the reactions cannot be reached, and the concentration of NO molecules still remains close to the value obtained at a peak value of the temperature. According to the oxidation mechanism explained by Zeldovich, called *thermal NOx formation*, the main reactions leading to NO formation are the following:

$$O + N_2 \rightarrow NO + N$$

$$N + O_2 \rightarrow NO + O$$

$$N + OH \rightarrow NO + H$$

The last reaction is relatively less important.

In the following sections, the influence of three critical factors, that are the air-fuel ratio, the spark timing and the residuals, on the formation of nitrogen oxides in spark-ignition engines will be analysed. Understanding the impact of these factors is essential to optimize the engine performance and to reduce harmful emissions. By examining the interplay between these variables and their effect on NOx formation, this study aims to provide valuable insights into the mechanisms driving NOx emissions and to identify potential strategies for mitigating their impact. This analysis will contribute to the development of cleaner and more efficient automotive technologies, supporting the ongoing efforts to achieve sustainable mobility.

1.6.2.1 A/F Ratio

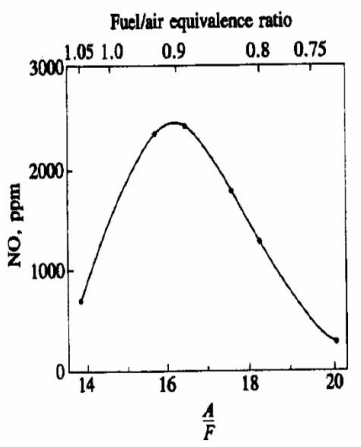

Figure 10 - NOx Consumption As Function Of The Air-Fuel Ratio [5]

As stated some lines before, the main reason for the formation of NOx is the high temperature, so, as a consequence, the air-fuel ratio that guarantees a high enough temperature contributes significantly to the formation of NOx. The peak combustion temperatures are achieved at an air-fuel ratio (λ) of approximately 0.9. However, in fuel-rich mixtures, the limited availability of oxygen inhibits the formation of nitrogen oxides. The formation of NOx reaches its maximum in slightly lean mixtures ($\lambda \cong 1.1$), where the temperatures remain elevated and sufficient oxygen is present behind the flame front, thus creating the optimal conditions for NO formation. Near the stoichiometric value, a 10% variation in the air-fuel ratio results in a 30-40% variation in NOx emissions.

1.6.2.2 Spark Advance

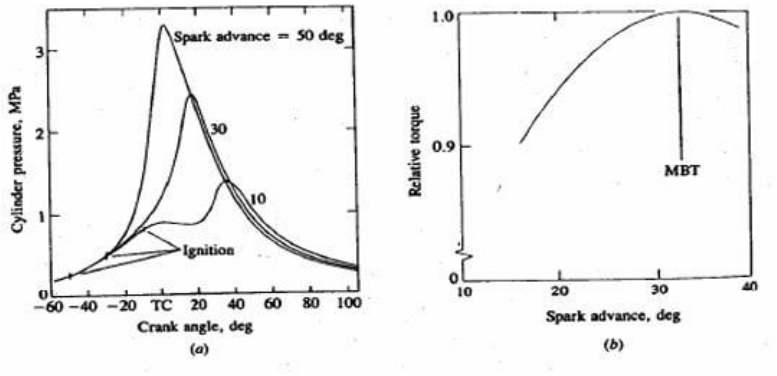

Figure 11 - a) Cylinder Pressure As Function Of The Spark Advance. b) Brake Torque As Function Of The Spark Advance [6]

An increasing spark advance leads to higher peak pressures and temperatures within the combustion chamber. This, in turn, results in elevated levels of nitrogen oxides emissions. The relationship between spark advance and NOx formation is significant, as advancing the spark timing enhances the combustion process, causing the air-fuel mixture to burn more rapidly and completely. Consequently, the higher combustion temperatures facilitate the formation of NOx, which are primarily generated through high-temperature oxidation reactions of nitrogen present in the air. Therefore, careful management of spark timing is crucial to control NOx emissions and ensure an optimal engine performance. As the spark timing is retarded, the efficiency of the engine is derated. Consequently, a trade-off between nitrogen oxides emissions and brake-specific fuel consumption must be established. However, near the maximum brake torque timing, the sensitivity of the brake mean effective pressure to spark timing is low, whereas the sensitivity of NOx emissions to spark timing is high; for instance, a spark timing adjustment that results in a 10% reduction in torque can lead to a 50% reduction in NOx emissions.

1.6.2.3 Residuals

Residual gases, which are the burned gases from the previous cycle, act as diluents in the unburned gas mixture. As the concentration of residual gases increases, the peak temperature reached during the combustion process decreases, thereby inhibiting the formation of nitrogen oxides. This effect is non-linear, and a 10% exhaust gas recirculation (EGR) can result in more than a 50% reduction in NOx emissions. However, the maximum EGR rate must be limited below 20% due to the deterioration of combustion quality, which includes increased coefficient of variation of indicated mean effective pressure (COV_{imep}) and higher hydrocarbon emissions. In addition to this, the exhaust gas recirculation technology is not used in most of spark ignition engines.

1.6.3 HC Emission

Up to approximately 9% of the fuel is not involved in the primary combustion process, resulting in a 6% loss in the indicated mean effective pressure. Within the cylinder, a significant portion of unburnt hydrocarbons (HC), ranging from 50% to 80%, undergoes oxidation. Additionally, up to 40% of the HC that is expelled from the cylinder is further oxidized in the exhaust port. Ultimately, a small fraction of the fuel, approximately 1% to 2%, is expelled at the tailpipe without undergoing complete combustion: this incomplete combustion process contributes to the overall emissions and efficiency losses in the engine. The concentration of unburned hydrocarbons at the tailpipe of spark-ignition engines is approximately 1% of the fuel. Despite the seemingly high combustion efficiency, these relatively low emission levels can be primarily attributed to post-flame oxidation reactions, occurring both within the cylinder and in the exhaust ports. While post-flame oxidation effectively reduces HC emissions, it adversely impacts the engine efficiency: this is due to the fact that the chemical energy of the fuel is converted into the enthalpy of exhaust gases rather than being utilized for piston work. Less than 50% of HC emissions consist of unburned fuel; the majority comprises partial oxidation products and pyrolysis products, which are highly reactive and contribute significantly to photochemical smog formation. In spark-ignition engines, several mechanisms contribute to the formation of hydrocarbons: the mixture trapped in crevice volumes accounts for 30-60% of the total HC emissions in a warmed-up engine; the fuel trapped in the oil layer contributes to 5-30% of the total HC emissions; the flame quenching at the combustion chamber walls is responsible for 5-20% of the total HC emissions; bulk quenching or incomplete combustion, which is usually significant only for air-fuel ratios that are much greater than 1 or with high levels of exhaust gas recirculation, also plays a role. Additionally, fuel trapped by deposits can contribute to 0-25% of the total HC emissions. The significance of each mechanism can vary considerably depending on the engine's operating conditions.

1.6.3.1 Wall Quenching

The flame front generally extinguishes before it reaches the combustion chamber walls due to the presence of a thermal boundary layer. In this layer, the mixture temperature is close to the wall temperature (approximately 400 K on the liner), which is insufficient for oxidation reactions to occur. The thickness of this thermal boundary layer can vary between 0.04 and 0.2 mm and it is inversely proportional to the in-cylinder pressure. This means that this mechanism is more important at part load: the lower the pressure, the higher the thickness of the layer. When two cold walls are positioned opposite to one another, the minimum distance between them that still allows the flame front to propagate is significantly greater than the thickness of the thermal boundary layer on a single wall. Specifically, this minimum distance is approximately five times the thickness of the thermal boundary layer; consequently, the minimum crevice region in which the flame can propagate is between 0.2 and 1 mm. This phenomenon is crucial in understanding the behaviour of flame propagation in confined spaces and its impact on combustion efficiency and emissions.

1.6.3.2 Crevices

During the compression phase, as the pressure increases, a portion of the air-fuel mixture is forced into the crevices of the combustion chamber, such as the spaces between the piston, liner, and rings, as well as the head gasket crevice. These regions cannot be reached by the flame front, preventing combustion from occurring within them. Subsequently, during the expansion stroke, when the pressure in the main combustion chamber drops below the pressure within the crevices, the trapped mixture flows back into the cylinder. However, this mixture is unable to complete its oxidation process, leading to incomplete combustion.

1.6.3.3 Oil Layer

During the compression stroke, fuel vapor can be absorbed by the oil layer on the cylinder liner due to the high fuel partial pressure. Subsequently, during the expansion stroke, as the fuel partial pressure decreases because fuel species are removed from the gas mixture by the combustion process, the oil layer releases the previously trapped hydrocarbon molecules. However, at this stage, these hydrocarbons are unable to complete their oxidation process. The solubility of fuel in the oil varies depending on the characteristics of the fuel molecules: it increases with the molecular weight of the hydrocarbon molecule and is negligible for light gas molecules such as methane or propane. Additionally, solubility is significantly influenced by temperature: lower temperatures result in higher solubility.

1.6.3.4 Bulk Quenching

As the combustion process nears its conclusion and the peak pressure is reached, the flame front's propagation speed across the combustion chamber diminishes. This deceleration is due to the reduction in pressure and temperature of the mixture caused by the expansion. If the temperature drops too rapidly, the flame front may cease to advance, resulting in unburned portions of the mixture. This phenomenon is more prevalent in slow combustion processes, such as those involving lean mixtures or high residual gas concentrations. Additionally, if the mixture surrounding the spark plug is not conducive to flame propagation, for example, due to an excessive concentration of residuals, misfiring events may occur.

1.6.3.5 Deposits

Deposits on the intake valve absorb fuel during acceleration transients and subsequently release it during deceleration phases. This process results in a mixture enleanment during tip-in and enrichment during tip-out, thereby increasing hydrocarbon (HC) emissions during transient conditions. However, these deposits are not

necessarily detrimental: they can be beneficial as they may lead to a reduction in fuel consumption. This occurs because the absorbed fuel is released during deceleration, and this can improve the overall fuel efficiency of the engine.

Additionally, deposits on the combustion chamber walls can trap and release fuel in a manner that is similar to the oil layer, leading to an increase in HC emissions as the engine ages. However, these deposits can also fill part of the crevice volumes and reduce heat exchange between the gases and the walls. As a result, combustion temperatures increase, causing a decrease in HC emissions as deposits accumulate over time.

1.6.3.6 Cold Start

During cold starts, hydrocarbon (HC) emissions rise significantly due to incomplete fuel evaporation. In port fuel injection (PFI) engines, fuel injection typically occurs when the intake valves are closed, allowing for effective fuel vaporization before the intake stroke. This vaporization is facilitated by the heat from the hot valve stem and backplate, as well as the mixing with hot residual gases that flow back into the exhaust port when the intake valve opens. However, during cold starts, a substantial fraction of the fuel fails to vaporize, necessitating mixture enrichment to achieve a near-stoichiometric mixture with the more volatile fraction of the fuel. Consequently, HC emissions during cold starts can increase by up to 50% for an engine starting at 0°C.

1.6.3.7 Operating Parameters

In the following section, the focus will be on the three operating parameters that significantly influence hydrocarbon emissions in internal combustion engines. These parameters include the air-fuel ratio, the spark timing and the residual gases. Each of these factors plays a crucial role in determining the efficiency of the combustion process and the resulting HC emissions. A detailed examination of these parameters provides a comprehensive understanding of their impact on HC emissions, similarly to the previously conducted analysis for nitrogen oxides emissions. Firstly, the influence of the air-fuel ratio on hydrocarbon emissions can be examined: HC emissions tend to be elevated in rich mixtures, not because of a lack of oxygen (which would result in carbon monoxide formation), but rather due to the increased severity of fuel trapping in crevices, the oil layer, and wall quenching phenomenon. Conversely, in lean mixtures, bulk quenching and misfire events become the dominant factors. HC emissions are typically minimized in slightly lean mixtures, with an air-fuel ratio of approximately 1.15 times the stoichiometric ratio. However, a trade-off with brake-specific fuel consumption must be considered. In lean mixtures, the relationship between HC emissions and spark timing changes: as the mixture becomes leaner, the flame front speed decreases, and this increases the significance of bulk quenching and the likelihood of incomplete combustion with reduced spark advance values. Next, let's consider the influence of spark timing on hydrocarbon emissions. As spark timing is advanced, the peak

pressure within the combustion chamber increases. This heightened pressure exacerbates the trapping of the air-fuel mixture in crevices and the oil layer, leading to higher HC emissions. Additionally, the gas temperatures at the end of the exhaust stroke are lower, which hinders the post-flame oxidation process, making it more challenging and slower. Consequently, the incomplete oxidation of hydrocarbons contributes to elevated HC emissions. Finally, let's examine the influence of residual gases on hydrocarbon (HC) emissions. As the percentage of exhaust gas recirculation (EGR) increases, the concentration of HC emissions also rises. This increase is primarily due to the heightened significance of bulk quenching and the occurrence of misfire events. Bulk quenching occurs when the flame front is unable to propagate through the entire air-fuel mixture, leading to incomplete combustion. Misfire events, on the other hand, happen when the mixture fails to ignite altogether. Both of these phenomena become more pronounced with higher EGR levels, as the presence of residual gases dilutes the air-fuel mixture and reduces the overall combustion efficiency. Consequently, the increased EGR percentage results in higher HC emissions.

2. MODEL DESCRIPTION

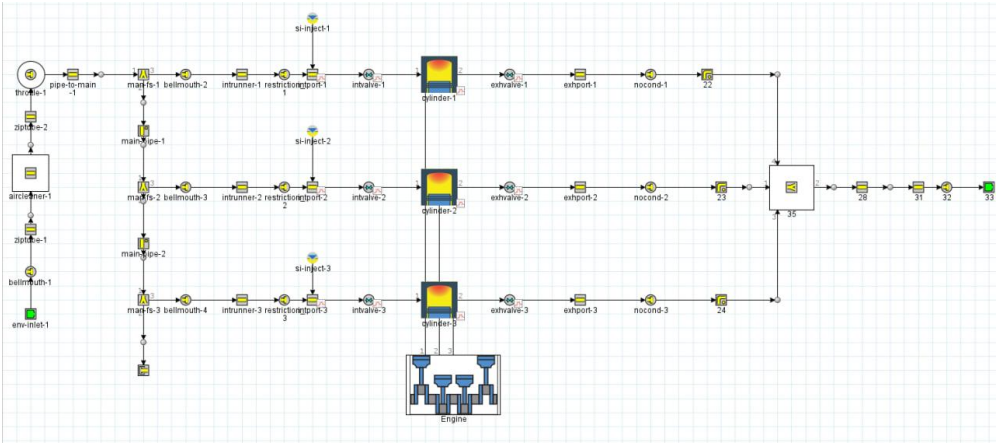

Figure 12 - GT-Power Engine Model

2.1 Features of The Engine

The FPT S8000 engine is a robust and efficient 3-cylinder, 2.9-liter diesel engine designed for industrial applications. This engine is known for its reliability, compact design and performance, making it a popular choice in various sectors, including agriculture, construction, and power generation. As previously stated, this engine has already been converted into a Spark Ignition engine, so some features are different from the original ones, in order to be able to run different fuels.

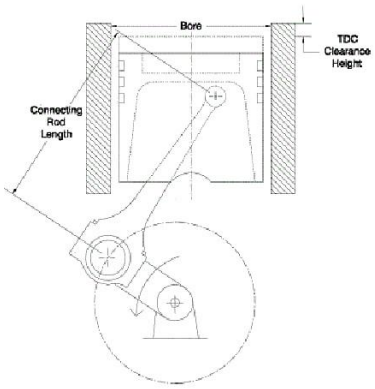

Figure 13 - Cylinder Geometry [2]

In the following table, the main characteristics of the engine and the geometric data of a single cylinder can be observed, respectively.

S8000 FPT ENGINE FEATURES	
Numbers of Cylinder	3
Bore	104 mm
Stroke	115 mm
Connecting Rod Length	174.2 mm
TDC Clearance High	11.5 mm
Displacement	0.977 L
Compression Ratio	11:1
Aspiration	Naturally Aspirated
Injection System	Multiport Injection System
Valves per Cylinder	2
Firing Order	1-2-3

Table 1 - Engine Features

2.2 Intake System

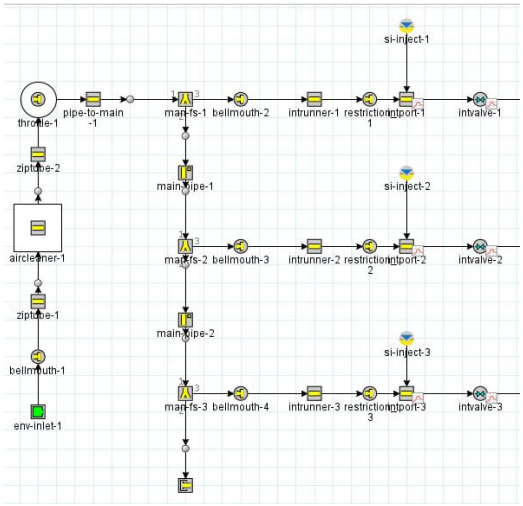

Figure 14 - Intake System Of The GT-Power Model

In the following section, a comprehensive analysis of the engine intake system will be provided, encompassing the pathway from the pick-up point to the intake port. This examination will delve into the various components and mechanisms involved in the intake process. The discussion will begin with an overview of the air intake system, including the air filter, which removes particulate matter and contaminants from the incoming air. Following this, the focus will shift to the throttle body, which regulates the airflow into the engine on the basis of the driver's input. The intake manifold, responsible for distributing the air evenly to each cylinder, will also be examined in detail. Additionally, the influence of the intake system on engine efficiency, power output, and emissions will be explored.

First of all, the ambient boundary conditions have been set, with the pressure equal to 1 bar and the temperature equal to 300 K. According to these conditions, the amount of intake air changes, as well as the amount of injected fuel and, subsequently, the performances of the engine. So, this hypothesis affects the obtained results, because a different value strictly changes the performances. Once the diameter and the length of the air filter are set, as well as the relative tubes that connect it with the pick-up point, the intake manifold has been created. The intake manifold comprises a series of general flow splits and pipes. A diagram of the manifold, along with the method employed to discretize the manifold, is presented below [2].

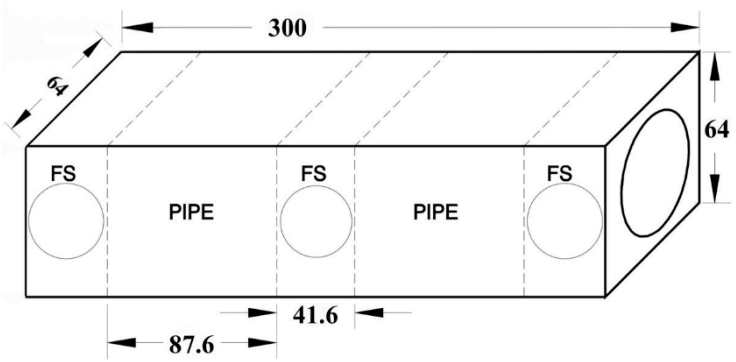

Figure 15 - Intake Manifold Used In The Model [2]

When discretizing a manifold, there are several steps to follow. First, the target discretization length has to be identified. For a general performance analysis, the discretization length should be approximately 0.4 times the bore diameter in the intake system and 0.55 times the bore diameter in the exhaust system. In this model, the bore diameter is 104 mm, resulting in an intake side discretization length of 41.6 mm. Next, the location of the flow splits (FS) has to be determined, ideally allocating one discretization length to each flow split. Flow splits are placed first because they always represent one sub-volume and cannot be further discretized. Using the overall dimensions, the remaining length for the pipes connecting the flow splits is calculated. The target discretization length for the intake system has to be applied to the pipes as well. The final component required for the intake manifold is an orifice. In most manifolds, the transition from the manifold to the runners is designed to be very smooth. Utilizing a default orifice in this location would introduce additional expansion and contraction losses to the system, which are not representative of actual conditions. Therefore, a non-default smooth orifice connection, known as a *"bellmouth"*, is necessary.

Finally, the intake runner and the intake port has been created for each cylinder. Between each of them, a restrictor has been put, with the aim to take the pressure losses of the real engine into account. The discharge coefficient and the diameter of these restrictions are tuned in order to obtain a volumetric efficiency that is as close as possible to the one of the real engine. Of course, in order to develop a model that has to be predictive, the value of the discharge coefficient should not be far from a common orifice one, and, in fact, during the optimisation process, the range within which this value can change has been the 1% of the typical orifice discharge coefficient value, that is 0.6.

For what concerns the intake and exhaust valves, the cam timing angle, the valve lift profiles and the discharge coefficients have been set. As the company did not provide the necessary data, a default discharge coefficient, scaled by a factor of *"x"*, was applied, allowing it to be adjusted during the optimisation process to ensure that the volumetric efficiency matches the actual value.

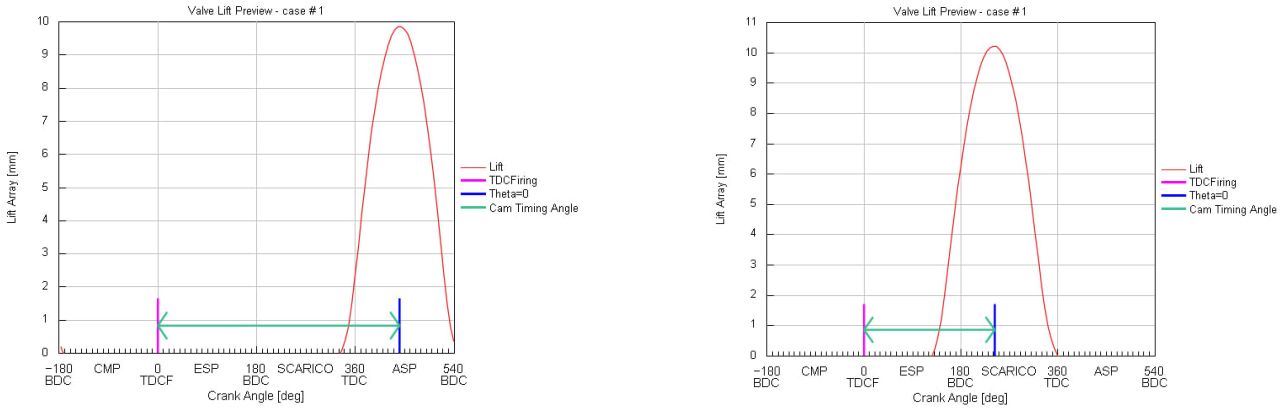

Figure 16 - Intake Valve Lift and Exhaust Valve Lift

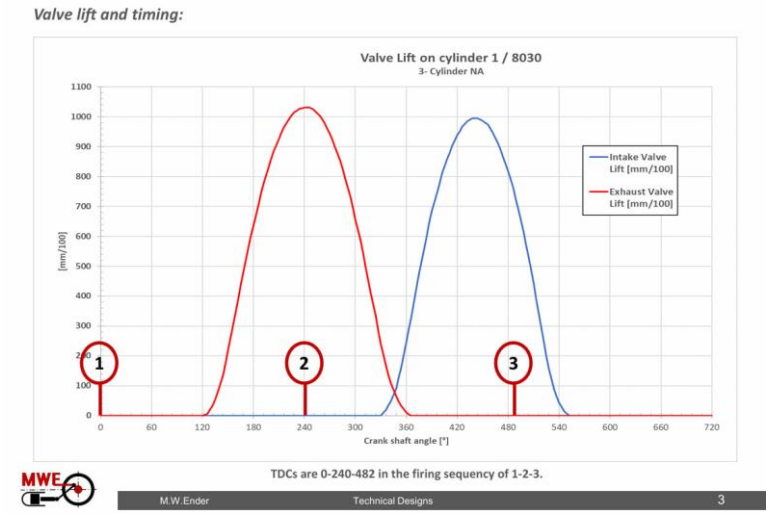

Figure 17 - Valve Lifts Provided By The Company

2.3 Injection System

The fuel injection system adopted for the s8000 engine is a multi-port system, characterised by a closed-valve, sequential injection strategy and an injector delivery rate equal to 12 g/s.

The following figure shows a part of the real cylinder head, which was sectioned to create the CAD model of the engine, as it is an old engine and the company does not have such data available.

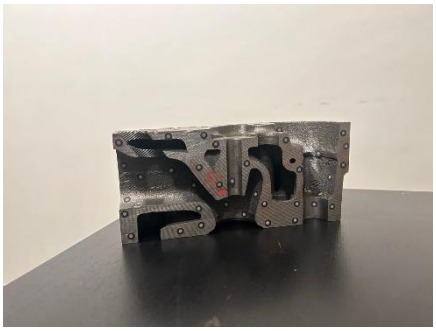

Figure 18 - Section Of The Original Engine Head

Instead, in the following figure, the injector seat can be appreciated: it is machined into the cylinder head, since, as said before, this engine was a CI engine.

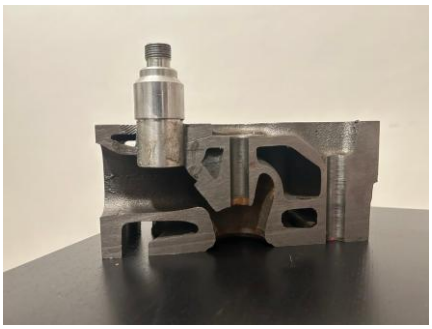

Figure 19 - Section Of The Engine Head with The Installed Spark Plug Seat

In the subsequent section, a comprehensive analysis of the injection systems in spark-ignition engines will be presented. This examination will delve into the various components and mechanisms involved in the fuel injection process, elucidating their roles and interactions in ensuring optimal engine performance. By exploring the intricacies of these systems, the aim is to provide a thorough understanding of their significance in the overall functioning of spark-ignition engines.

2.3.1 Requirements of The Fuel Metering System

First off, the fuel metering system must satisfy different requirements according to the operating conditions of the engine, so both steady-state conditions (idle, part load and full load) and transient conditions (fast enough variation of load and speed to ensure a desired acceleration or deceleration and a proper warm-up, for example during a cold start).

At wide open throttle condition, so at full load, the fuel metering system has to be able to ensure a slightly rich mixture, in order to increase the brake power of the engine, as it leads to a lower exhaust gas temperature and to a charge cooling with fuel vaporization, which results in an increase of the volumetric efficiency, due to an higher density of the air, and in a lower risk of knock, due to a lower temperature of the mixture.

For what concerns the part load condition, the fuel metering system has to be able to ensure a stoichiometric mixture in order to increase the fuel conversion efficiency as much as possible, since only a stoichiometric mixture can lead to a fast enough combustion process. Besides this, in some spark ignition engines at part load, a certain rate of the exhaust gas recirculation is allowed, as this leads to a higher fuel conversion efficiency due to a higher expansion work, because of the changes in thermodynamic properties of the mixture, to a higher flow rate at the intake due to a more open throttle valve, resulting in an higher intake pressure, and to lower heat losses to the walls due to a lower burned gas temperature. As load reduces, due to the valve overlap, which results in increase of the internal dilution of the mixture with the residual burned gasses of the previous cycle, a lower dilution of the mixture can be tolerated.

In addition to this, before the approval of emission regulations for vehicle in early 1990s, some engines were operated lean to further leverage the advantages of the dilution, but this led to issues in fulfilling emission regulations, as at lean mixture the after treatment mixture must be endowed with a lean NOx catalyst, since only the three-way-catalyst is not able to reduce the NOx. Moreover, increasing the proportion of excess air or the amount of exhaust gas recirculation (EGR) decelerates the combustion process and heightens the cycle-to-cycle variability; consequently, the degradation in combustion stability imposes a limit on the extent of dilution that an engine can accommodate.

At idle, instead, no EGR is tolerated and the fuel metering system has to provide a stoichiometric or slightly rich mixture in order to improve the combustion stability.

Regardless of the employed method, the fuel metering systems in spark-ignition (SI) engines must regulate the fuel mass and mix it with air to meet the engine's complex mixture requirements. This objective can be achieved through one of the following physical principles: the carburettor involves utilizing the pressure drop created by the airflow through a converging-diverging nozzle to meter the appropriate fuel flow; alternatively, injection relies on the pressure increase generated in the fuel by a suitable pump to inject a fuel spray into the induced air [1].

2.3.2 Carburettor

Historically, carburettors were widely used due to their operational simplicity. However, in recent decades, increasingly stringent emissions regulations have made it necessary to adopt injection systems in passenger car SI engines. This is because the main principle at the base of the carburettor is the venturi effect: the carburettor is, in fact, a simple restriction, as, in correspondence to its minimum cross section, a small pipe is located, so to connect the inner side of the restriction with a fuel tank at ambient pressure. This system is designed in such a way that the air flow rate through the restriction produces a delta pressure, and, thanks to this decrease of pressure, the fuel enters in the air steam. At the end, according to the air flow rate, so to the delta pressure, the amount of fuel injected is proportional to it, ensuring a stoichiometric ratio. But this system has limits that do not guarantee the stoichiometric condition: in fact, if the accelerator suddenly increases, the air flow rate increases as well, and if it reaches a value that is too high, the so called *"chocking"* phenomenon can happen. This means that the air flow rate is increasing excessively, while the delta pressure at the restriction does not increase proportionally any longer and, instead, it remains constant. As a result, the mixture entering in the cylinder is leaner. In addition, if the air flow rate is too low, the produced delta pressure cannot be high enough to overcome the fuel surface tensions, which are strictly related to the viscosity of the fuel, and the mixture is leaner. Today, carburettors are primarily used in SI engines for minor applications.

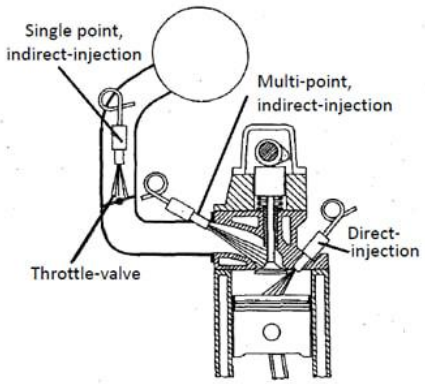

Figure 20 - Different SI Fuel Metering Systems [1]

2.3.3 Port-Fuel Injection System

Various gasoline injection systems have been developed for spark-ignition (SI) engines, each based on different solutions for the main components of the system. The injector can be positioned either outside the combustion chamber, where the fuel is injected into the intake system (indirect-injection, port-fuel injection or PFI), or on the head of each cylinder, where the fuel is directly injected into the combustion chambers (direct injection or GDI) [1].

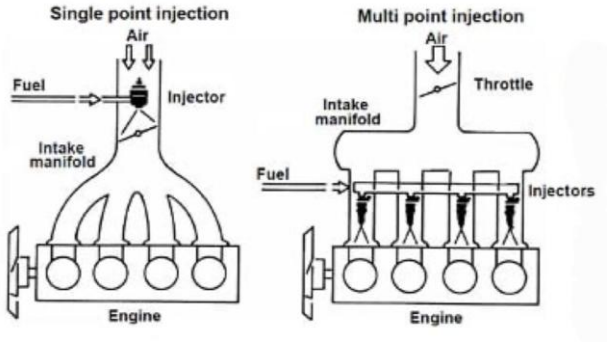

Figure 21 – Port-Fuel Injection Systems [1]

Single-point injection systems, which replaced carburettors, involve placing a single injector upstream to the throttle valve, where the traditional carburettor was located. While this solution is simple and cost-effective, it does not provide precise control over fuel distribution among the cylinders and the air/fuel ratio. In addition, other drawbacks concern problems during the transient condition, since part of the fuel gets blocked on the walls of the intake manifold and the vaporization of the fuel is not used in the best potential way. On the other hand, such system offers several advantages, including, as previously mentioned, being simple and cost-effective, as well as a better atomization, since the mixture flows through the throttle valve, and a good mixing.

In contrast, multi-point injection systems, which are now widely used, inject gasoline into the air stream near the intake port of each cylinder, leading to a more rapid engine response. The injection occurs during the initial part of the intake stroke, allowing sufficient time to the liquid spray to mix with the air and evaporate, forming a homogeneous mixture before the combustion begins and ensuring a uniform air/fuel ratio. In addition, such system increases the brake power through an improved volumetric efficiency, as the fuel vaporization is more related to the air steam rather than the high temperature of intake manifold's walls, and it provides a more uniform fuel distribution due to one injector for each cylinder. There are various strategies to enhance the engine performance with the multi-point injection system; in the past, through mechanical injectors, the fuel was injected in two steps: the majority was injected and temporarily stored in front of the intake valve, while the remaining portion was injected directly during the intake process. Nowadays, with electronically controlled injectors, the fuel is injected intermittently towards the intake valves according to three different strategies: simultaneous or full group injection, group injection, and sequential injection. The first strategy involves commanding all injectors at the same time; the second strategy is similar but commands the injectors in groups, for example, in a four-cylinder engine, the injectors are commanded in groups of two; finally, the most widely adopted strategy today is sequential injection, where each injector is commanded separately. Besides this, simultaneous and group injection strategies, coupled with an higher amount of injected fuel, allowed a robust engine start. However, these two strategies were abandoned from Euro3 regulations because of their too high emissions. On the other hand, also the sequential injection strategy has some disadvantages, since the exact time of the injection for each cylinder must be known, and so, a sensor must be used in the crankshaft to

distinguish which is the firing one between the two TDCs. This, of course, leads to higher costs of the system and higher required time.

However, port injection systems have some problems related to the fact that the fuel is not injected directly into the cylinder, but it impinges the intake walls or the surfaces of the intake valves. The mixture inside the combustion chamber is, indeed, globally but not locally homogeneous, so there are rich and lean pockets in the cylinder; the fuel may not be fully vaporized as it enters the engine and the distribution of fuel in the cylinders is not exactly equal. All these factors lead to a non-perfect mixture entering the cylinders. Besides this, even under fully warmed-up engine conditions, a small percentage of fuel is carried into the cylinder as a liquid. During cold engine starting, a substantial amount of additional fuel, beyond the quantity that is required to produce a stoichiometric in-cylinder mixture if fully vaporized, is injected in the initial injections: this is because, at low ambient temperatures, only a moderate fraction of the injected fuel vaporizes. However, with excess liquid fuel in the intake port from the initial injections, subsequent injections must be reduced below the nominal stoichiometric requirement to vaporize and burn the initial excess. Any liquid film on the intake port or valve walls introduces additional fuel transport processes, including deposition, liquid transport, and evaporation. During engine transients, such as vehicle accelerations and decelerations, when engine fuel requirements and manifold conditions change, transient air and fuel flow phenomena do not vary with time in the same manner, as fuel has a much longer time constant than the air process. The fuel metering system must implement strategies to compensate for transient phenomena: one approach involves analysing the liquid fuel mass on the walls (wall wetting) of the intake port and valve as one or more "puddles". The volume of fuel in the puddle increases with increasing load and speed. Such models have been primarily used to develop fuel metering strategies that compensate for the fuel transport lag. So, as stated, if the engine speed and the load increase, the thickness of this layer increases, and, as result, the amount of fuel that is injected into the cylinder is lower, leading to an enleanment until another steady-state condition is reached, while the thickness remains constant. For instance, during a tap-in manoeuvre, that is a transient condition, this kind of metering systems lead to a slower response of the fuel flow with respect to the air one and to an increased thickness of the *"puddles' layer"*. As a consequence, if any control strategy is implemented, a mixture that is leaner than the desired one is obtained, leading to a lower brake mean effective pressure during this transient condition, and to a lower performance of the engine with respect to the one desired by the driver. Vice versa, the opposite effect is obtained when the driver releases the accelerator pedal, since, in this case, the brake mean effective pressure is higher due to an enrichment of the mixture.

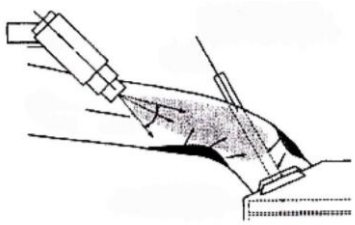

Figure 22 - Puddle Layer

2.3.4 Direct Injection System

The Gasoline Direct Injection (GDI) technology represents a significant advancement in the field of internal combustion engines, particularly for spark-ignition engines. Unlike traditional port fuel injection systems, where the fuel is injected into the intake manifold, GDI systems inject fuel directly into the combustion chamber. This direct injection method offers several advantages, including improved fuel efficiency, enhanced power output, and reduced emissions.

One of the primary benefits of GDI technology is its ability to provide precise control over the air-fuel mixture within the combustion chamber. This precision allows for the optimization of the combustion process, resulting in better fuel economy and lower levels of harmful emissions. Additionally, GDI systems can operate with a stratified charge, where a richer mixture is present near the spark plug and a leaner mixture is present elsewhere in the combustion chamber. This stratification enables an efficient combustion and further reduces fuel consumption.

The implementation of GDI technology also addresses the issue of engine knock, which is a common challenge in high-compression engines. By injecting fuel directly into the combustion chamber, GDI systems can better manage the temperature and pressure conditions, thereby minimizing the risk of knock and allowing for higher compression ratios. This capability is particularly advantageous in turbocharged and downsized engines, where knock resistance is crucial for performance and efficiency.

Moreover, GDI technology facilitates the use of advanced combustion strategies, such as homogeneous charge compression ignition (HCCI) and controlled auto-ignition (CAI). These strategies aim to achieve ultra-lean combustion, further enhancing fuel efficiency and reducing emissions. The flexibility of GDI systems in adapting to various combustion modes makes them a versatile and valuable technology in the pursuit of cleaner and more efficient engines.

In conclusion, Gasoline Direct Injection (GDI) technology offers numerous benefits that contribute to the advancement of internal combustion engines. Its ability to provide precise control over the air-fuel mixture, reduce engine knock, and enable advanced combustion strategies positions GDI as a leading technology for achieving higher fuel efficiency and lower emissions in modern SI engines.

2.4 Engine Cylinder

GT-POWER requires a series of information and inputs in order to be able to perform the desired combustion process. Unfortunately, much of this information was not provided by the company, as it was not obtained during the test bench, and, therefore, a series of data was assumed based on some made hypotheses.

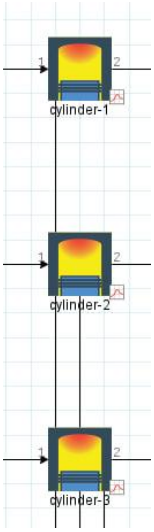

Figure 23 - Engine Cylinders In GT-Power Model

2.4.1 Wall Temperature

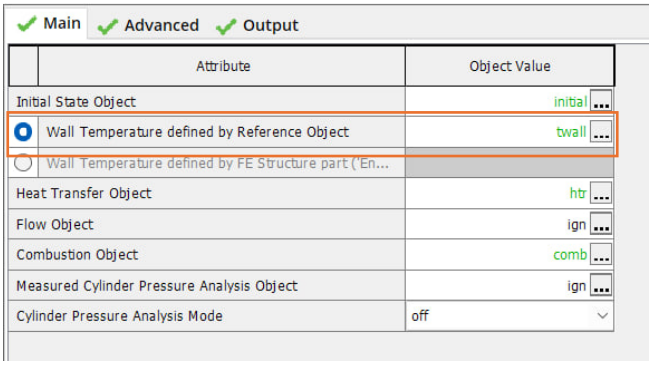

Figure 24 - Wall Temperature Object In The GT-Power Model

For what concerns the wall temperature, the software requires three parameters: the temperature of the head surface, including the valve face temperature, which, in the absence of specific head temperatures, has typical values at full load that range from 550 to 600 K; the piston temperature, which denotes the temperature of the piston surface or the designation of a dependency reference object, and, if specific piston temperatures are unavailable, typical values at full load range from 550 to 600 K; the cylinder temperature, which pertains to

the temperature of the cylinder, and, in the absence of specific cylinder temperatures, has typical value at full load of 400 K.

For this model, the assumed values are reported in the following table.

Head Temperature	550 K
Piston Temperature	590 K
Cylinder Temperature	450 K

Table 2 - Temperature Values Used

2.4.2 Heat Transfer Object

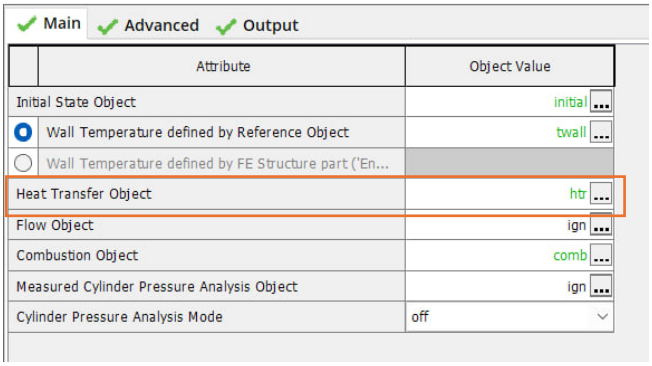

Figure 25 - Heat Transfer Object In The GT-Power Model

For what concerns the heat transfer object, the in-cylinder heat transfer is calculated using a formula that closely emulates the classical Woschni correlation without swirl. The primary distinction lies in the treatment of heat transfer coefficients during the period in which the valves are open: during this period, the heat transfer is increased by inflow velocities through the intake valves and by backflow through the exhaust valves. This method is recommended when measured swirl data is unavailable. The multiplier for the convective heat transfer is set to 1 as default.

2.4.3 Combustion Object

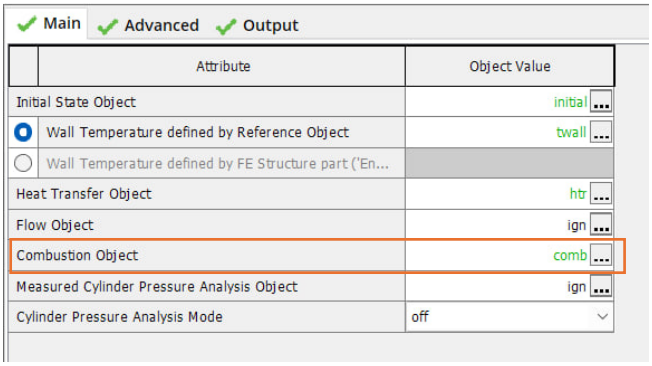

Figure 26 - Combustion Object In The GT-Power Model

As regards the combustion model, for this application the combustion burn rate for spark ignition engines has been imposed using the Wiebe function. The anchor angle, also called the centre of gravity of the combustion, which is the number of crank angle degrees between the TDC and typically the 50% combustion point of the Wiebe curve, has to be set, as well as the duration, in crank angle, of Wiebe combustion curve and the Wiebe exponent. In addition, as the company has only provided the spark advance, all the previously mentioned data has to be assumed. First of all, the anchor angle is calculated according to the following formula, in order to express it as a function of the spark advance:

$$MFB50\% = \left(\frac{combustion\ duration}{2} + \Delta\theta_{0-10}\right) - SA$$

where the combustion duration and the spark advance are the two inputs, while $\Delta\theta_{0-10}$ is the duration in crank angle of the development phase of the combustion and $MFB50$ is the anchor angle. To better understand this formula, it is suggested to have a look at the following figure of the mass fraction burned, where the formula is shown graphically.

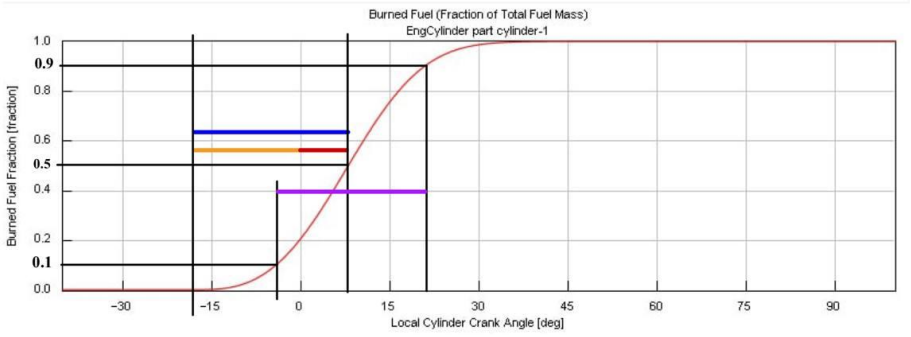

Figure 27 - Graphical Expression Of How The Formula Is Obtained

The combustion duration is represented in purple, while the first term of the formula, that is half of the combustion duration plus the development phase duration, is represented in blue; the spark advance is in yellow and, as a result, the anchor angle is in red.

In order to use this formula, two main assumptions are considered:

- $\Delta\theta_{0-10}$ is constant and equal to 13.9 °CA (this value is obtained experimentally);
- the spark advance has been calculated as the difference between the TDC, that corresponds to 0 °CA in the figure, and the crank angle when the burned mass fraction starts to be different from zero.

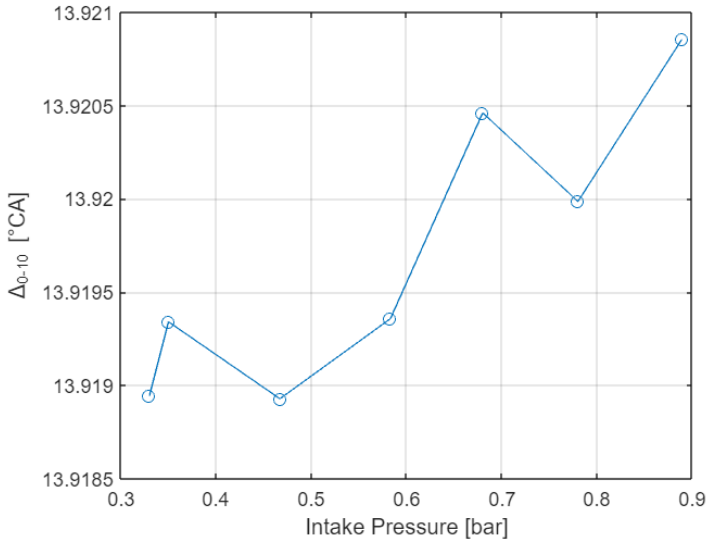

Figure 28 - Development Phase Duration

As can be appreciated from the previous figure, that represents the development phase duration relatively to different spark advances (the ones provided by the company), the first assumption is not so far from the reality, thus it can be considered to be valid.

For what concerns the other two data, the following table shows the relative values assumed for this model.

Combustion Duration	25 °CA
Wiebe Exponent	2

Table 3 - Values Used In The Combustion Object In The GT-Power Model

These two values are the default ones.

2.5 Engine Cranktrain

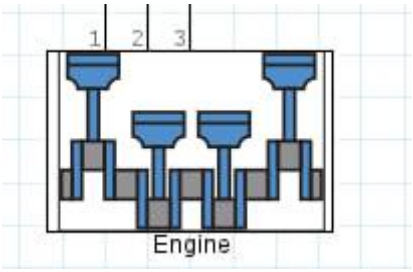

Figure 29 - Engine Cranktrain In The GT-Power Model

This template is used to model the kinematics and rigid dynamics of common reciprocating internal combustion engine cranktrain configurations in GT-POWER engine performance models.

Attribute	Unit	Object Value
Engine Type		4-stroke
Speed or Load Specification		speed
Engine Speed	See Case S...	[RPM]
Engine Friction Object or FMEP	bar	friction
Start of Cycle (CA at IVC)		[start_of_cycle]
Enable Cylinder Other than #1 Fire First (Beta)		
Crankcase Pressure	bar	def

Figure 30 - Engine Friction Object In The GT-Power Model

As illustrated in the preceding figure, among the various data required by GT-POWER, in addition to the two inputs, namely the engine rotational speed and the cycle start, which were provided by the company, there also are data relatively to the engine friction.

The engine friction model used in GT-POWER is the one based on the Chen-Flynn model, in which the friction mean effective pressure (FMEP) is obtained as follows:

$$FMEP = FMEP_{const} + A \cdot Pressure_{max} + B \cdot MeanPistonSpeed + C \cdot MeanPistonSpeed^2$$

where $FMEP_{const}$ is the constant term of the FMEP, A is the cylinder pressure dependence term, while B and C are the piston speed dependence terms. These two last terms are the default ones, while $FMEP_{const}$ and A have been calibrated resorting to a MATLAB Tool, in order to obtain the desired Brake Power. According to the different versions of the model, these values change, because the Brake Power that is obtained before the calibration of the frictions is different. This calibration has been done in order to still comply with the Chen-Flynn friction model, and so to obtain, at the end, a predictive model.

3. EXPERIMENTAL DATA

The engine was tested under a load step, with a power that is increased through 5 kW increments from 0 kW to a maximum of 30 kW, at two different rotational speeds: 1500 RPM and 1800 RPM. As mentioned in the introduction, the used fuels were methanol and ethanol. The following figures illustrate the tests that have been conducted respectively with methanol and ethanol at both rotational speeds.

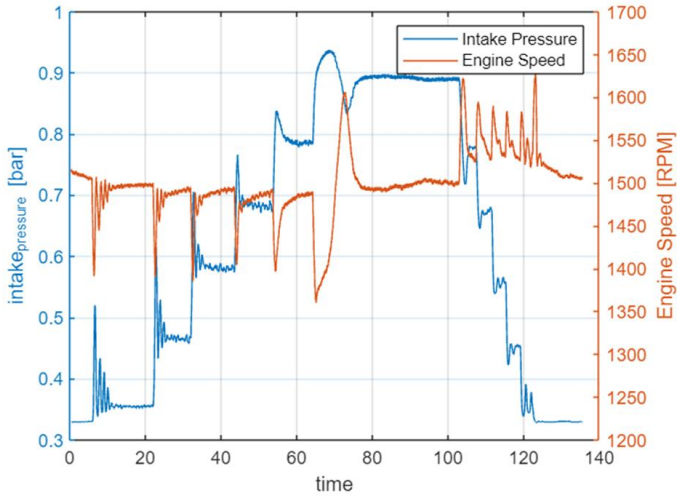

Figure 31 - Test Done With The Methanol At 1500 RPM

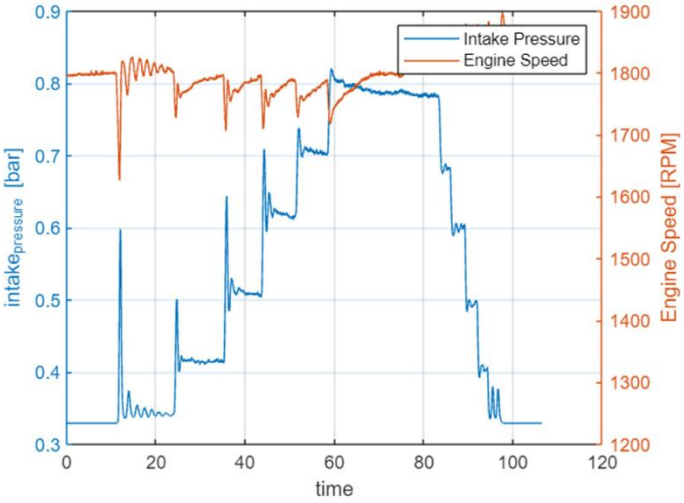

Figure 32 - Test Done With The Methanol At 1800 RPM

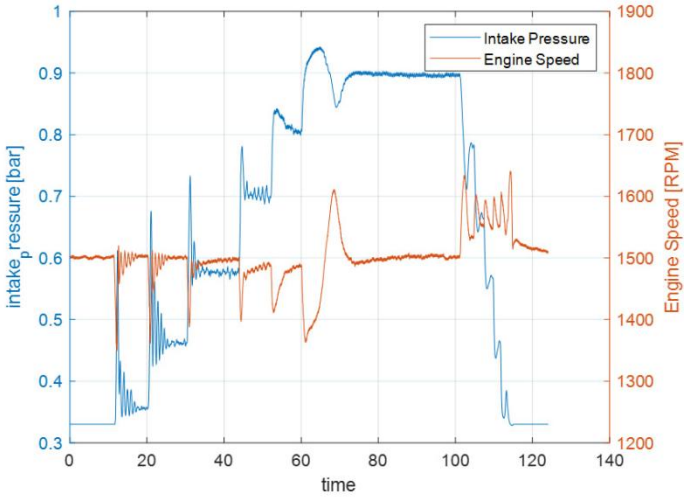

Figure 33 - Test Done With The Ethanol At 1500 RPM

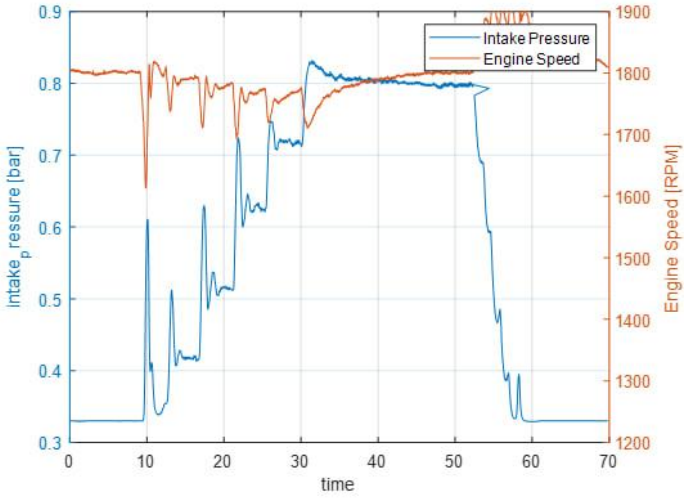

Figure 34 - Test Done With The Ethanol At 1800 RPM

As can be appreciated from the figures above, by increasing the load, both the curves of the intake pressure and the RPM start a transient period, so an oscillating behaviour. In some cases this oscillatory behaviour does not conclude before the commencement of the subsequent load step, and, as a consequence, since all the data are measured during the steady-state conditions for each step (more precisely, a very slow transient condition rather than steady-state condition), this may lead to errors in the comparison between the obtained results of the GT-POWER model and the real ones. In the following sections, the data provided by the company are shown, and, as a result, these are the data that have been compared with the results obtained by the implemented model in order to verify whether it actually is valid and predictive or not.

3.1 Intake Pressure

By knowing the values of the intake pressure at each time instant, an average of these values during the time intervals in which the transient period can be considered concluded was calculated, thus only during the steady-state period for each load. The obtained values are reported in the following table.

methanol	1500 RPM	0.35	0.467	0.583	0.68	0.78	0.889	bar
	1800 RPM	0.3424	0.4148	0.5097	0.6203	0.7065	0.7892	bar
ethanol	1500 RPM	0.3565	0.4624	0.5792	0.7017	0.8143	0.8975	bar
	1800 RPM	0.3455	0.4187	0.5141	0.6258	0.7172	0.8015	bar

Table 4 - Intake Pressure Values

The throttle valve in the model can be seen as a common restriction that, according to the equivalent hole diameter of the cross section, provides a pressure drop and, as a result, a different intake pressure in function of the load. Because of this, in order to obtain the desired values downstream the throttle valve, an optimisation process has been performed, leading to an equivalent diameter of the valve.

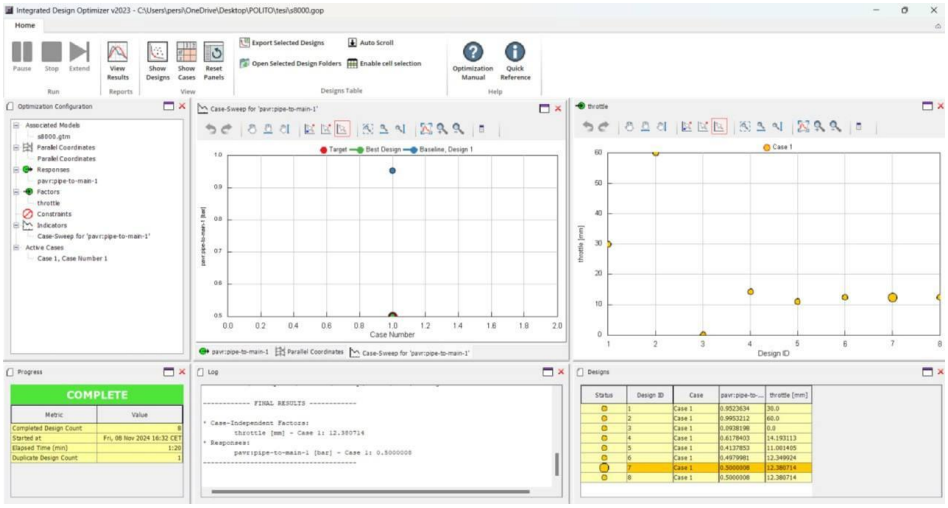

Figure 35 - Example Of The Optimisation Procedure

3.2 Injected Mass

The injected mass per single cycle and per single cylinder was calculated using the consumption data provided by the company. These data were obtained by weighing the fuel tank, thereby determining the consumption as the difference in the tank's weight after a few seconds of observation for each load step. The following tables show the consumption values obtained by the company for both the methanol and ethanol at 1500 RPM and 1800 RPM respectively.

kW	kg initial	kg final	Δkg in 2 min	Δkg per minute	Δg per minute	consumption in kg/min
5	13.992	13.764	0.228	0.114	114	0.114
10	13.725	13.442	0.283	0.1415	141.5	0.1415
15	13.404	13.046	0.358	0.179	179	0.179
20	12.995	12.577	0.418	0.209	209	0.209
25	12.525	12.038	0.487	0.2435	243.5	0.2435
30	11.902	11.324	0.578	0.289	289	0.289

Table 5 - Injected Fuel Mass For The Methanol At 1500 RPM

kW	kg initial	kg final	Δkg in 2 min	Δkg per minute	Δg per minute	consumption in kg/min
5	11.184	10.971	0.213	0.1065	106.5	0.1065
10	10.942	10.655	0.287	0.1435	143.5	0.1435
15	10.613	10.252	0.361	0.1805	180.5	0.1805
20	10.2	9.77	0.43	0.215	215	0.215
25	9.684	9.192	0.492	0.246	246	0.246
30	9.122	8.527	0.595	0.2975	297.5	0.2975

Table 6 - Injected Fuel Mass For The Methanol At 1800 RPM

kW	kg initial	kg final	Δkg in 2 min	Δkg per minute	Δg per minute	consumption in kg/min
5	13.138	12.963	0.175	0.0875	87.5	0.0875
10	12.944	12.71	0.234	0.117	117	0.117
15	12.69	12.408	0.282	0.141	141	0.141
20	12.39	12.045	0.345	0.1725	172.5	0.1725
25	12.019	11.609	0.41	0.205	205	0.205
30	11.403	10.934	0.469	0.2345	234.5	0.2345

Table 7 - Injected Fuel Mass For The Ethanol At 1500 RPM

kW	kg initial	kg final	Δkg in 2 min	Δkg per minute	Δg al minute	consumption in kg/min
5	10.814	10.642	0.172	0.086	86	0.086
10	10.612	10.372	0.24	0.12	120	0.12
15	10.342	10.05	0.292	0.146	146	0.146
20	10.014	9.652	0.362	0.181	181	0.181
25	9.61	9.201	0.409	0.2045	204.5	0.2045
30	9.155	8.665	0.49	0.245	245	0.245

Table 8 - Injected Fuel Mass For The Ethanol At 1800 RPM

The injected mass per cylinder per cycle is computed through the following formula:

$$\dot{m}_f = m_f \cdot i \cdot \frac{n}{m}$$

$$=> m_f = \frac{\dot{m}_f}{i \cdot \frac{n}{m}}$$

Where $\dot{m}_f$ is the consumption in g/min, i is equal to the number of cylinders, n is the revolution speed of the engine in RPM, m is the term that accounts for the cycle frequency, which is equal to 4 for four-stroke internal combustion engines, and m_f is the injected mass per cylinder per cycle.

3.3 Brake Specific Fuel Consumption

The brake specific consumption ($bsfc$) for each case is computed through the following formula:

$$bsfc = \frac{\dot{m}_f}{P_b}$$

The following tables show the $bsfc$ values obtained by the company for both the methanol and ethanol at 1500 RPM and 1800 RPM respectively.

kW	$bsfc$ in g/kWh
5	1368
10	849
15	716
20	627
25	584.4
30	578

kW	$bsfc$ in g/kWh
5	1278
10	861
15	722
20	645
25	590.4
30	595

Table 9 - Bsfc Values For the Methanol At Both The Engine Speed

kW	$bsfc$ in g/kWh
5	1050
10	702
15	564
20	517.5
25	492
30	469

kW	$bsfc$ in g/kWh
5	1032
10	720
15	584
20	543
25	490.8
30	490

Table 10 - BSFC Values For the Ethanol At Both The Engine Speed

3.4 Fuel Conversion Efficiency

The fuel conversion efficiency (η_f) for each case is computed through the following formula:

$$\eta_f = \frac{1}{bsfc \cdot LHV}$$

where $bsfc$ is the brake specific consumption, while LHV is the lower heating value of the relative fuel.

The following tables show the η_f values obtained by the company for both the methanol and ethanol at 1500 RPM and 1800 RPM respectively.

kW	η_f in %
5	11.9620
10	19.2740
15	22.8540
20	26.0980
25	28.0010
30	28.3110

kW	η_f in %
5	12.8040
10	19.0050
15	22.6640
20	25.3700
25	27.7160
30	27.5020

Table 11 - Fuel Conversion Efficiency Values For the Methanol At Both The Engine Speed

kW	η_f in %
5	12.8410
10	19.2070
15	23.9060
20	26.0540
25	27.4050
30	28.7490

kW	η_f in %
5	13.0650
10	18.7270
15	23.0880
20	24.8310
25	27.4720
30	27.5170

Table 12 - Fuel Conversion Efficiency Values For the Ethanol At Both The Engine Speed

3.5 Volumetric Efficiency

The volumetric efficiency (λ_v) for each case is computed through the following formula:

$$\lambda_v = \frac{\alpha_{stoc} \cdot m_f}{\rho_a \cdot V_D}$$

where α_{stoc} is the stoichiometric air-fuel ratio, m_f is the injected fuel mass per cylinder, ρ_a is the air density, equal to 1.204 Kg/m^3 , and V_D is the engine displacement.

The following tables show the λ_v values obtained by the company for both the methanol and ethanol at 1500 RPM and 1800 RPM respectively.

kW	λ_v
5	0.2769
10	0.3437
15	0.4348
20	0.5077
25	0.5915
30	0.6482

kW	λ_v
5	0.2156
10	0.2905
15	0.3654
20	0.4352
25	0.498
30	0.6022

Table 13 - Volumetric Efficiency Values For the Methanol At Both The Engine Speed

kW	λ_v
5	0.2957
10	0.3954
15	0.4764
20	0.5829
25	0.6927
30	0.7924

kW	λ_v
5	0.2422
10	0.3379
15	0.4111
20	0.5097
25	0.5758
30	0.6899

Table 14 - Volumetric Efficiency Values For the Ethanol At Both The Engine Speed

4. RESULTS

The objective of this chapter is to present the results of my work, which concerns the development of a GT-Power model of the real engine. To validate this model, it is essential to compare the data obtained from the company, as described in the previous chapter, with the results generated by the model. Additionally, to create a predictive model for both methanol and ethanol fuels, and for both rotational speeds of 1500 RPM and 1800 RPM, three versions of the model have been implemented. The following sections will analyse in detail the different inputs for each version.

4.1 Different Inputs

The three versions differ due to variations in the design of the intake manifold. These differences arise from changes in the data related to the orifice inserted in the intake line to account for real losses in the intake environment, which are not accounted for in the model. Additionally, there are differences in the percentage reduction of the flow discharge coefficient of the intake valve and, finally, in the coefficients characterizing the Chen-Flynn model used to obtain the engine friction. As already explained, the engine friction model used in GT-POWER is the one based on the Chen-Flynn model, in which the friction mean effective pressure (FMEP) is obtained as follows:

$$FMEP = FMEP_{const} + A \cdot Pressure_{max} + B \cdot MeanPistonSpeed + C \cdot MeanPistonSpeed^2$$

The following table shows these values.

	Version 1	Version 2	Version 3
Restriction Diameter [mm]	26.6422	32	41.6
Cd [-]	0.6157	0.6412	1
X [-]	0.9872	0.9905	1
A [-]	0.007753	0.007753	0.01
$FMEP_{const}$ [bar]	1.0371	1.0371	1
B $\left[\frac{bar}{\frac{m}{s}}\right]$	0.08	0.08	0.08
C $\left[\frac{bar}{(\frac{m}{s})^2}\right]$	$8 \cdot 10^{-4}$	$8 \cdot 10^{-4}$	$8 \cdot 10^{-4}$

Table 15 - The Different Inputs For The Three Versions

The third version of the model has no restriction, since the restriction diameter is equal to the nominal value of the intake port, and both the discharge coefficients of the restriction and the intake valve are not scaled.

4.2 Comparison Between The Versions With Methanol

The following plots show the differences between the three versions for what concerns the Brake Power, the Brake Specific Fuel Consumption, the Volumetric Efficiency, the fuel conversion efficiency and the Injected fuel mass.

4.2.1 Brake Power For With Methanol At 1500 RPM

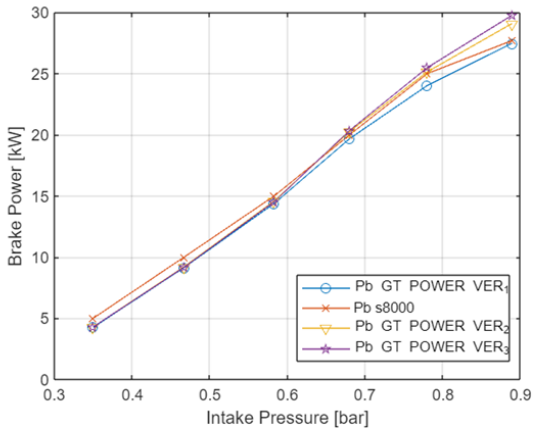

Figure 36 - Brake Power For Each Version

The curves show the same trend, but the closest to the red one, which is the curve of the real engine, is the one of the first version, as can be further verified analysing the errors in the following figure.

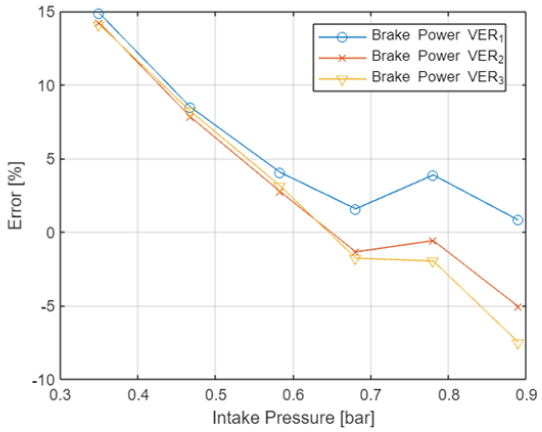

Figure 37 - Brake Power errors For Each Version

The errors are quite high at low load, due to a lower accuracy of the model at these conditions, because of a lower amount of intake air at these conditions and, as a consequence, a lower Brake Power, resulting in higher relative errors. As the load increases, it can be observed that the curve corresponding to the first version is closer to zero. This can be better understood by analysing the following figure, where the three versions are represented by three different colours. The darkest colour represents the first version, while progressively lighter shades represent the second and third versions respectively.

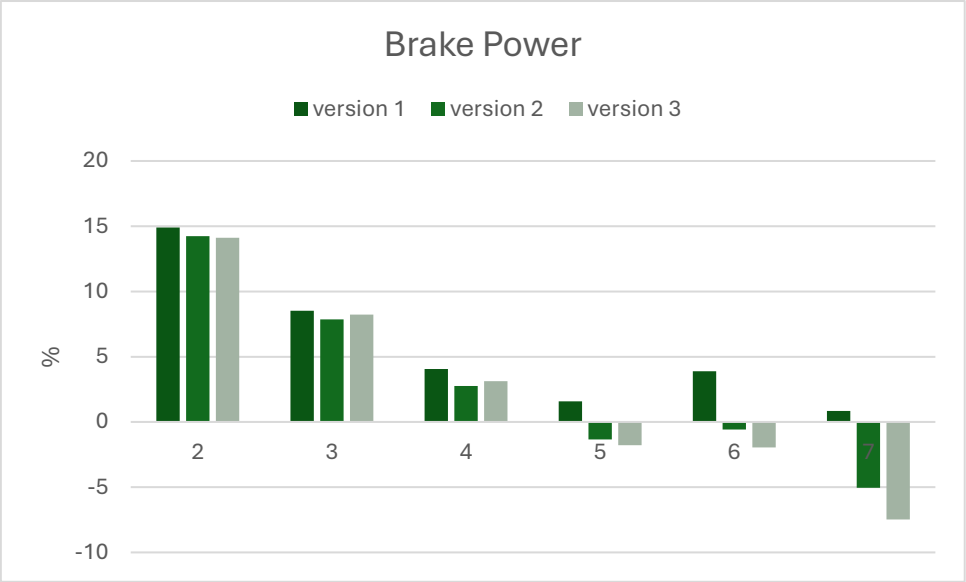

Figure 38 - Brake Power Errors For Each Version

4.2.2 Brake Specific Fuel Consumption With The Methanol At 1500 RPM

For what concerns the Brake Specific Fuel Consumption, in this case the curves of the three versions show the same behaviour of the real one as well. So, the three versions of the model can be used as a predictive model of the real engine.

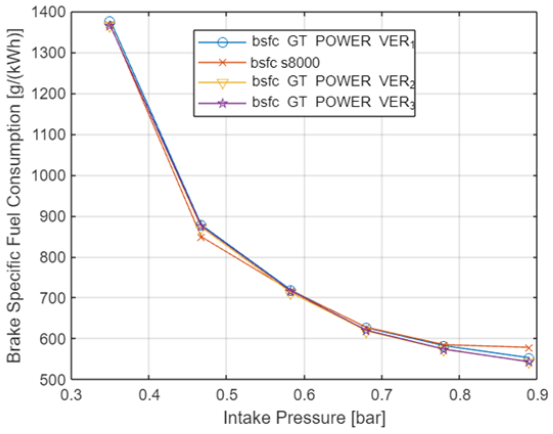

Figure 39 - Brake Fuel Conversion For Each Version

By analysing the errors, it is possible to state that the implemented friction model, despite it being different for the three versions, allows for errors in the brake specific fuel consumption (BSFC) that are not too distant from

the real case: in fact, they all are below 6%. In this case, again, the version that yields the best results is the first one.

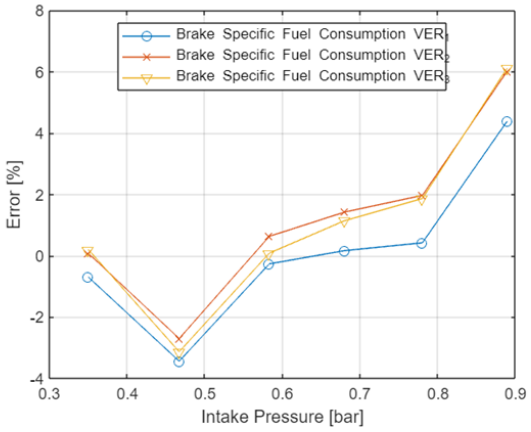

Figure 40 - Brake Specific Fuel Consumption Errors For Each Version

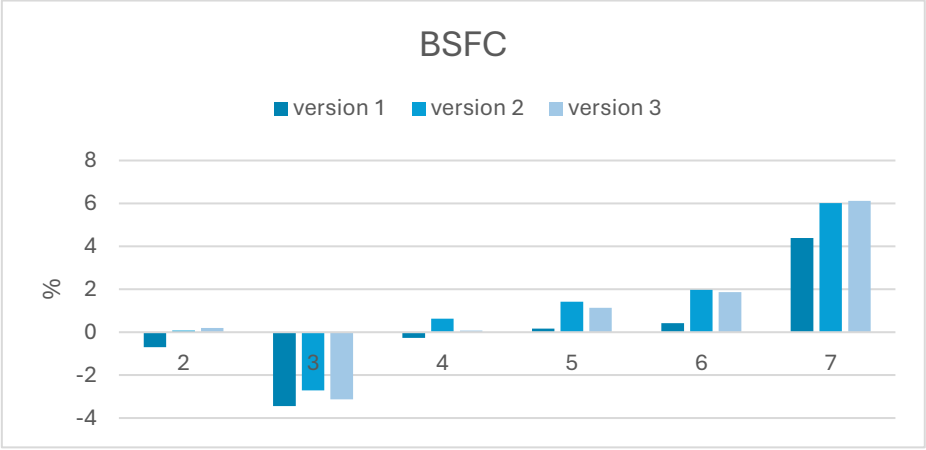

Figure 41 - Brake Specific Fuel Consumption Errors For Each Version

4.2.3 Volumetric Efficiency With The Methanol At 1500 RPM

The volumetric efficiency of the three versions is much higher than the one of the real engine, and this is mainly due to the fact that it is not easy to take all the losses into account in the intake manifold of the real engine; also, the three versions are optimised taking into account the other operating condition of the engine as well, that is with a revolution speed of 1800 RPM. Indeed, by increasing the speed, the pressure of the intake air decreases, leading to a lower volumetric efficiency, since the losses through a restriction are proportional to the square of the flow speed, which is, by turn, proportional to engine revolution speed. Of course, the difference between the three versions can be attributed to the fact that, from the first to the last version, the

losses introduced in the intake manifold decrease progressively. This is because both the diameter of the introduced restriction and the corresponding flow discharge coefficient, as well as the variation in the discharge coefficient of the intake valve, increase. As previously mentioned, the third version is characterized by the absence of the restriction and by no reduction in the discharge coefficient.

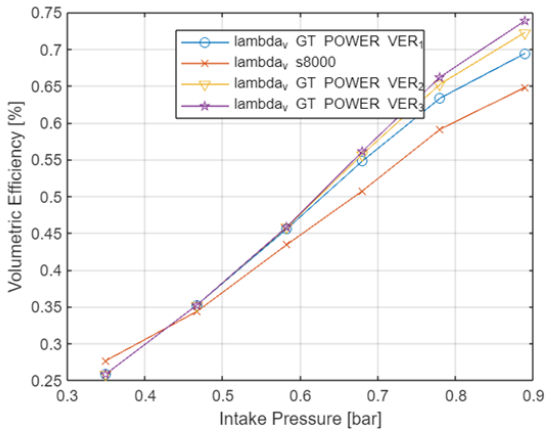

Figure 42 - Volumetric Efficiency For Each Version

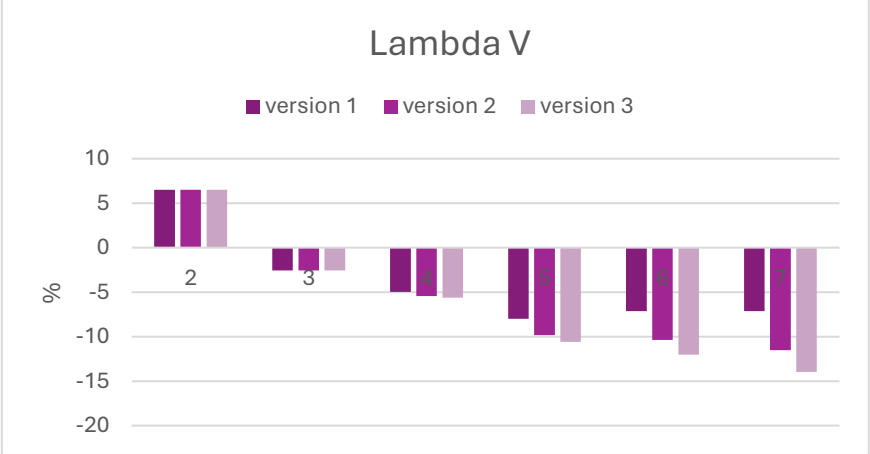

Figure 43 - Volumetric Efficiency Errors For Each Version

4.2.4 Fuel Conversion Efficiency With The Methanol At 1500 RPM

The curves of the fuel conversion efficiency show a similar trend of the one of the real engine, but, also for this parameter, the GT-POWER efficiency is higher than the real one. This is probably due to the assumptions that have been made for the combustion object reported in the previous chapter. However, the obtained values are not so far from the typical fuel conversion efficiency value of SI engines at full load conditions.

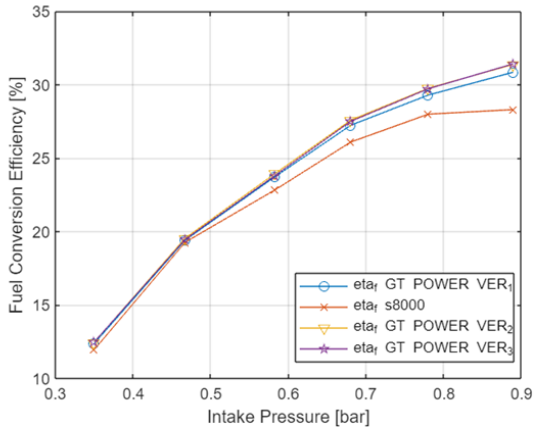

Figure 44 - Fuel Conversion Efficiency For Each Version

4.2.5 Injected Fuel Mass With The Methanol At 1500 RPM

As already appreciated with the Brake Power, the curves have the same trend of the curve of the real engine, but at low load the errors are more significant than the ones at higher load, due to the higher accuracy of the model.

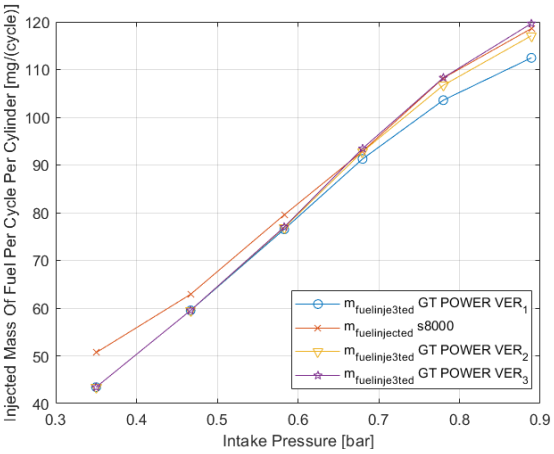

Figure 45 - Injected Fuel Mass For Each Version

From the point of view of the injected fuel mass, the third version is the closest to the real engine behaviour, because of the higher volumetric efficiency.

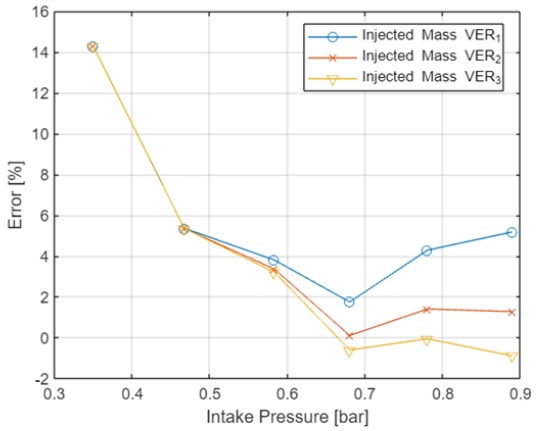

Figure 46 - Injected Fuel Mass Errors For Each Version

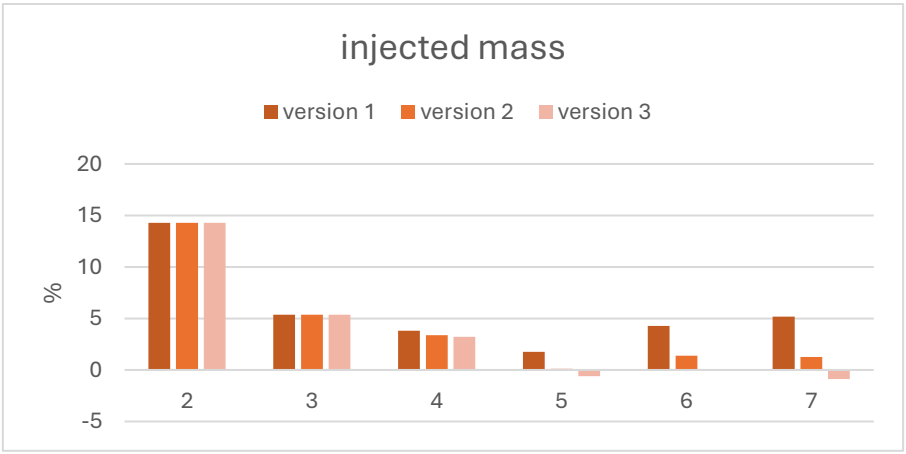

Figure 47 - Injected Fuel Mass Errors For Each Version

4.2.6 Intake Pressure With The Methanol At 1500 RPM

The following figure shows the intake pressure values of the three versions. An analysis of the intake pressure holds a critical relevance, as, of course, a value that turns out to be significantly different from that of the real engine can negatively affect the obtained data and, consequently, the results of the analysis of the three versions. This is because different intake pressure values result in different densities of the intake air mass, and, consequently, of the injected fuel mass and the obtained power.

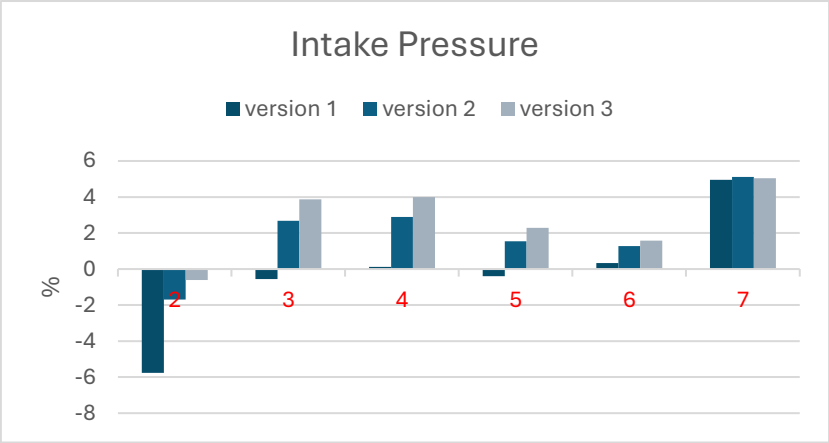

Figure 48 - Intake Pressure Errors For Each Version

These values refer to the pressure downstream to the restriction and, therefore, in the intake port. As can be appreciated from the figure, the errors in the intake pressure are lower for version one, excluding the first case where high errors are expected. These errors for all versions were accepted during the optimization procedure so to achieve a behaviour of the model as close as possible to the real one.

4.2.7 Brake Power With The Methanol At 1800 RPM

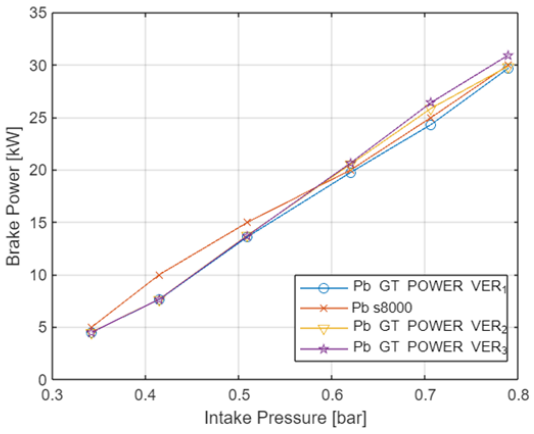

Figure 49 - Brake Power For Each Version

As can be observed from the figure, at low loads the error is quite high due to the fact that the friction model is calibrated for 1500 RPM and, as a result, by increasing the revolution speed of the engine, the engine frictions

increase as well, leading to a lower Brake Power at lower load. However, as the load increases, the error becomes progressively smaller, as evidenced by the trend of the curves for the three versions, which increasingly align with the one of the real engine.

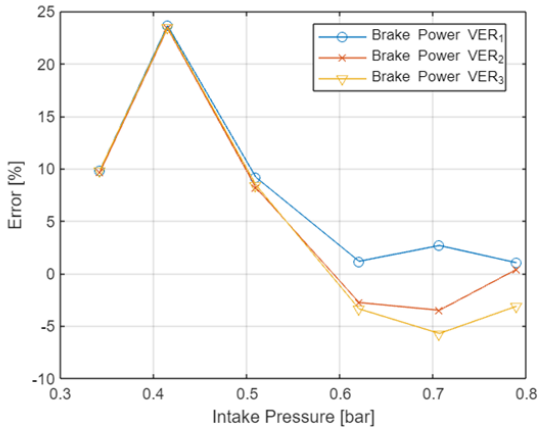

Figure 50 - Brake Power Errors For Each Version

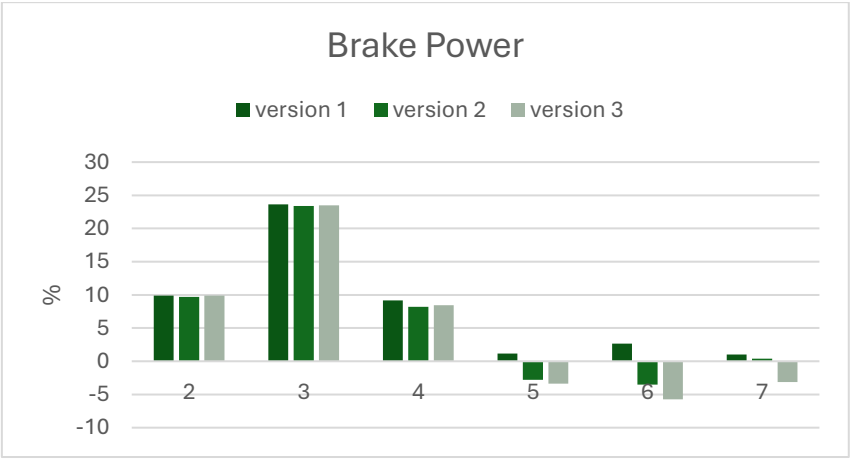

Figure 51 - Brake Power Errors For Each Version

From the Brake Power point of view, the first version seems to perform better for both the two operating conditions. However, it will be demonstrated that this version does not work appropriately for the ethanol.

4.2.8 Brake Specific Fuel Consumption With The Methanol At 1800 RPM

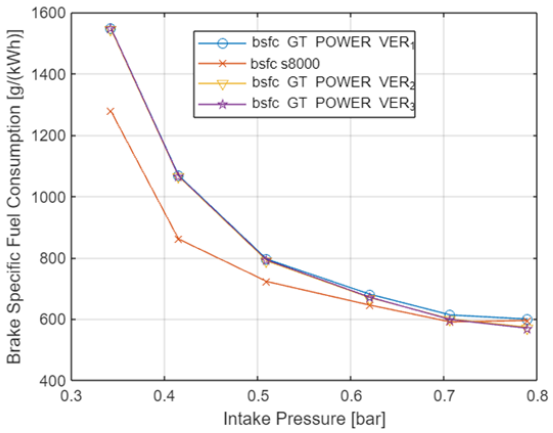

Figure 52 - Brake Specific Fuel Conversion For Each Version

As already established from the analysis of the brake power, at low load the frictions of the model are higher than the real one, since, in order to implement a predictive model, the friction model is the Chen-Flynn one, which limits the two coefficients that take the contribution of the engine speed to the friction mean effective pressure into account. In fact, a lower value of these two coefficients could lead to a better behaviour of both the brake power and BSFC curves; however, this overcomes the limits set by the Chen-Flynn model.

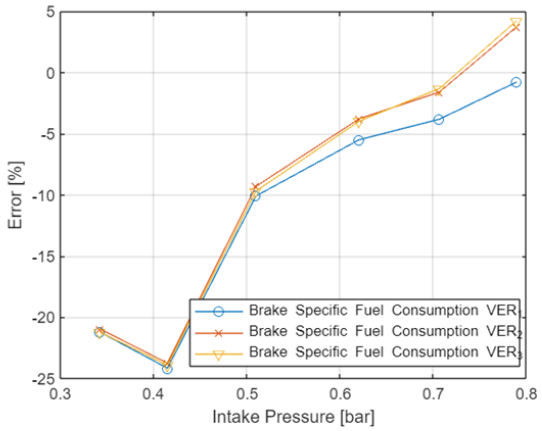

Figure 53 - Brake Specific Fuel Conversion Errors For Each Version

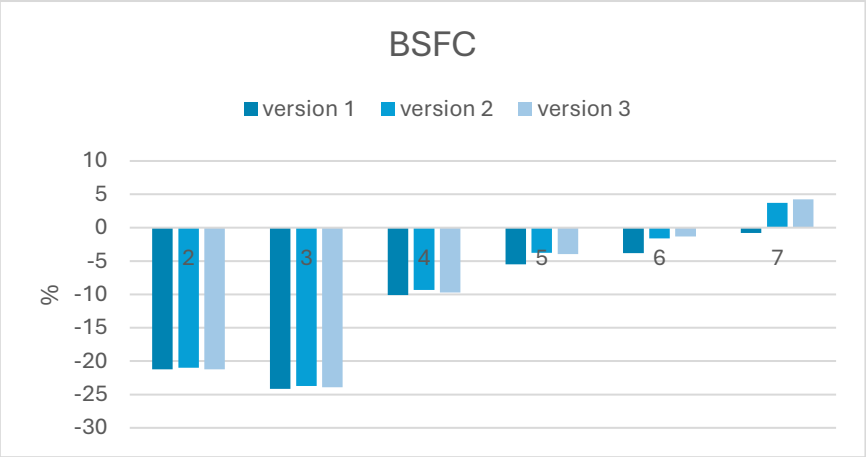

Figure 54 - Brake Specific Fuel Conversion Errors For Each Version

4.2.9 Volumetric Efficiency With The Methanol At 1800 RPM

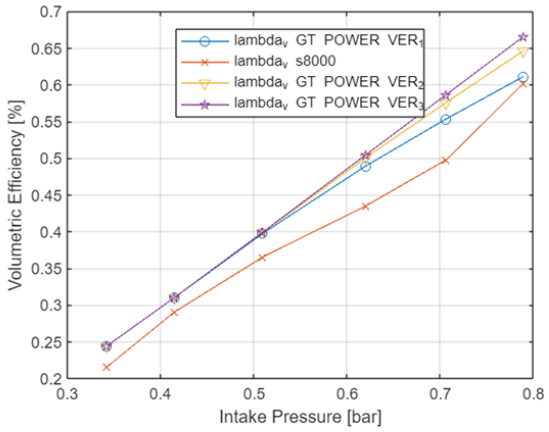

Figure 55 - Volumetric Efficiency For Each Version

Also for this operating condition, the volumetric efficiency obtained by the three versions of the model is much higher than the one of the real engine, since all the real engine losses during the intake phase are not easy to be taken into account. Of course, the difference between the curves could also be due to the approximation made during the implementation of the model and to possible imperfections during the measurement of the data of the real engine.

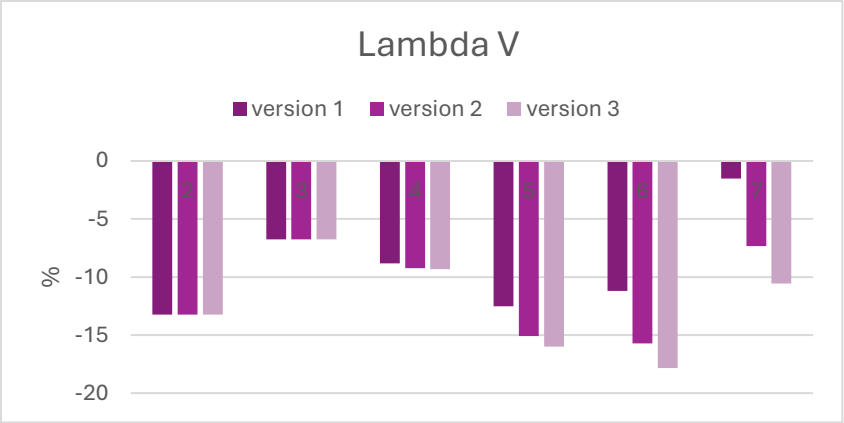

Figure 56 - Volumetric Efficiency Errors For Each Version

4.2.10 Fuel Conversion Efficiency With The Methanol At 1800 RPM

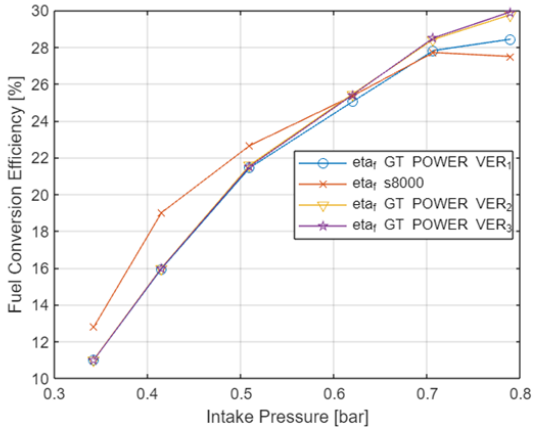

Figure 57 - Fuel Conversion Efficiency For Each Version

The same errors analysed with the brake power and the BSFC at low load can be also appreciated by analysing the figure above, in which, for the same reason, the errors between the obtained curves and the red one tend to be progressively lower as the load increases.

4.2.11 Injected Fuel Mass With The Methanol At 1800 RPM

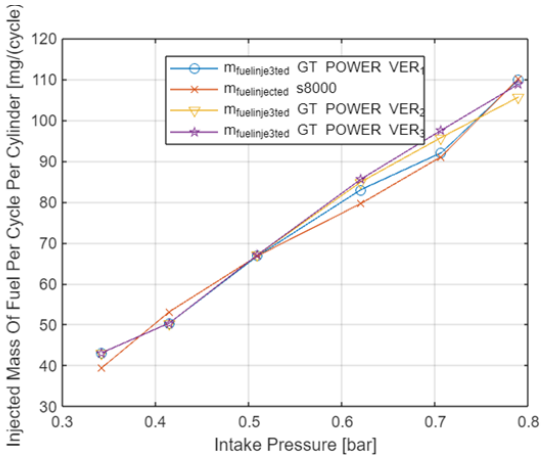

Figure 58 - Injected Fuel Mass For Each Version

For what regards the injected fuel mass, all three versions tend to closely follow the curve of the real engine, as can be understood by analysing the following figure and table where the errors are reported. In this case as well, version one of the model better follows the behaviour of the real engine. However, as previously mentioned, this version unfortunately does not perform well with ethanol.

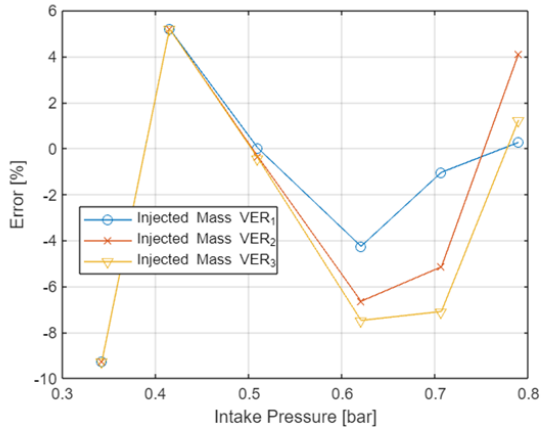

Figure 59 - Injected Fuel Mass Errors For Each Version

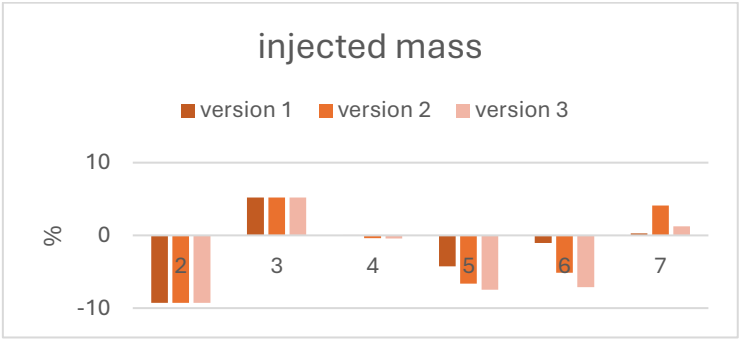

Figure 60 - Injected Fuel Mass Errors For Each Version

4.3 Comparison Between The Versions With Ethanol

In the following chapter, the same analysis conducted with methanol has been performed with ethanol as well for both rotational speeds. Therefore, the graphs concerning the Brake Power, the Brake Specific Fuel Consumption, the Volumetric Efficiency, the fuel conversion efficiency and the Injected fuel mass will show the difference between the three versions and the real engine.

4.3.1 Brake Power For With Ethanol At 1500 RPM

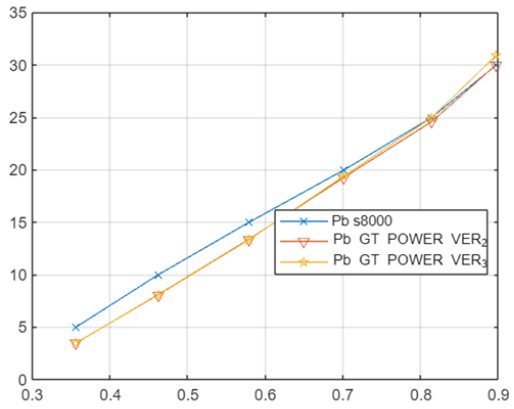

Figure 61 - Brake Power For Each Version

As can be observed in the figure, only versions two and three of the model were analysed. This is because, as previously mentioned, version one did not function correctly with ethanol. Consequently, the other two versions were implemented to sacrifice some performance with methanol but gain with ethanol.

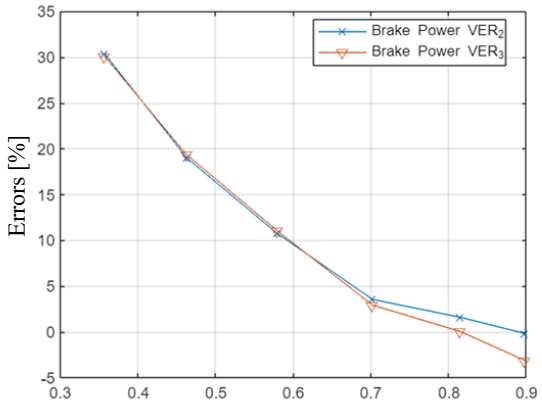

Figure 62 - Brake Power Errors For Each Version

Regarding the errors, at low loads, these errors are quite significant, both because the friction model was calibrated with methanol and also due to the lower accuracy of the models at low loads. However, as the load increases, the error decreases, reaching an almost negligible error at full load with the second version.

This can be better understood by analysing the following figure, where the two versions are represented by two different colours. The darkest colour represents the second version, while lighter shade represents the third version.

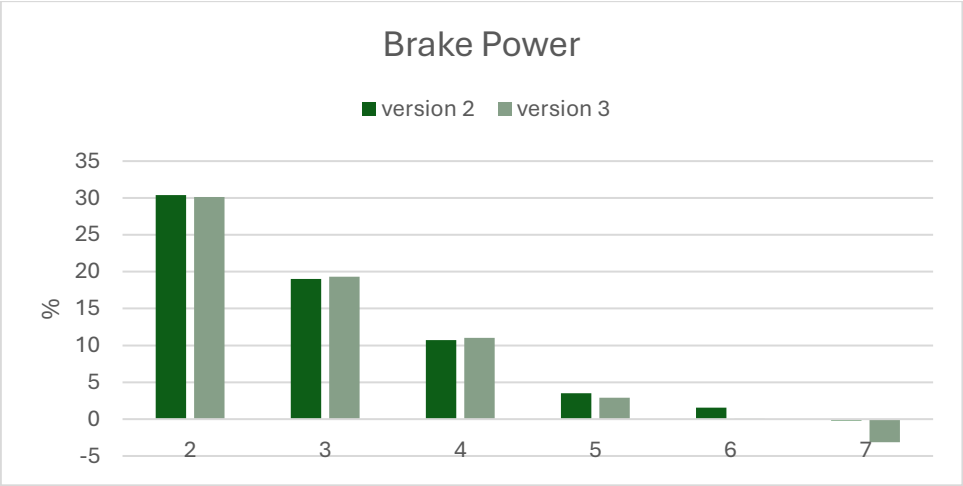

Figure 63 - Brake Power Errors For Each Version

4.3.2 Brake Specific Fuel Consumption With The Ethanol At 1500 RPM

As regards the Brake Specific Fuel Consumption, also in this case the curves of the two versions show almost the same behaviour, which is not so far from the real one. So, both of the versions of the model can be used as a predictive model of the real engine.

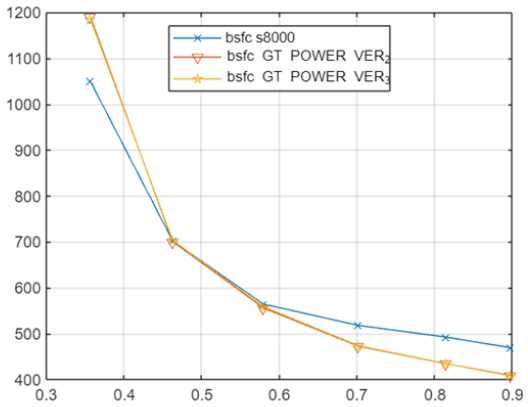

Figure 64 - Brake Specific Fuel Conversion For Each Version

By analysing the errors, it can be observed that the implemented friction model, despite it being different for the two versions, allows for errors in the brake specific fuel consumption (BSFC) that are not too distant from one another. On the other hand, the relative error with the BSFC of the real engine is significant high, as expected, since, as already mentioned, at low load the frictions are higher than the real ones. Instead, at high load the errors are high probably due to a non-correct measurement of the fuel consumption, since, as it will be demonstrated in the subsequent chapter concerning the injected fuel mass, the real engine is consuming more than it should under these operating conditions and with these air-fuel ratios and combustion efficiencies.

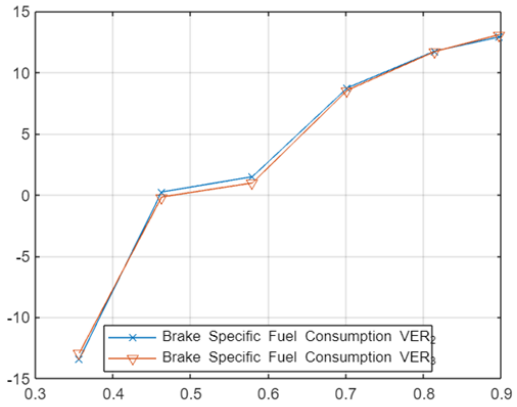

Figure 65 - Brake Specific Fuel Conversion Errors For Each Version

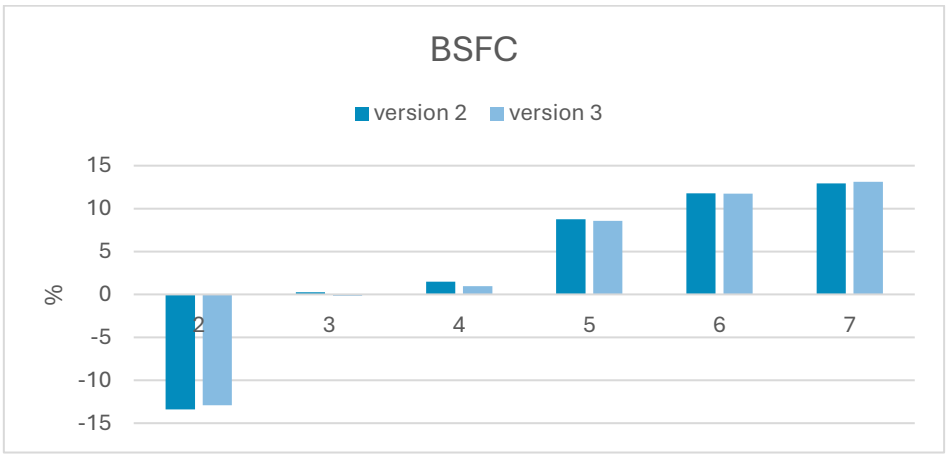

Figure 66 - Brake Specific Fuel Conversion Errors For Each Version

4.3.3 Volumetric Efficiency With The Ethanol At 1500 RPM

The volumetric efficiency of both versions is lower than that of the actual engine. This discrepancy primarily arises from the difficulty in accurately accounting for all the losses occurring in the intake manifold of the real engine. Additionally, the two versions have been optimized considering both the operating conditions of the engine.

The distinction between the two versions can be attributed to the progressive reduction in losses within the intake manifold. This reduction is a result of an increase in the diameter of the introduced restriction, the corresponding flow discharge coefficient and the variation in the discharge coefficient of the intake valve. As previously stated, the third version is characterized by the elimination of the restriction and the absence of any reduction in the discharge coefficient.

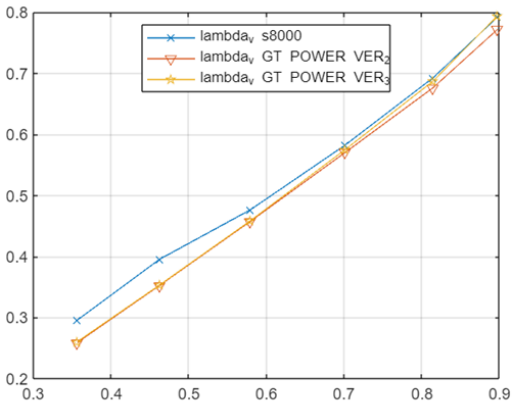

Figure 67 - Volumetric Efficiency For Each Version

At low load, the errors of the two versions can be considered more or less the same, while for increasing loads the curve that is relative to the third version seems to be closer to the curve of the s8000 engine: in fact, at full load, the relative error tends to zero.

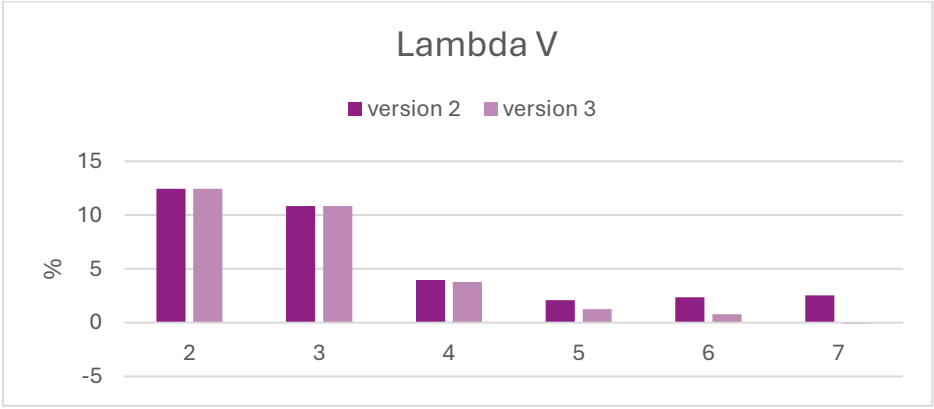

Figure 68 - Volumetric Efficiency Errors For Each Version

4.3.4 Fuel Conversion Efficiency With The Ethanol At 1500 RPM

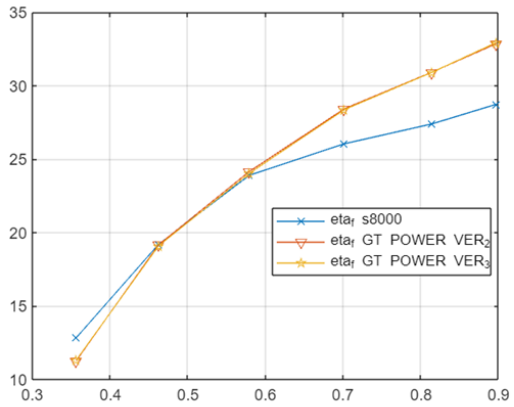

Figure 69 - Fuel Conversion Efficiency For Each Version

The behaviour of the fuel conversion efficiency curves for the two versions is as expected, exactly opposite to that of the BSFC in terms of error relatively to the real engine curve. Therefore, considering the absolute value of the errors, these errors can be attributed to the same reasons as those of the BSFC. So, at low load, these errors are due to the friction model, while at high load due to an incorrect measurement of the fuel consumption.

4.2.5 Injected Fuel Mass With The Ethanol At 1500 RPM

As it can be appreciated analysing the following figure, the curves have the same trend of the curve of the real engine, but for both low load and high load the error values are significantly high. Orientatively, as seen with the other plots, the behaviour of the two models is quite the same.

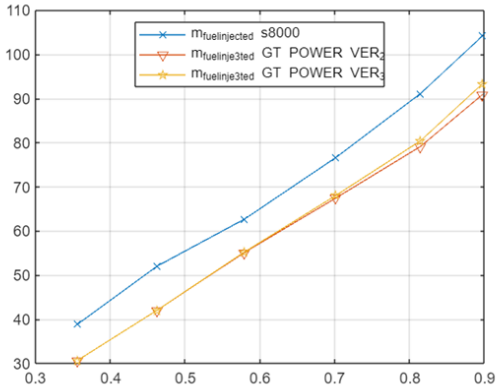

Figure 70 - Injected Fuel Mass For Each Version

These errors can be better noticed from the following figure and table.

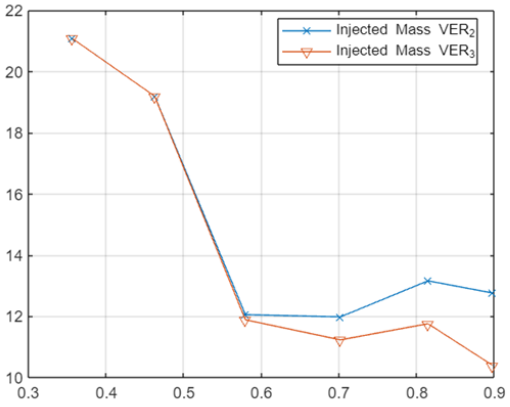

Figure 71 - Injected Fuel Mass Errors For Each Version

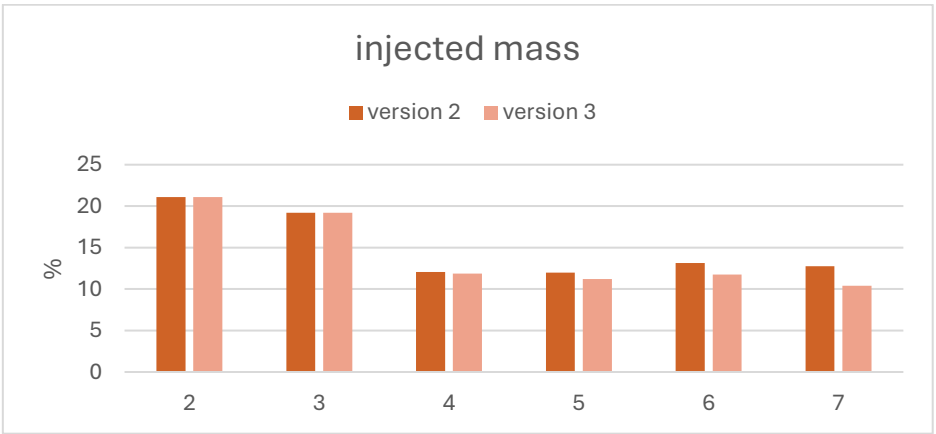

Figure 72 - Injected Fuel Mass Errors For Each Version

As previously mentioned, the substantial difference between the behaviour of the implemented models and the real engine may be due to incorrect measurement of the real engine's fuel consumption. This is because, as stated in the chapter concerning the data acquired from the company, the consumption measurements were based on weighing the fuel tank over a certain period to obtain the fuel flow rate. This procedure was carried out for all loads. To avoid considering the transient phase during measurement, that is when the load increases by one step, the operator waited a certain number of seconds before starting the measurement. However, mainly with ethanol, as seen in the *figure 33* and in the *figure 34*, it is clear that the steady-state phase of the engine, when the measurements were taken, is significantly shorter than the transient phase, or almost imperceptible. Therefore, these small imperfections strongly affect the results that have been obtained with the software, as it always operates in steady-state conditions. Additionally, by observing the same figures, it can be verified that the engine's rotational speed is not perfectly equal to the desired speed; instead, it is slightly lower due to the transient phase caused by the load change. Knowing that the injected mass is inversely proportional to the engine's rotational speed, if the latter is lower, then this implies that the mass is greater than that obtained from GT-POWER, as the software always operates at a constant speed. To verify this statement, a simple calculation was performed, in particular computing the injected fuel mass as a function of power, considering only the fuel conversion efficiency, and then, in the subsequent two calculations, considering the error of the volumetric efficiency with respect to the real engine as well; finally, the error of the brake power with respect to the real engine one was introduced in the calculation as well. The computation was conducted with the following formulas:

$$m_{f\,CALC} = \frac{P_b}{\eta_f \cdot \frac{n}{m} \cdot LHV}$$

$$m_{f\,CALC\,2} = \frac{P_b}{\eta_f \cdot \frac{n}{m} \cdot LHV} \cdot error_1$$

$$m_{f\,CALC\,3} = \frac{P_b}{\eta_f \cdot \frac{n}{m} \cdot LHV} \cdot error_2$$

where P_b is the brake power, η_f is the fuel conversion efficiency, n is the engine speed, $m = 2$ for the four stroke engines, LHV is the lower heating value of the fuel, $error_1$ and $error_2$ are the errors with respect to the volumetric efficiency and to the brake power, respectively.

In the following figure these fuel masses are plotted.

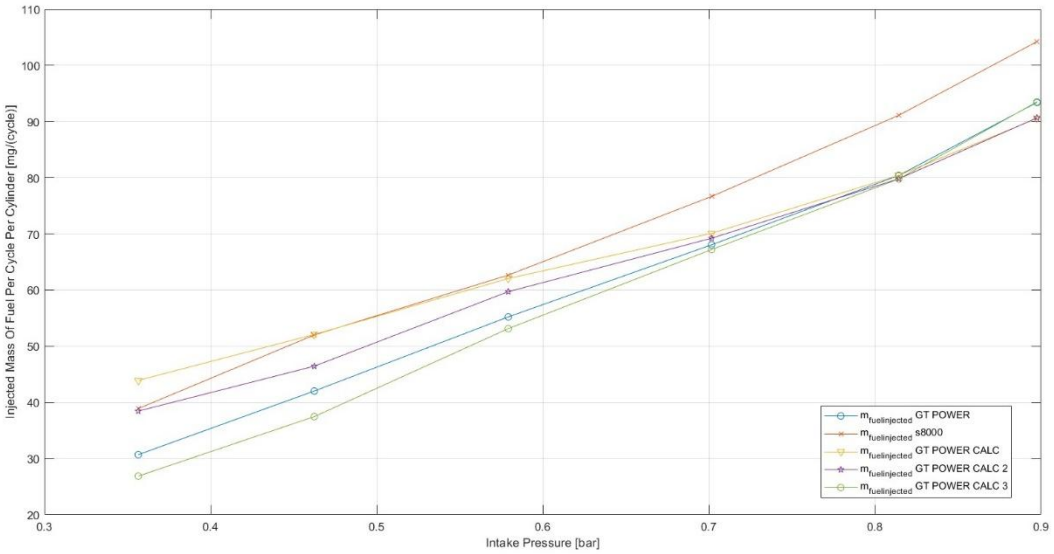

Figure 73 - Comparison Between The Real and The Supposed Injected Fuel Mass

As it can be appreciated from the figure above, the last calculated mass is very close to the one obtained by the third version of the GT-POWER model, as expected.

4.3.6 Intake Pressure With The Ethanol At 1500 RPM

The following figure shows that the intake pressure values of the two versions are very low, so this means that a good optimalisation is done for the ethanol at this operating condition.

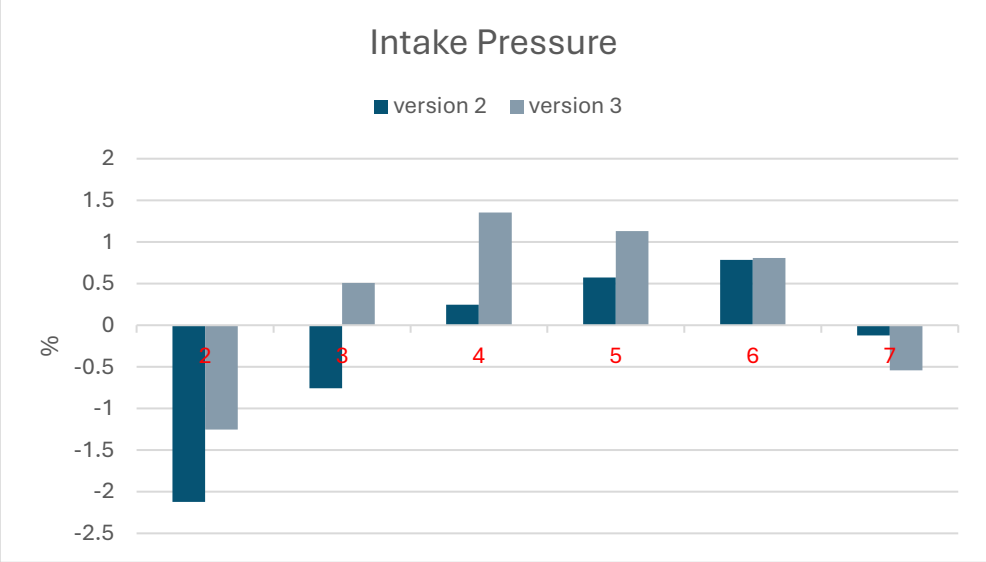

Figure 74 - Intake Pressure Errors For Each Version

4.3.7 Brake Power With The Ethanol At 1800 RPM

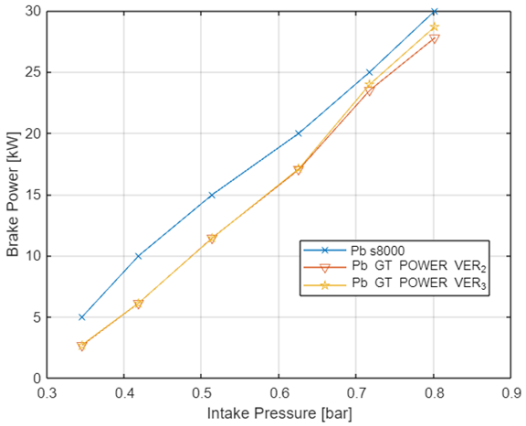

Figure 75 - Brake Power For Each Version

As illustrated in the figure, at low loads the error is relatively high, because the friction model is calibrated for 1500 RPM. Consequently, as the engine speed increases, frictional losses also rise, resulting in lower brake power at reduced loads. However, as the load increases, the error progressively decreases, as demonstrated by the convergence of the curves for both versions, which increasingly align with the actual engine behaviour.

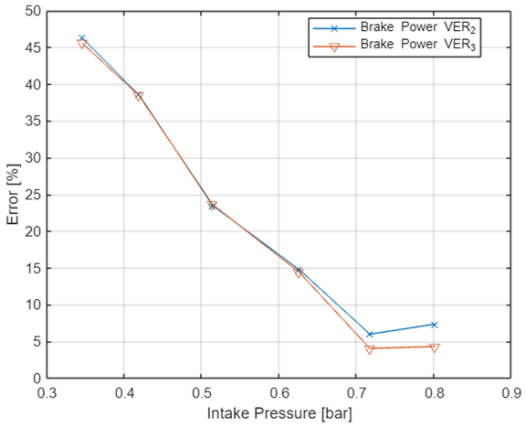

Figure 76 - Brake Power Errors For Each Version

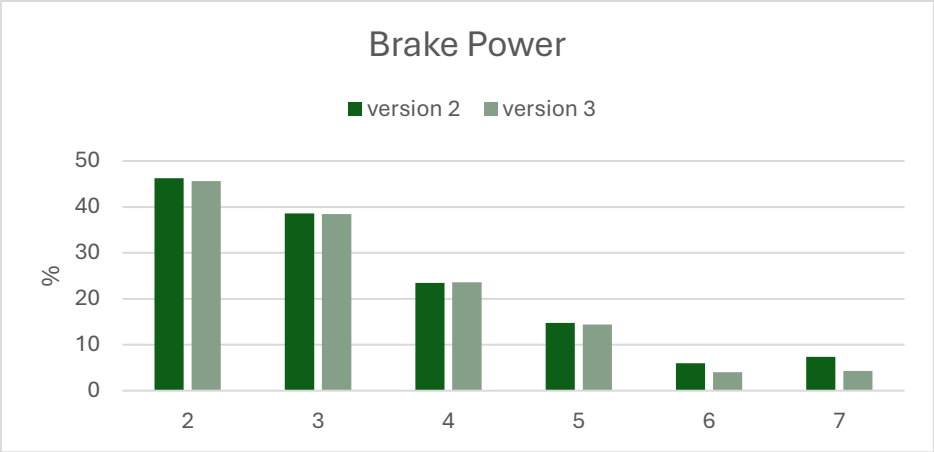

Figure 77 - Brake Power Errors For Each Version

4.3.8 Brake Specific Fuel Consumption With The Ethanol At 1800 RPM

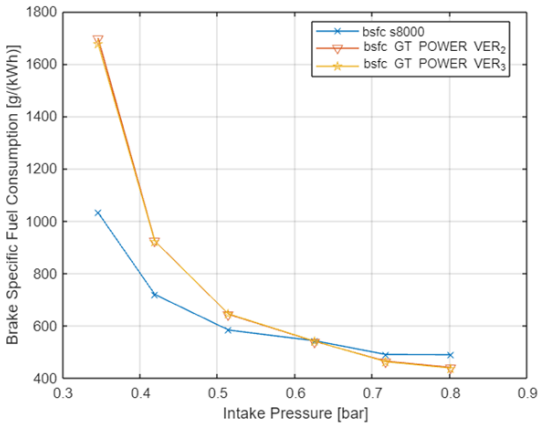

Figure 78 - Brake Specific Fuel Consumption For Each Version

As previously understood when dealing with the brake power, the model exhibits higher friction at low loads compared to real-world conditions. This discrepancy arises because, as discussed in the previous chapter, the friction model employed in the predictive framework is the Chen-Flynn model, which constrains the two coefficients that account for the influence of engine speed on the friction mean effective pressure. A reduction in these coefficients could potentially improve the accuracy of both the brake power and the brake-specific fuel consumption (BSFC) curves. However, such adjustments would exceed the limitations imposed by the Chen-Flynn model. Conversely, at high loads, the errors are likely significant due to an inaccurate measurement of fuel consumption. As will be demonstrated in the following chapter on injected fuel mass, the

real engine consumes more fuel than expected under these operating conditions, given the corresponding air-fuel ratios and combustion efficiencies.

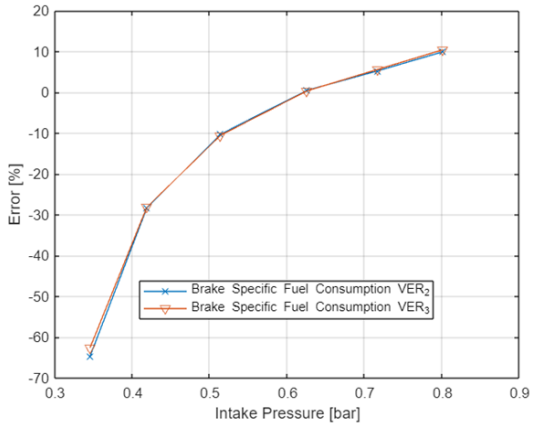

Figure 79 - Brake Specific Fuel Consumption Errors For Each Version

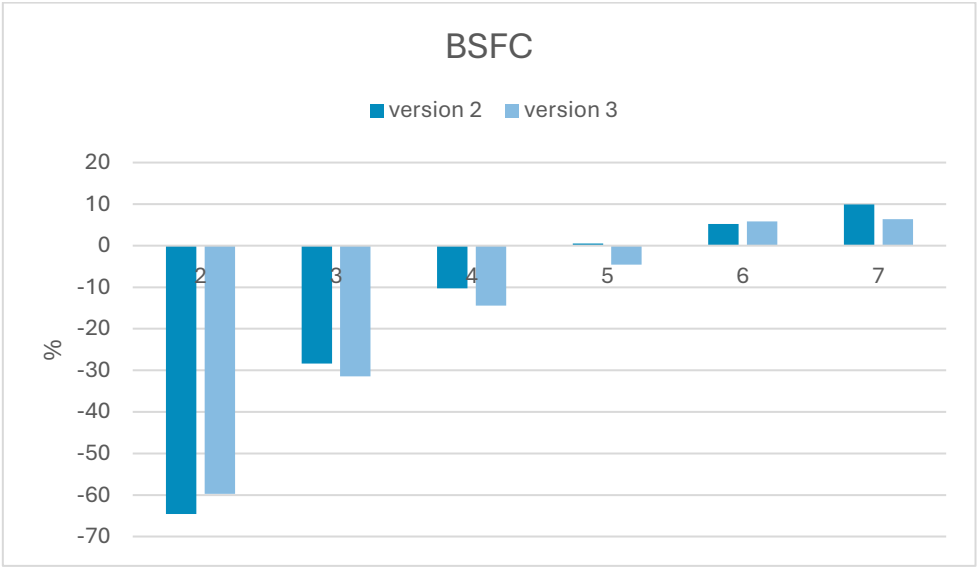

Figure 80 - Brake Specific Fuel Consumption Errors For Each Version

4.3.9 Volumetric Efficiency With The Ethanol At 1800 RPM

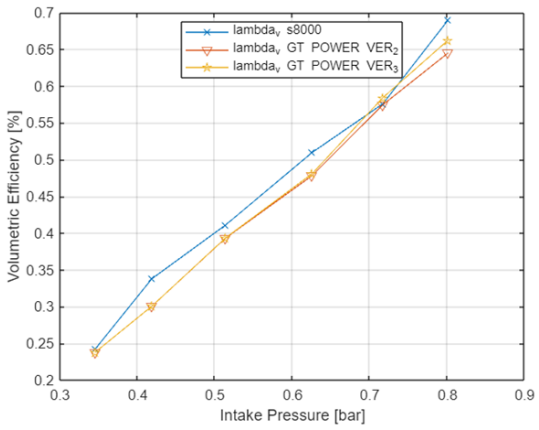

Figure 81 - Volumetric Efficiency For Each Version

The volumetric efficiency of both versions is lower than that of the actual engine, primarily due to the challenges in accurately accounting for all losses occurring in the real engine's intake manifold. Moreover, both versions have been optimized while considering the engine's operating conditions. The difference between the two versions stems from the progressive reduction of intake manifold losses; this reduction is achieved by increasing the diameter of the introduced restriction, improving the corresponding flow discharge coefficient, and modifying the intake valve's discharge coefficient. As previously mentioned, the third version is distinguished by the complete removal of the restriction and the absence of any reduction in the discharge coefficient.

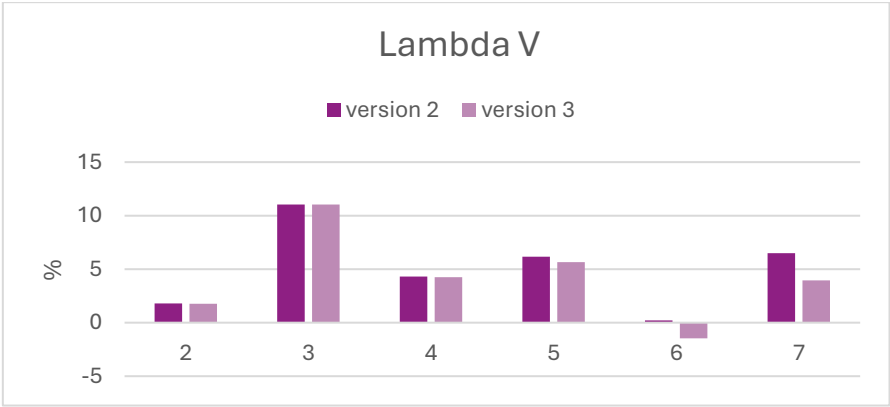

Figure 82 - Volumetric Efficiency Errors For Each Version

4.3.10 Fuel Conversion Efficiency With The Methanol At 1800 RPM

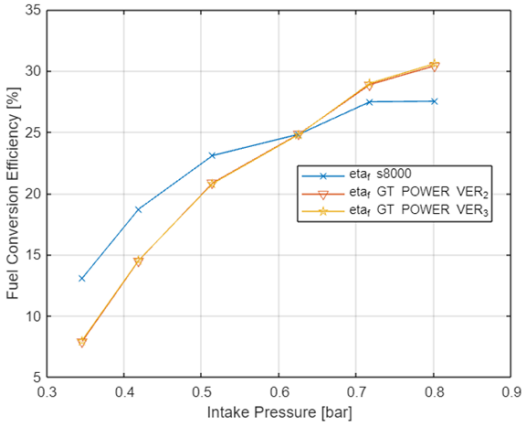

Figure 83 - Fuel Conversion Efficiency For Each Version

The same errors at low load, analysed with the brake power and the BSFC, can also be appreciated by analysing the figure above, where, for the same reason, the errors between the obtained curves and the red one tend to be lower and lower by increasing the load.

4.3.11 Injected Fue Mass With The Methanol At 1800 RPM

As illustrated in the following figure, the curves exhibit the same overall trend as that of the real engine. However, at both low and high loads, the error values are significantly high. Generally, as observed in other plots, the behaviours of the two models remain quite similar.

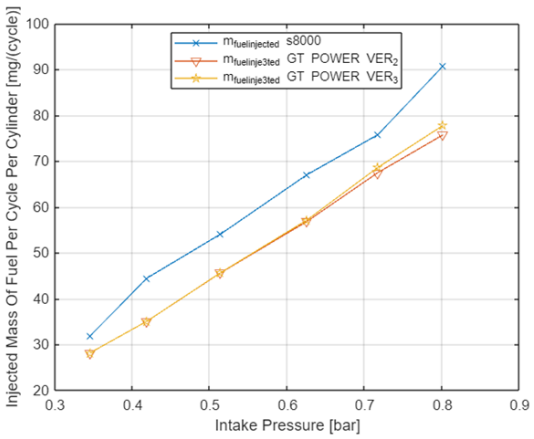

Figure 84 - Injected Fuel Mass For Each Version

The errors of the injected mass can be better appreciated by analysing the following figure and table.

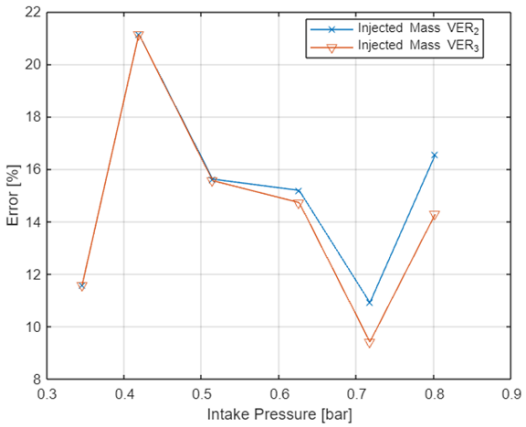

Figure 85 - Injected Fuel Mass Errors For Each Version

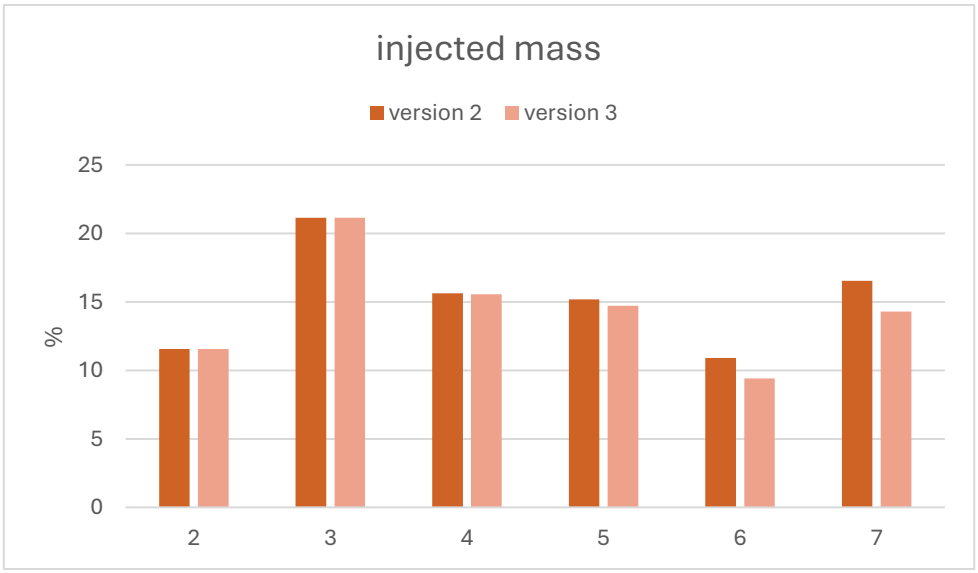

Figure 86 - Injected Fuel Mass Errors For Each Version

As previously discussed, a key factor contributing to the discrepancy between the implemented models and the real engine is likely the inaccurate measurement of the real engine's fuel consumption. According to the chapter on data acquired from the company, fuel consumption measurements were obtained by weighing the fuel tank over a set period to determine the fuel flow rate. This procedure was conducted for all load conditions. To minimize the influence of transient phases, i.e., the period when the load increases by one step, the operator waited a predetermined number of seconds before beginning the measurement. However, particularly in the case of ethanol, as shown in the *figure 34*, it is evident that the steady-state phase, during which measurements were taken, is significantly shorter than the transient phase or almost imperceptible. These minor inaccuracies can have a considerable impact on the software's results, as the model operates strictly under steady-state conditions. Furthermore, the same figure reveals that the engine's rotational speed does not precisely match the desired speed but is, instead, slightly lower due to the transient phase induced by load changes. Given that the injected fuel mass is inversely proportional to engine speed, a lower rotational speed results in a greater injected mass compared to the values predicted by GT-POWER, where the system always operates at a constant speed.

To validate this hypothesis, a simple calculation was performed, determining the injected fuel mass as a function of power. Initially, only the fuel conversion efficiency was considered. Subsequently, two additional calculations were carried out: one incorporating the error in the volumetric efficiency relatively to the real engine and another accounting for the error in the brake power relatively to the real engine.

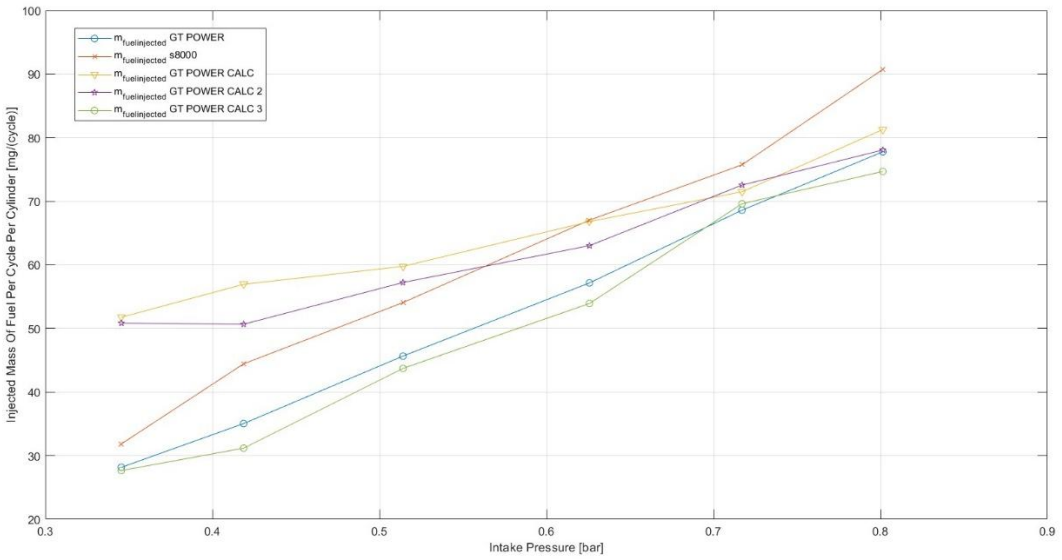

Figure 87 - Comparison Between The Real and The Supposed Injected Fuel Mass

4.4 Final Version

The final version that was chosen is the third one, because it functions correctly for both fuels. Compared to the second version, this model does not present any restriction in the intake system and does not change the flow discharge coefficient of the intake valve from the default value, resulting in an even more predictive model. In addition to this, it is important to specify that some figures do not have any value, since they cannot be divulgated.

4.4.1 Performance and Emissions at 1500 RPM

The following figures represent the results in terms of performance and emissions of the two fuels at an engine speed equal to 1500 RPM.

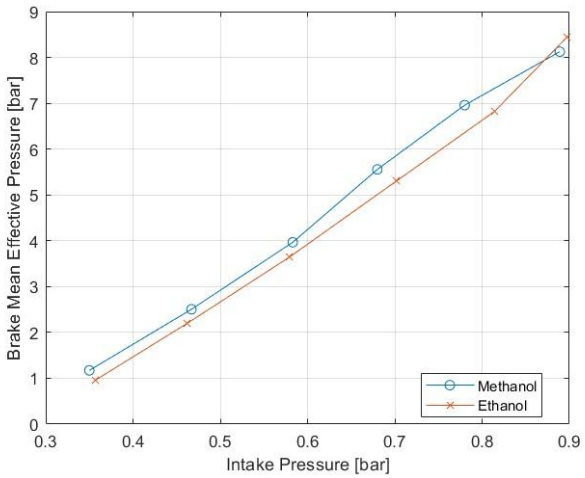

Figure 88 - Brake Mean Effective Pressure For Both The Fuels

The figure above shows the brake mean effective pressure for both the fuels. As can be observed, the load for each case is slightly different, which obviously affects the brake mean effective pressure values for the two fuels at each load. With an increasing intake pressure, more air, and consequently more fuel, can be expected, resulting in a higher power output. The reason why methanol exhibits a slightly higher brake mean effective pressure compared to ethanol can be attributed to various factors, such as a different spark advance or simply different dosages for each load. In the initial analysis, this may be due to a higher ratio of lower heating value to stoichiometric air-fuel ratio for methanol compared to ethanol, leading to a higher brake mean effective pressure.

The same trend can be observed in the figure below, where the mean maximum pressures are represented.

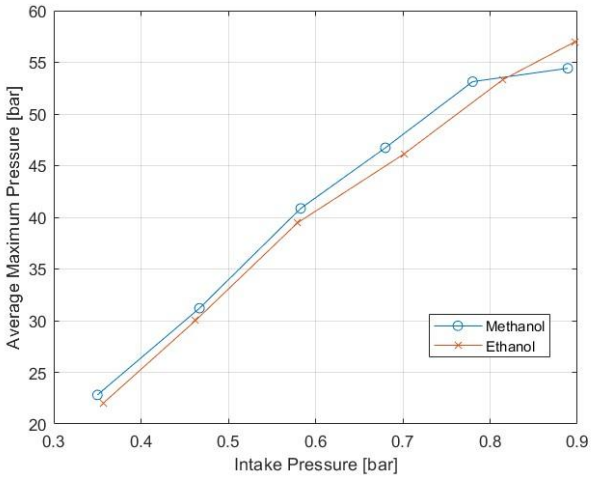

Figure 89 - Averaged Maximum Pressure For Both The Fuels

The figure below shows the combustion efficiencies. These high values can be a result of the assumptions made to create the combustion object used by the software. The lowest value for the ethanol can be attributed to a too high spark advance, which can result in a lower flame propagation and, at the end, in a lower combustion efficiency.

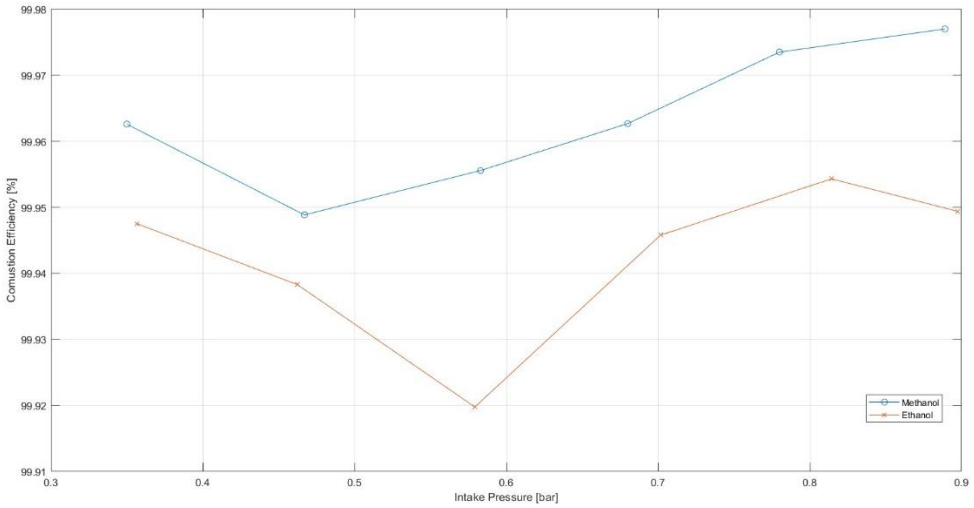

Figure 90 - Combustion Efficiency For Both The Fuels

As previously seen in the preceding chapter, the friction model was calibrated by adjusting the constant and the coefficient that account for the peak cylinder pressure in the Chen-Flynn model. The following figures respectively show the friction values obtained using the MATLAB tool after calibration and the friction mean effective pressure obtained with the software for both fuels. As can be observed, the curves can more or less be superposed.

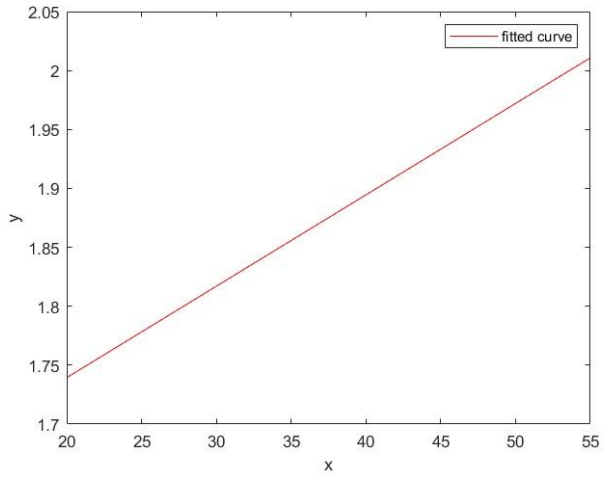

Figure 91 - Friction Values For Each Load In Matlab

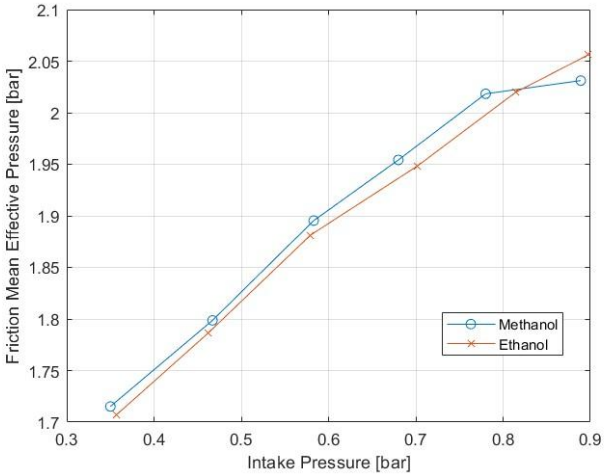

Figure 92 - Friction Mean Effective Pressure For Both The Fuels

The following figures show the mass fraction burned for each load. The trend of the curves for the two fuels is indicatively the same, since it is strictly connected to the values of the spark advance. Indeed, the values of the spark advance are, of course, different for the two fuels, but their trend is quite the same, as can be observed in the *figure 99* and in the *figure 100*. Therefore, the mass fraction burned tends to shift to higher crank angles as the spark advance decreases. In fact, by observing the trend of the spark advance, or MFB50, since they are connected through the equation described in the previous chapter, it can be verified that the MFB50 and the corresponding mass fraction burned curve, related to the maximum load, correspond to a crank angle after

TDC firing. Conversely, at lower loads, characterized by higher spark advances, the MFB50 and the corresponding mass fraction burned curve correspond to a crank angle before TDC.

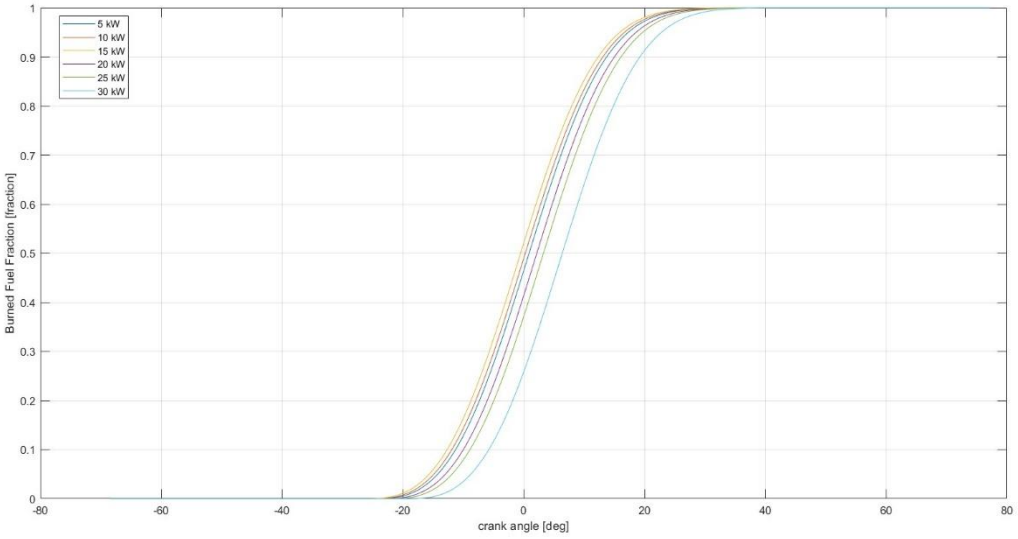

Figure 93 - Burned Fuel Fraction For Each Load With The Methanol

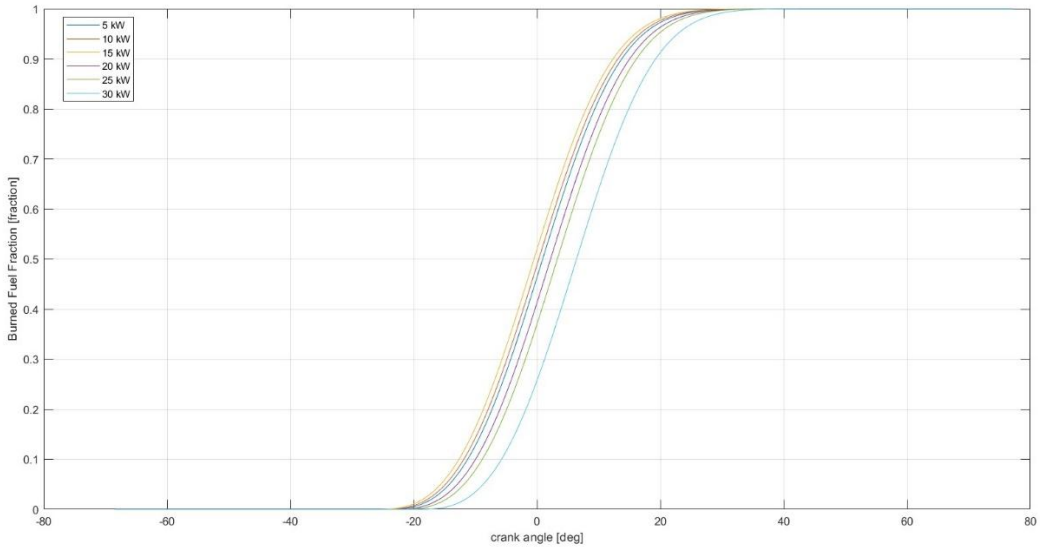

Figure 94 - Burned Fuel Fraction For Each Load With The Ethanol

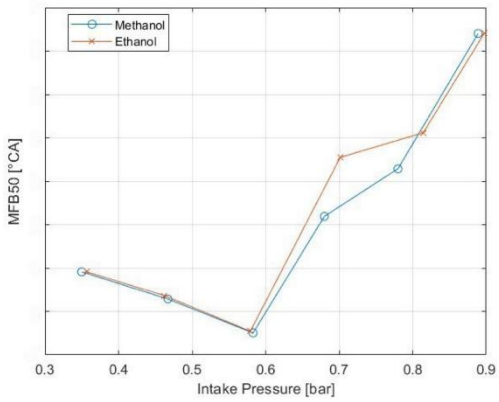

Figure 95 - MFB50 For Both The Fuels

The following figures show the heat transfer coefficient used in the Woschni model for each load. The trend for both the fuels is quite the same, and that is that, by increasing the load, the energy release by the oxidation of the fuel increases as well, resulting in a higher heat transfer through the wall of the combustion chamber. By analysing the temperature in the combustion chamber in the *figure 98*, by increasing the load, the temperature increases until the condition of the maximum value is reached, while, after that peak, the temperature starts to slowly decrease. Indeed, as it can be seen in the figures relative to the heat transfer coefficient, the increment of the heat transfer coefficient is progressively higher passing from 5 kW to 15 kW than from 15 kW to the maximum load.

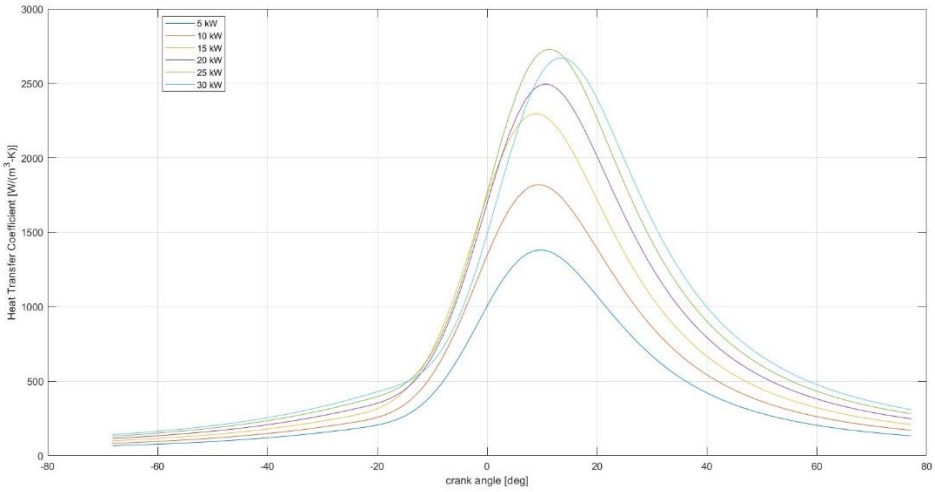

Figure 96 - Heat Transfer Coefficient For Each Load With The Methanol

By analysing the figure relative to the methanol, it can be observed that the previously described trend is interrupted at maximum load. In fact, under these conditions, a lower peak heat transfer coefficient can be observed compared to the previous load. This can be explained by a maximum combustion efficiency, due to a faster flame propagation and, consequently, a more complete oxidation process, and, as mentioned earlier, a slightly lower peak temperature.

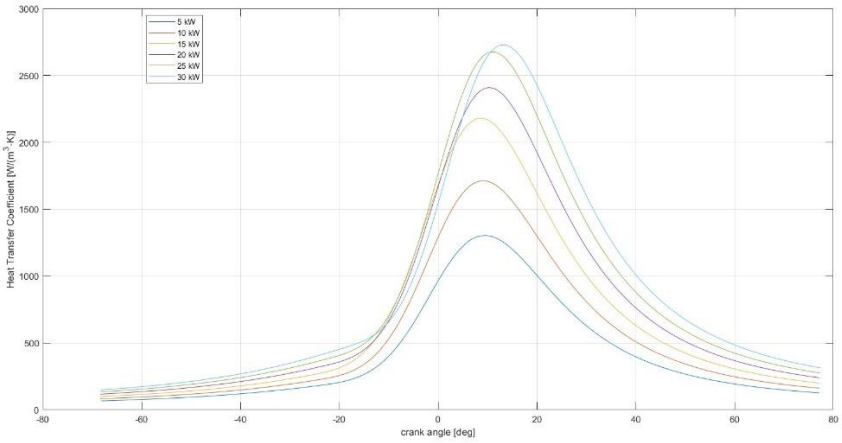

Figure 97 - Heat Transfer Coefficient For Each Load With The Ethanol

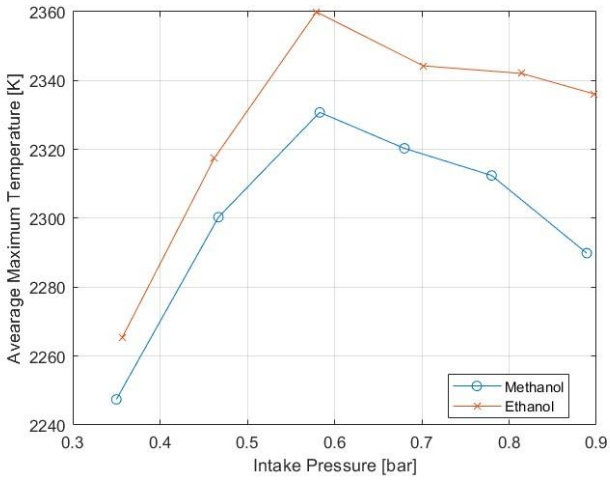

Figure 98 - Maximum Temperature For Both The Fuels

The following figure reports the comparison between the data provided by the company, that is the spark advance, and the relative start of the combustion obtained by the software, which corresponds to the spark advance used as input in GT-POWER. In fact, according to the previously described formula that connects the centre of gravity of the combustion (the desired input of the software) with the spark advance provided by the company, the start of the combustion is assumed to be the crank angle when the mass fraction burned starts to be different from zero. This leads to an overlooking of the potential delays due to the ignition delay of the fuel and possible delays between the command sent by the ECU and the actual spark advance. So, this justifies the small gap between the two curves. In addition, it can also be appreciated from the two figures of the spark advance relative to the two fuels what was previously hypothesized as a justification for the differences between the brake mean effective pressure values for each loads for both fuels. Indeed, a higher spark advance could lead to higher in-cylinder pressure and, as a result, to higher *bmep*.

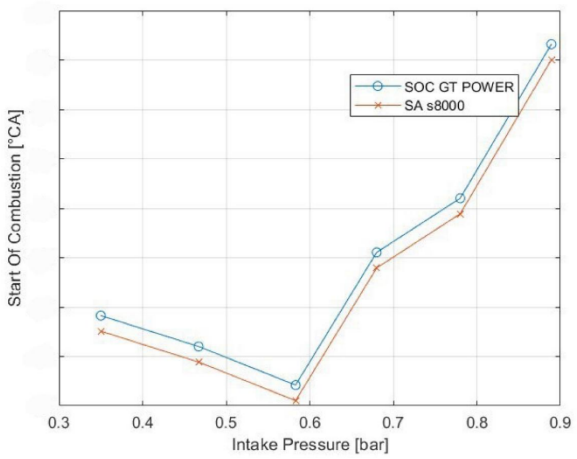

Figure 99 - Spark Advance With The Methanol

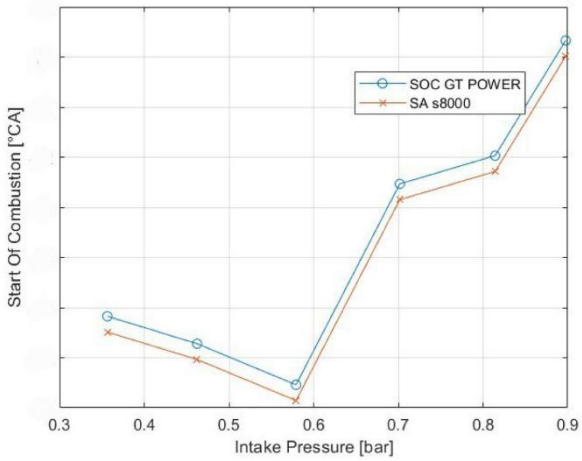

Figure 100 - Spark Advance With The Ethanol

The following figures respectively depict the emissions for methanol and ethanol, as well as the dosage for both fuels as a function of load. Analysing hydrocarbon emissions for both fuels, as the load increases, the throttle valve opens wider, the pumping cycle losses decrease, the air-fuel mixture becomes denser, and the combustion more complete, resulting in lower emissions. The values of these emissions in terms of g/kWh are quite small, as shown in the *figure 103*, where the dosage for each load is consistently lean, resulting in high combustion efficiency.

Analysing CO emissions, these decrease as well with increasing load, due to higher combustion efficiency and because the increasing load leads to a higher air-fuel ratio, resulting in a leaner mixture and thereby increasing the fuel conversion efficiency. For ethanol, this decreasing trend is interrupted in the third and final operating condition, which can be explained by analysing the dosage as a function of load. Under these conditions, there is a slight enrichment of the mixture, resulting in a reduction in the oxidation process efficiency.

A similar trend is observed with CO_2 emissions, which tend to decrease with increasing load. The CO_2 emissions for the two fuels are quite similar for each load, even though methanol should produce less CO_2 since it contains less carbon per unit mass compared to ethanol. This result can be explained by comparing the BSFC for both fuels; for methanol, the BSFC values are significantly higher.

Regarding NOx consumption, the trends are rather peculiar for both fuels, as they are characterized by a decreasing pattern with occasional increases. This can be due to two possible causes: the rise in temperatures, which facilitates the increase in NOx emissions, and a non-constant dosage for the different loads. In addition, the methanol produces lower NOx emissions than the ethanol, since it is characterized by a lower flame temperature and a higher oxygen content in its molecular structure, promoting more uniform combustion.

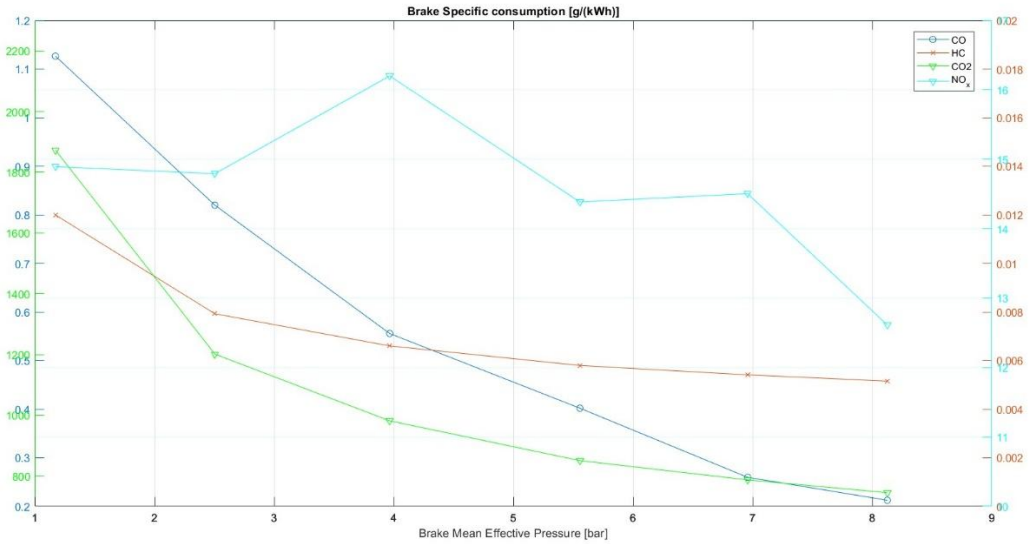

Figure 101 - Emission Values For Each Load With The Methanol

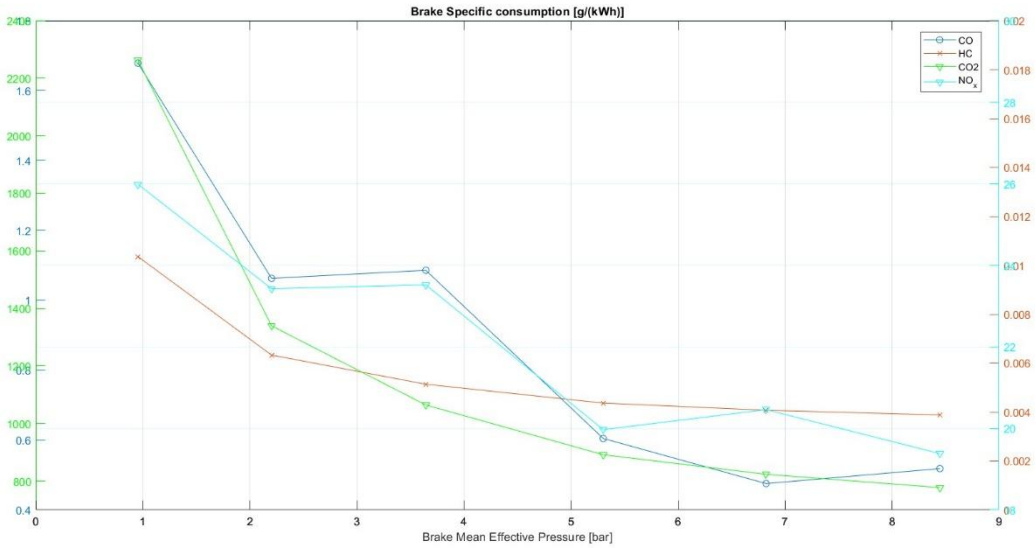

Figure 102 - Emission Values For Each Load With The Ethanol

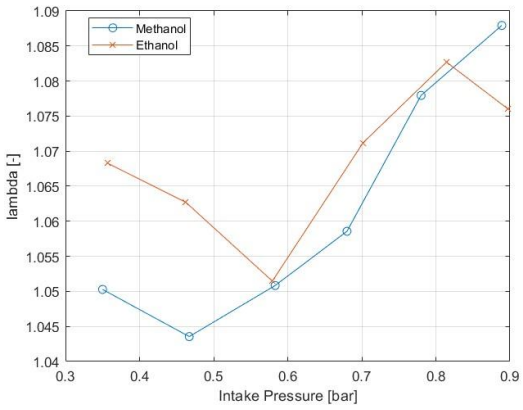

Figure 103 - lambda values For Both The Fuels

By analysing the *figure 103*, which shows lambda as a function of load, a rather peculiar trend can be observed, as one would expect a richer mixture with increasing load, thereby gaining in terms of knock resistance and performance. However, in this case, the mixture becomes increasingly leaner: this may be due to the fact that, by making the mixture leaner, the combustion efficiency increases, and therefore the fuel conversion efficiency improves. Additionally, both methanol and ethanol have high knock resistances, so the choice of a richer charge with increasing load to reduce charge temperatures and the risk of knock is unnecessary given the high resistance of the two fuels. In fact, they have RON values of 106 and 109, respectively.

4.4.2 Performance and Emissions at 1800 RPM

The following figures represent the results in terms of performance and emissions of the two fuels at an engine speed equal to 1800 RPM.

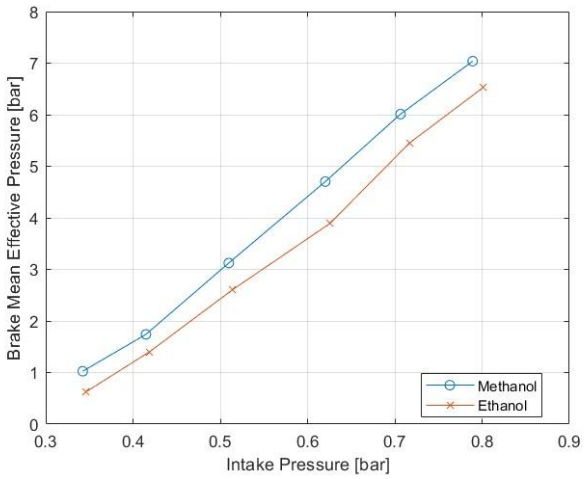

Figure 104 - Brake Mean Effective Pressure For Both The Fuels

The figure above shows the brake mean effective pressure for both the fuels. As can be observed, also at this operating condition the methanol exhibits an higher brake mean effective pressure due to the possible same reasons already analysed for 1500 RPM, that are a different spark advance or simply different dosages for each load, or also a higher ratio of lower heating value to stoichiometric air-fuel ratio for methanol compared to ethanol, leading to a higher brake mean effective pressure. Besides this, another possible reason is the much higher volumetric efficiency obtained with the methanol than the one obtained with the ethanol.

The same trend can be observed in the figure below, where the mean maximum pressures are represented.

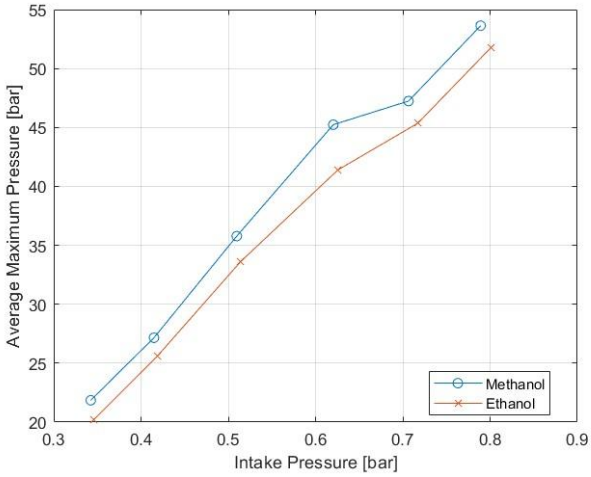

Figure 105 - Averaged Maximum Pressure For Both The Fuels

The figure below shows the combustion efficiencies. These high values can be a result of the assumption done to create the combustion object used by the software. The lowest value, that is, of course, still high for the methanol, can be due to a rich air-fuel ratio, which can result in a lower flame propagation and, at the end, in a lower combustion efficiency.

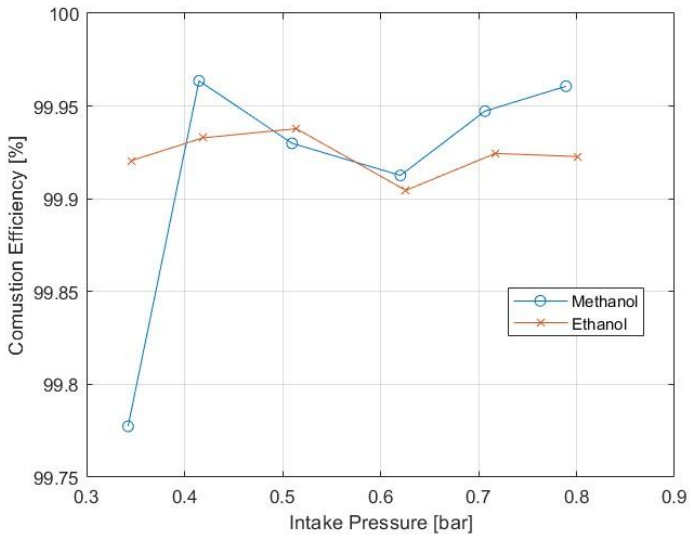

Figure 106 - Combustion Efficiency For Both The Fuels

As previously seen in the preceding chapter, the friction model was calibrated by adjusting the constant and the coefficient that accounts for the peak cylinder pressure in the Chen-Flynn model. The following figures respectively show the friction values obtained using the MATLAB tool after calibration and the friction mean effective pressure obtained with the software for both fuels. As can be observed, also at this engine speed the curves show the same trend, as expected.

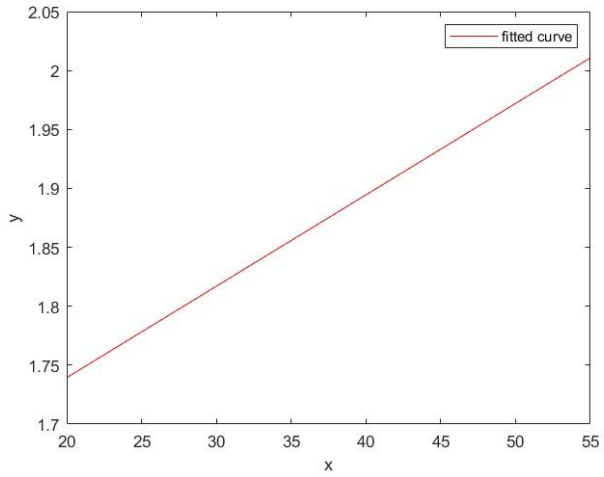

Figure 107 - Friction Values For Each Load In Matlab

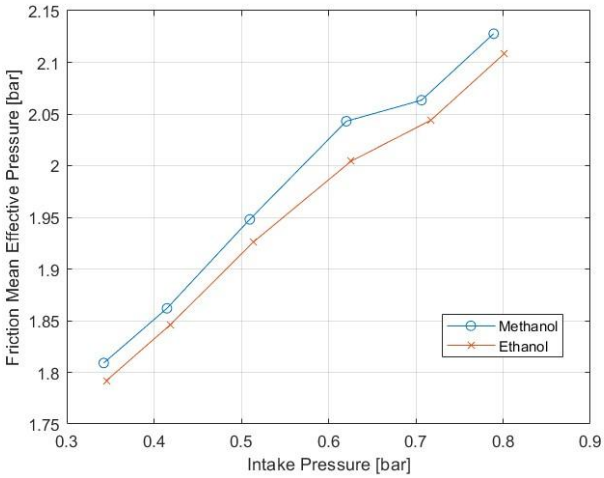

Figure 108 - Friction Mean Effective Pressure For Both The Fuels

The subsequent figures illustrate the mass fraction burned for each load. The curve trends for the two fuels are approximately the same, as they are closely linked to the values of the spark advance. Although the spark advance values differ for the two fuels, their trends are quite similar, as shown in the *figure 115* and *figure 116*. Consequently, the mass fraction burned tends to shift to higher crank angles as the spark advance decreases. By examining the trend of the spark advance, or MFB50, which are connected through the equation described in the previous chapter, it can be observed that the MFB50 and the corresponding mass fraction burned curve, related to higher spark advance (which means that the combustion is triggered far from the TDC), correspond to a crank angle before the TDC. On the other hand, the ones related to the lower spark advance (that is the combustion is triggered closer to the TDC), correspond to a crank angle before the TDC, but closer to it, or, even, after it.

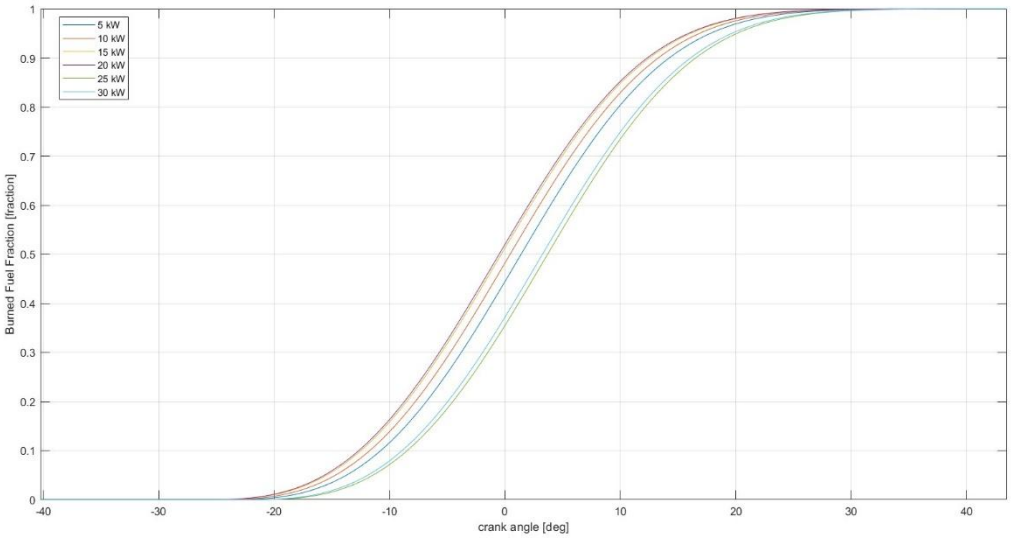

Figure 109 - Burned Fuel Fraction For Each Load With The Methanol

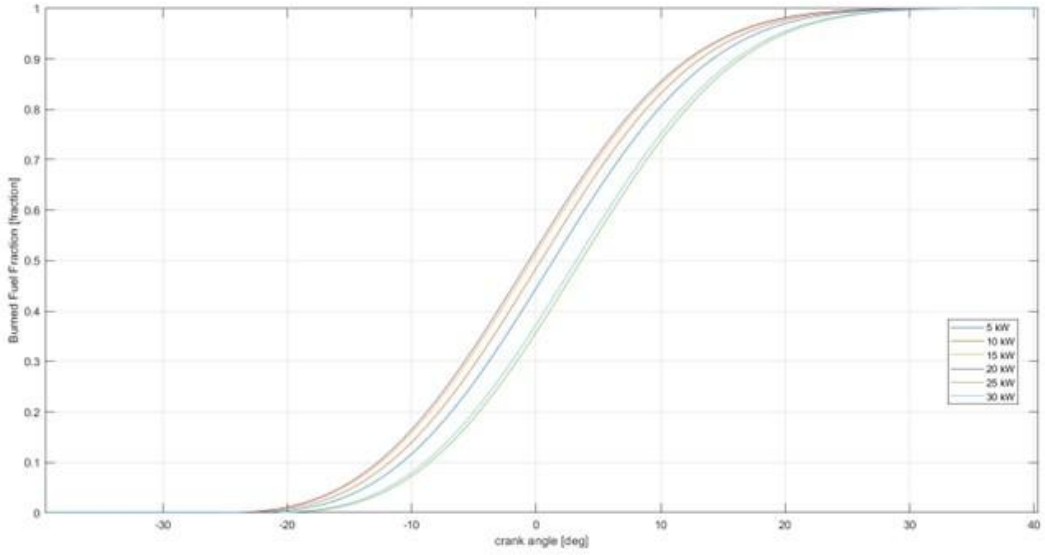

Figure 110 - Burned Fuel Fraction For Each Load With The Ethanol

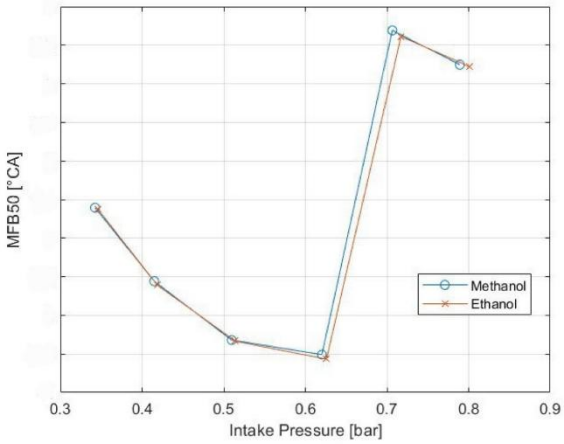

Figure 111 - MFB50 For Both The Fuels

The next set of figures illustrates the heat transfer coefficient employed in the Woschni model for varying loads. Both fuels display similar trends: as the load increases, the energy released during the fuel oxidation also rises, resulting in a greater heat transfer through the combustion chamber walls. From the temperature data shown in *figure 114*, it is evident that, as the load increases, the temperature also increases until it peaks, and then it gradually declines. This pattern is mirrored in the heat transfer coefficient figures, where the increase is more pronounced when moving from 5 kW to 15 kW, compared to the transition from 15 kW to maximum load. Upon examining both figures, a notable deviation from the established trend is observed at maximum load. In these conditions, the peak heat transfer coefficient is lower than that of the previous load. This anomaly can be attributed to the attainment of maximum combustion efficiency, facilitated by faster flame propagation and a more thorough oxidation process, accompanied by a slightly lower peak temperature, as previously mentioned.

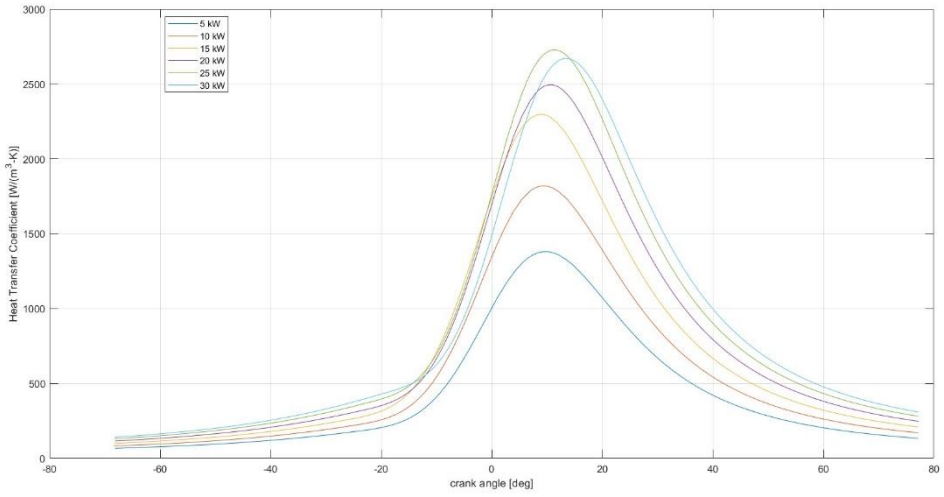

Figure 112 - Heat Transfer Coefficient For Each Load With The Methanol

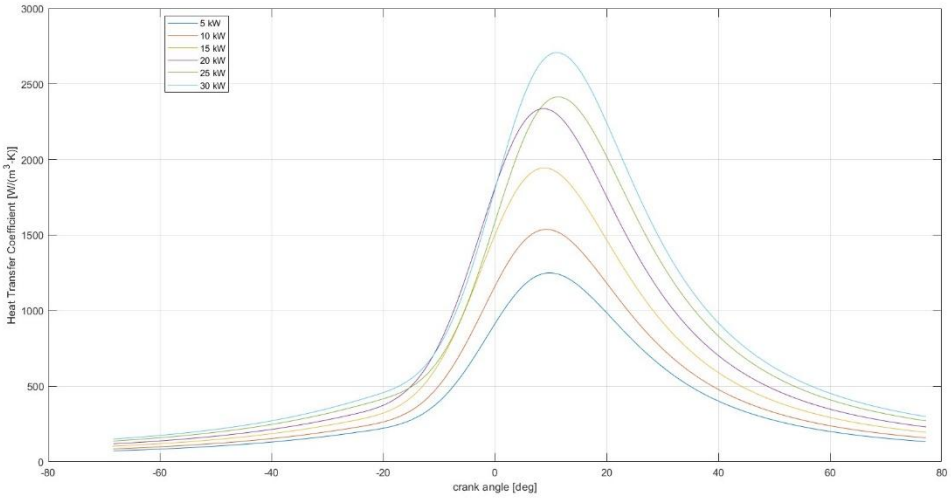

Figure 113 - Heat Transfer Coefficient For Each Load With The Ethanol

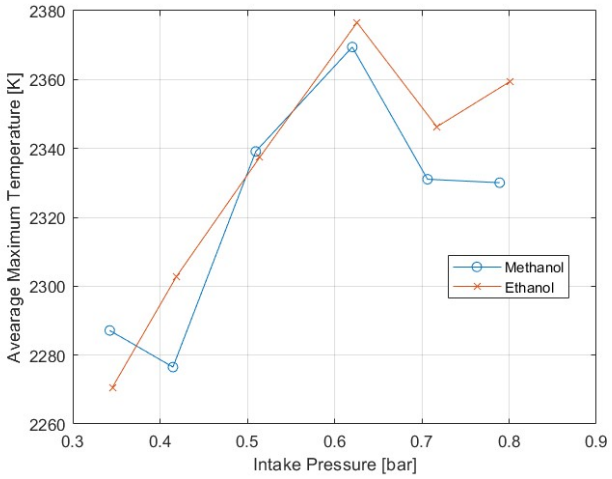

Figure 114 - Maximum Temperature For Both The Fuels

The following figures present a comparison for both the fuels between the company's data on spark advance and the relative start of combustion obtained from the software, which corresponds to the spark advance used as input in GT-POWER. According to the previously described formula that links the centre of gravity of the combustion (the desired input for the software) with the spark advance provided by the company, the start of combustion is assumed to be the crank angle at which the mass fraction burned becomes non-zero. This approach disregards potential delays caused by the ignition delay of the fuel and possible discrepancies between the command sent by the ECU and the actual spark advance. Consequently, this accounts for the small discrepancy observed between the two curves.

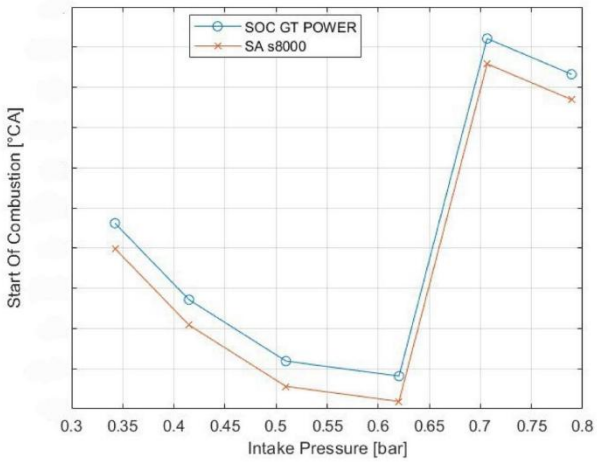

Figure 115 - Spark Advance With The Methanol

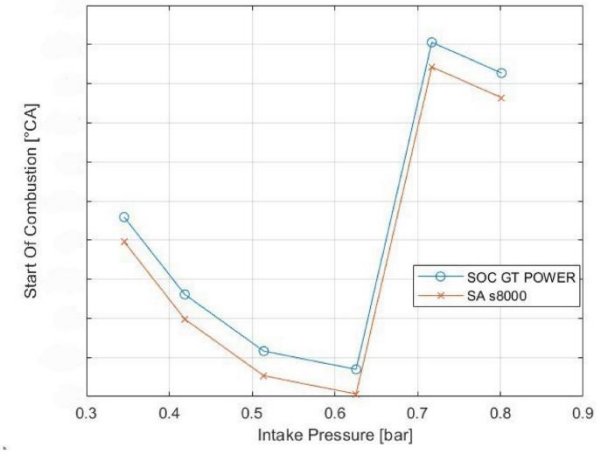

Figure 116 - Spark Advance With The Ethanol

The following figures respectively depict the emissions for methanol and ethanol, as well as the dosage for both fuels as a function of load. Analysing hydrocarbon emissions for both fuels, as the load increases, the throttle valve opens wider, the pumping cycle losses decrease, the air-fuel mixture becomes denser, and the combustion more complete, resulting in lower emissions. The values of these emissions are, in terms of g/kWh, quite small, as shown in the *figure 119*, where the dosage for each load is consistently lean, resulting in high combustion efficiency.

Analysing CO emissions, these too decrease with increasing load due to higher combustion efficiency and because the increasing load leads to a higher air-to-fuel ratio, making the mixture leaner and thereby increasing the fuel conversion efficiency. For the methanol, the first case is characterized by a rich mixture that results in higher values of CO and HC, as, with this air-fuel ratio, the mixture cannot completely oxidate. For ethanol, this decreasing trend is interrupted in the third operating condition, which can be explained by analysing the

dosage as a function of load. Under these conditions, there is a slight enrichment of the mixture, resulting in a reduction in the oxidation process efficiency.

A similar trend is observed with CO_2 emissions, which tend to decrease with increasing load. The CO_2 emissions for the two fuels are quite similar for each load, even though methanol produce less CO_2 since it contains less carbon per unit mass compared to ethanol.

Regarding NOx consumption, the trends are rather peculiar for both fuels, as they are characterized by a decreasing pattern with occasional increases. This can be due to two possible causes: the rise in temperatures, which facilitates the increase in NOx emissions, and a non-constant dosage for the different loads. In addition, the methanol produces lower NOx emissions than the ethanol, since it is characterized by a lower flame temperature and a higher oxygen content in its molecular structure, promoting more uniform combustion.

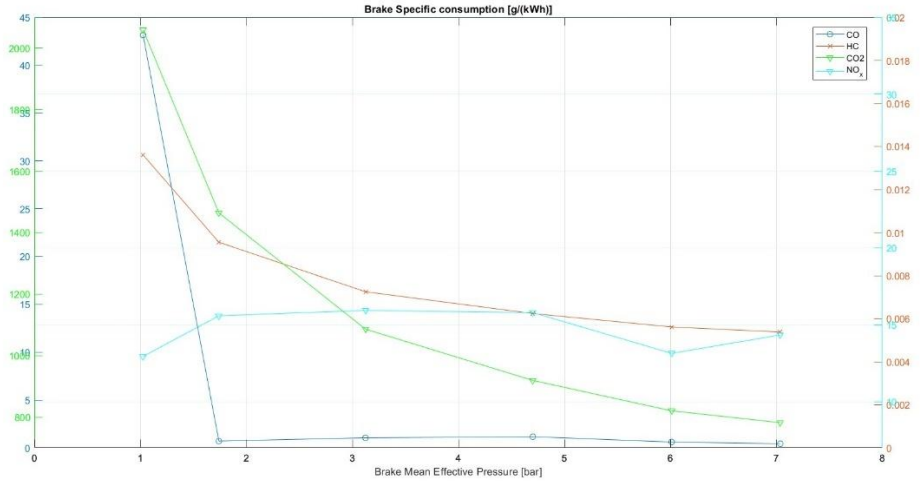

Figure 117 - Emission Values For each Load With The Methanol

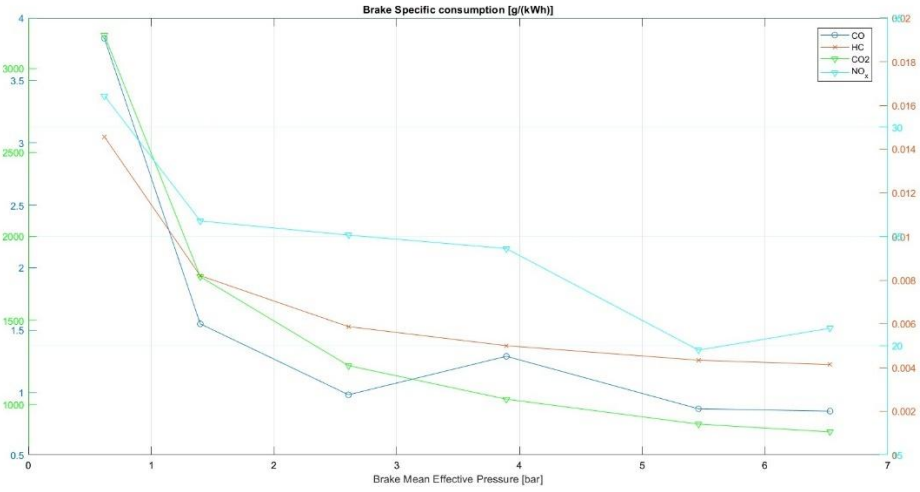

Figure 118 - Emission Values For Each Load With The Ethanol

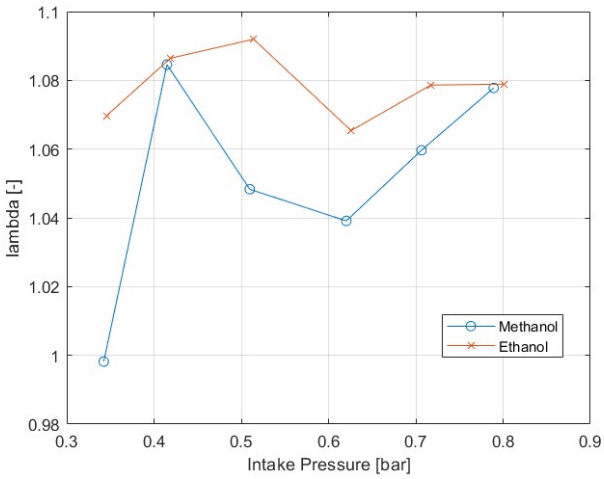

Figure 119 - Lambda Values For Both The Fuels

Upon examining the figure that depicts lambda as a function of load, a rather unusual trend emerges. Typically, one would expect a richer mixture with increasing load to enhance knock resistance and performance. However, in this scenario, the mixture becomes progressively leaner. This phenomenon might be attributed to the increase in the combustion efficiency and, consequently, in the fuel conversion efficiency, which occurs with a leaner mixture. Furthermore, both methanol and ethanol possess high knock resistances, eliminating the need for a richer mixture to reduce charge temperatures and mitigate the risk of knock as the load increases. Specifically, methanol and ethanol exhibit RON values of 106 and 109, respectively.

4.5 Syngas Analysis

Once it was verified that the model is predictive by comparing the results obtained with the few provided by the company, it was decided to test this model with a new gas, called *"Syngas"*, to once again verify the model's predictiveness, but also to observe how this gas affects the engine's performance. This is because the company will use this gas for another engine, much larger in size than the engine in consideration. Therefore, this analysis is fundamental to determine how this gas behaves with a smaller engine, and subsequently to extend this analysis to a larger engine. The Syngas (synthesis gas) is a fuel mixture primarily composed of hydrogen (H_2), carbon monoxide (CO), and small amounts of carbon dioxide (CO_2). It is produced through gasification of biomass, coal, or waste materials. In modern automotive and industrial applications, syngas is gaining attention as a cleaner alternative to conventional fossil fuels. It can be used in internal combustion engines, gas turbines, and fuel cells, offering potential reductions in greenhouse gas emissions. Additionally, syngas can serve as a feedstock for producing synthetic fuels like methanol or hydrogen, further supporting the transition to sustainable energy solutions. The interesting aspect of this syngas is that, since it is mainly derived from waste materials, instead of being discarded, it can be used as a fuel to produce energy that would otherwise be lost. Therefore, one should not expect high performances from the engine or a high efficiency, since this gas is composed of waste materials or substances with low calorific value. As a result, energy, albeit low, is being obtained from a substance that would otherwise be thrown away.

The composition of this gas has not been provided by the company as it is not yet in their possession. Therefore, after a series of attempts with various compositions of this substance according to different publications, the composition present in the article [11] referenced in the bibliography was used. This composition allows for obtaining plausible results in terms of BMEP, because the other tested compositions had higher percentages of already combusted gases, which do not participate in the oxidation process. For the same reason, this gas is injected in a gaseous state, as high injection pressures would have caused these substances to separate, leading to evaporation and, consequently, to the separation of the gas molecules.

Species	Molar Fraction	
	Syngas	Natural Gas
H_2	0.293	0.0
CO	0.287	0.0
CO_2	0.118	0.0024
N_2	0.030	0.0421
H_2O	0.272	0
CH_4	0.000	0.9488

Table 16 - Molar Fraction For Each Species In The Syngas

The figure above shows the molar fraction of the species present in this gas. As the software required the mass or volume fraction of the species, the following formula have been used for each species:

$$M_{fraction} = \frac{(M_{mol} \cdot n_{mol})}{M_{tot}} \cdot 100$$

where the $M_{fraction}$ is mass fraction, M_{mol} is the molar mass, n_{mol} is the number of mole and M_{tot} is the total mass.

Species	Mass [%]	Mass [g]
H_2	3.0	59.06528
CO	41.1	803.8899
CH_4	0.0	0
CO_2	26.5	519.3121
C_2H_6	0.0	0
N_2	4.3	84.0402
H_2O	25.0	490.0156
Tot	100	1956.323

Table 17 - Mass Fraction For Each Species In The Syngas

4.5.1 Performance and Emission at 1500 RPM

As already mentioned, for this fuel no data are available from the company, so the inputs data in terms of spark advance and start of the injection are the one of the methanol for simplicity. Regarding the air-fuel ratio, the chosen lambda value is 1.3, indicating a slightly lean mixture. This is because, with such a composition, a faster flame propagation and thus a higher combustion efficiency are achieved. This is due to the fact that different air-fuel ratio values caused an injection duration that exceeded the allowed stroke, resulting in no combustion.

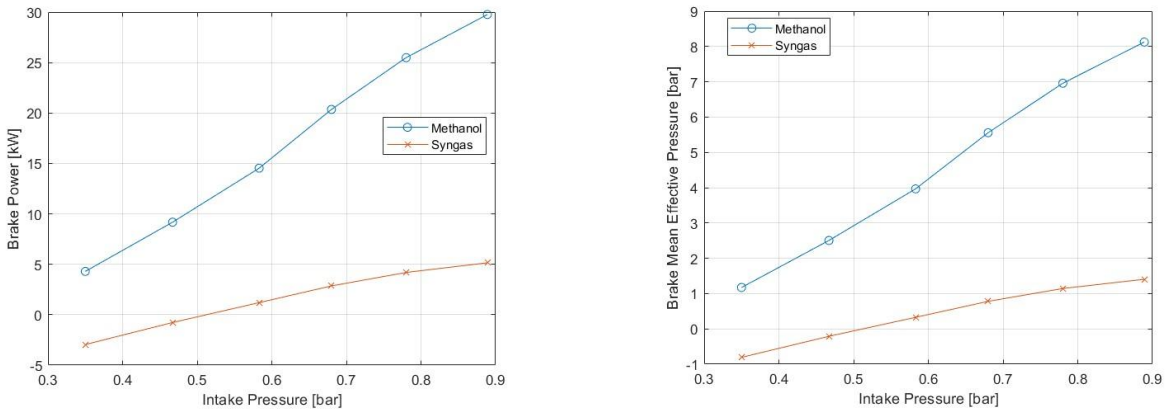

Figure 120 - Comparison Of Both The Brake Power And The Brake Mean Effective Pressure Between The One Obtained With Methanol And The One Obtained With The Syngas

The figures above show the comparison between the brake power and the brake mean effective pressure of the methanol and the syngas relatively. By analysing the brake power curves, it can be appreciated that the values of brake power for the syngas are the expected ones, since the lower heating value of the syngas is around one tenth of the methanol one. Of course, the greater difference between the two curves at high load is due to the implemented friction model, because of the coefficient of the Chen-Flynn model related to the maximum pressure; indeed, with the methanol, the reached pressure values are significantly higher than the one of the syngas, and, as a result, the engine frictions for the methanol are higher than the one of the syngas as well. For what concerns the low load values, the brake power is lower than zero because of two possible reasons, that are the fact that the syngas is not able to overcome the frictions due to its too low lower heating value, and also the fact that the implemented model shows a predictive behaviour at these conditions, as the engine frictions are higher than expected.

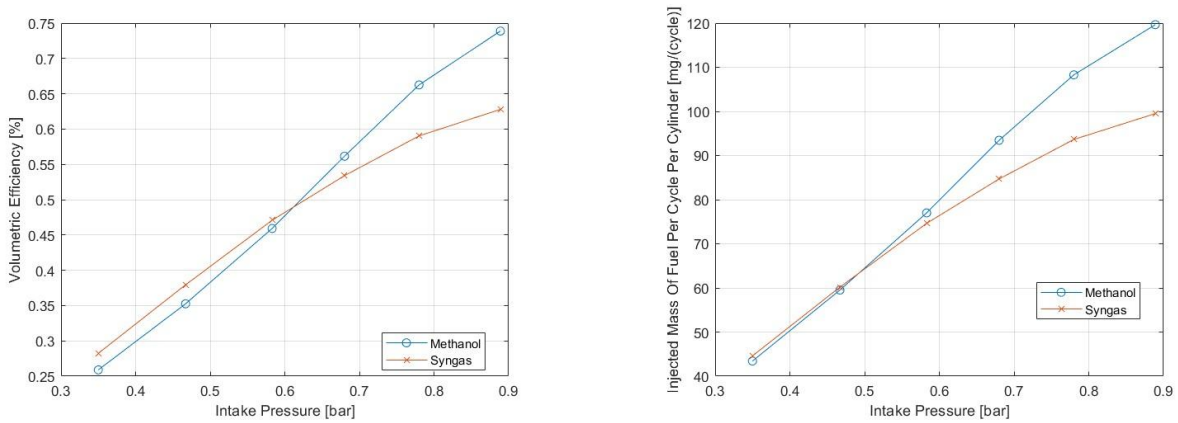

Figure 121 - Comparison Of Both The Volumetric Efficiency And The Injected Fuel Mass Between The One Obtained With Methanol And The One Obtained With The Syngas

The figures above show respectively the volumetric efficiency and the injected fuel mass for both the two fuels. The difference between the curves relatively to the injected mass is due to both the different volumetric efficiency values for each load and the different air-fuel ratio. For what concerns the difference between the two volumetric efficiencies, it stands in the fact that, since the syngas cannot be injected as liquid fuel because of the high injection pressures which cause the substances in the syngas to separate, leading to evaporation and consequently to the separation of the gas molecules, then it is injected in the gaseous state, leading to a reduction in the space available for the air due to the expansion of the gas molecules. This results in a reduction in the volumetric efficiency and in the brake power as well.

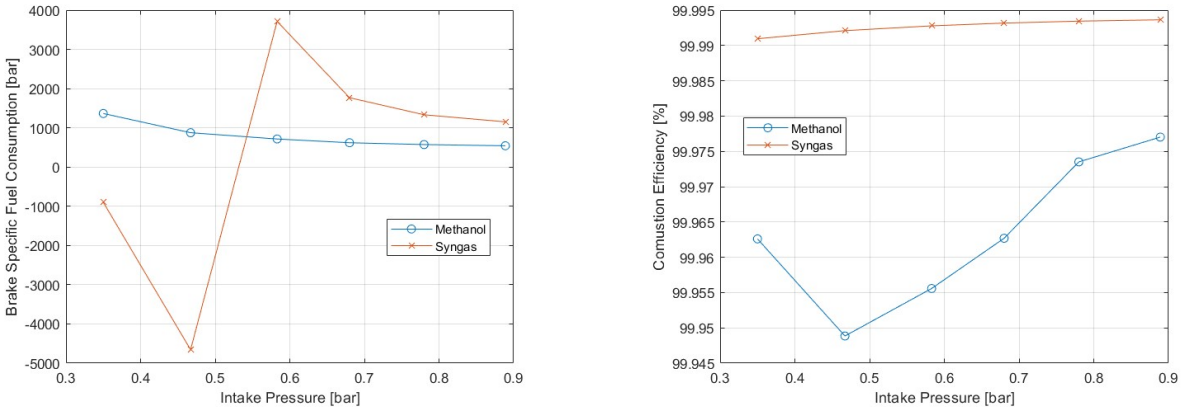

Figure 122 - Comparison Of Both The Brake Specific Fuel Consumption And The Combustion Efficiency Between The One Obtained With Methanol And The One Obtained With The Syngas

The figure above on the left shows the curves of the Brake Specific Fuel Consumption for the two fuels; at low loads the values are negative, as expected due to a negative brake power, so they cannot be taken into account during the analysis of this gas since, as already evaluated, this fuel is not able to work at these low load conditions. Of course, the higher values of BSFC at full load for the syngas are also expected due to a possibly not correct optimisation of the friction model, as it was specifically tuned for the methanol. For what concerns the combustion efficiency, in the figure on the right, the higher constant values for the syngas are the result of a constant air-fuel ratio, chosen in order to obtain a flame propagation that is as fast as possible.

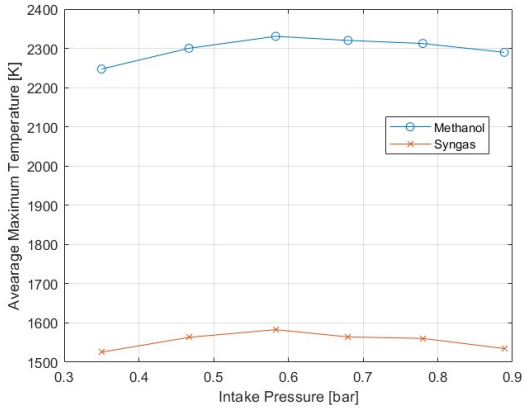

Figure 123 - Comparison Of The Maximum Temperature Between The One Obtained With Methanol And The One Obtained With The Syngas

The following figure shows the Emission Consumption of the syngas. As can be appreciated by analysing the *figure 123*, the too low temperature that is reached in the combustion chamber, due to a too low energy produced during the combustion process, produces nil emissions in terms of NOx consumption. For what concerns the other species, the consumptions of both the HC and the CO are very low at high load (the values reached at low loads cannot be taken into account since they are produced with a negative brake power, which

is not feasible), because of the too high combustion efficiency. As regards the CO_2 consumption, the obtained values are very high due to a too high brake specific fuel consumption.

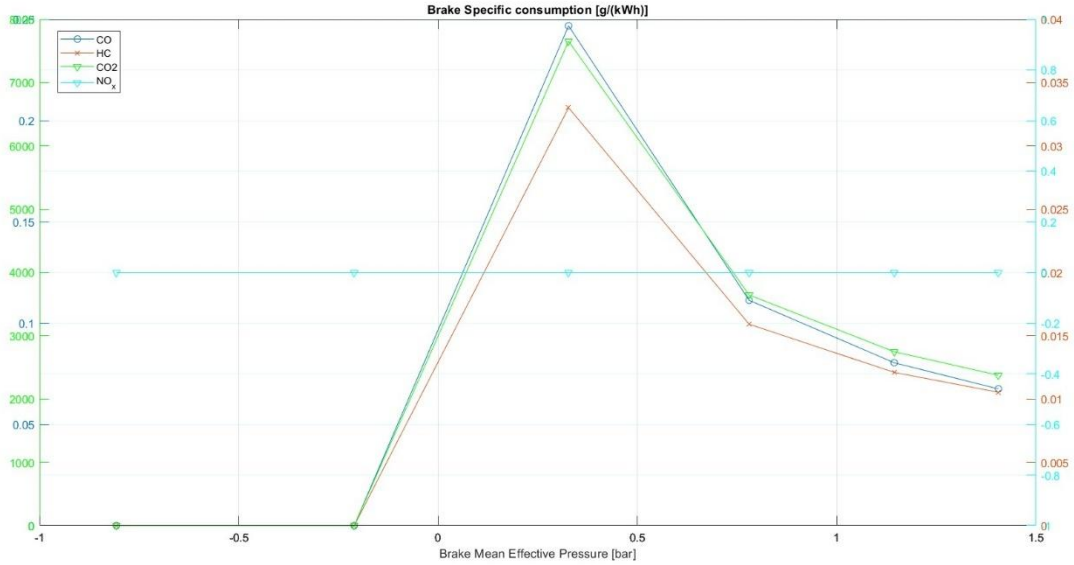

Figure 124 - Emission Values For Each Load With The Syngas

5 CONCLUSIONS

The purpose of this thesis is to implement a one-dimensional model of a retrofitted FPT s8000 3-cylinder engine using the GT-POWER software. Based on the data from the control unit and the data related to the engine's geometry, a model was developed. Furthermore, this model required additional information, which was hypothesized in order to develop it and make it predictive.

To verify the predictability of this model, some efficiency and consumption data were compared with those provided by the company. Regarding these data, the reliability of some tests conducted by the company during the measurement of these data was also analysed. Three different versions were created to choose the one that works best with the two fuels used by the company. Once the best version was found, the performance and emissions of the engine for both fuels were analysed.

It was observed that the engine performed better under high load conditions for both fuels, due to better accuracy of the tests, and hence of the data provided by the company (inputs used in the software), as well as a greater accuracy of the program itself. To further verify the predictability of the model, a test was conducted with syngas, which is of great importance to the company, as this gas will be used with engines characterised by significantly larger displacements than the studied engine. Therefore, an initial analysis on this engine, using the implemented model first, which results in a significant cost reduction for the company, allows for a preliminary impression of how this gas behaves.

BIBLIOGRAPHY

[1] Ishant Gupta, Shweta Kandari, Arvind Rajput, Mohd Asif, Anand Singh, *"Multipoint Fuel Injection System"*, International Journal of Engineering Research & Technology, 2013.

[2] GT-SUITE, Engine Performance Tutorials, 2023.

[3] GT-SUITE, Optimization Manual, 2023.

[4] Stephen G. Russ, Edward W. Kaiser, Walter O. Siegl, Diane H. Podsiadlik and Kathy M. Barrett, *"The Effect of Air/Fuel Ratio on Wide Open Throttle HC Emissions from a Spark-Ignition Engine"*, SAE technical Paper, 1994.

[5] Jason A. Lupescu, Timothy B. Chanko, Joel F. Richert, Adolfo A. Mauti, *"Effect of Fuel/Air Ratio Variations on Catalyst Performance and Hydrocarbon Emissions During Cold-Start and Warm-Up"*, SAE technical Paper, 2009.

[6] F.Millo, *"Knock in S.I. engines: a comparison between different techniques for detection and control"*, SAE Technical Paper, 1998.

[7] Yasuo Kaneko, Hiroyuki Kobayashi, Reijiro Komagome, *"The Effects of Exhaust Gas Recirculation and Residual Gas on Engine Emissions and Fuel Economy"*, SAE technical Paper, 1975.

[8] Moshe Matalona, FrancescoCret, *"The "turbulent flame speed" of wrinkled premixed flames"*, 2012.

[9] Mahmut Kaplan, *"Influence of swirl, tumble and squish flows on combustion characteristics and emissions in internal combustion engine"*, International Journal of automotive Engineering and Technologies, 2019.

[10] Kevin R. Lang and Wai K. Cheng, *"A Novel Strategy for Fast Catalyst Light-Off without the Use of an Air Pump"*,2007.

[11] Vincenzo Liso, Yingru Zhao, Wenyuan Yang and Mads Pagh Nielsen, *"Modelling of a Solid Oxide Fuel Cell CHP System Coupled with a Hot Water Storage Tank for a Single Household"*, Article, 2015.